

Functionalization of Graphene: Covalent and Non-Covalent Approaches, Derivatives and Applications

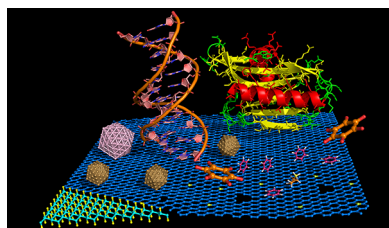
Vasilios Georgakilas,[†] Michal Otyepka,[‡] Athanasios B. Bourlinos,[‡] Vimlesh Chandra,[§] Namdong Kim,[§] K. Christian Kemp,[§] Pavel Hobza,^{‡,§,⊥} Radek Zboril,^{*,‡} and Kwang S. Kim^{*,§}

[†]Institute of Materials Science, NCSR "Demokritos", Ag. Paraskevi Attikis, 15310 Athens, Greece

[‡]Regional Centre of Advanced Technologies and Materials, Department of Physical Chemistry, Faculty of Science, Palacky University Olomouc, 17. listopadu 12, 771 46 Olomouc, Czech Republic

[§]Center for Superfunctional Materials, Department of Chemistry, Pohang University of Science and Technology, San 31, Hyojadong, Namgu, Pohang 790-784, Korea

[⊥]Institute of Organic Chemistry and Biochemistry, Academy of Sciences of the Czech Republic, v.v.i., Flemingovo nám. 2, 166 10 Prague 6, Czech Republic



CONTENTS

1. Introduction	6156
2. Functionalization by Covalent Bonding	6157
2.1. Covalent Attachment of Organic Functionalities to Pristine Graphene	6157
2.1.1. Addition of Free Radicals to sp ² Carbon Atoms of Graphene	6158
2.1.2. Addition of Dienophiles to Carbon–Carbon Bonds	6159
2.2. Covalent Attachment of Functionalities to Graphene Oxides	6162
2.2.1. Addition of Chromophores	6163
2.2.2. Covalent Linkage to Polymers	6164
2.2.3. Addition of Other Organic Molecules	6166
2.2.4. Starting from Partially Reduced Graphene Oxide	6168
2.3. Covalent Attachments of Hydrogen and Halogens toward Graphene Derivatives	6169
2.3.1. Graphane	6169
2.3.2. Fluorographene (Graphene Fluoride)	6172
3. Noncovalent Functionalization of Graphenes	6173
3.1. Graphene–Ligand Noncovalent Interactions: Theory	6173
3.1.1. Nonpolar Gas– π Interaction	6174
3.1.2. H– π Interaction	6174
3.1.3. π – π Interaction	6174
3.1.4. Cation– π Interaction	6174
3.1.5. π_{cation} – π Interaction	6174
3.1.6. Anion– π Interaction	6175
3.1.7. Graphene–Ligand Noncovalent Interaction	6175
3.2. Graphene–Ligand Noncovalent Interactions: Experiment	6175

4. Functionalization with Nanoparticles	6183
4.1. Deposition of Precious Metal Nanoparticles	6183
4.2. Deposition of Metal Oxide Nanoparticles	6185
4.3. Deposition of Quantum Dots	6189
4.4. Deposition of Other Nanoparticles	6191
5. Substitutional Doping	6192
6. Application of Functionalized Graphene	6194
6.1. Devices of Doped Graphene	6194
6.2. Multilayered Graphene Intercalates and Composites	6198
6.3. Electronic/Spintronic Devices Including Ultrafast DNA Sequencing	6201
6.4. Green Chemistry	6202
6.5. Bio-imaging	6204
7. Summary and Outlook	6205
Author Information	6205
Corresponding Author	6205
Notes	6205
Biographies	6205
Acknowledgments	6207
References	6207

1. INTRODUCTION

Graphene, the two-dimensional sp²-hybridized carbon, is currently, without any doubt, the most intensively studied material. This single-atom-thick sheet of carbon atoms arrayed in a honeycomb pattern is the world's thinnest, strongest, and stiffest material, as well as being an excellent conductor of both heat and electricity. It is no wonder that this two-dimensional material is considered, from the application viewpoint, to be even more promising than other nanostructured carbon allotropes, that is, 1-dimensional nanotubes and 0-dimensional fullerenes.

Since the first experimental evidence of the electronic properties of graphene in 2004,¹ a major focus of experimental research has been concentrated on the development of new synthetic routes enabling an effective production of well-defined sheets.^{2–18} The commonly applied methods include the micromechanical¹ or chemical exfoliation of graphite,¹³ chemical

Received: January 31, 2012

Published: September 25, 2012

vapor deposition (CVD) growth,^{6–12} and chemical, electrochemical, thermal, or photocatalytic reduction of graphene oxide (GO; in this review, GO represents graphene oxide, whereas graphite oxide is written in full) and fluorographene.^{15–18} The specific approaches involve, for example, reduction of other graphene derivatives like graphene fluoride toward single graphene nanoplatelets.

The developed methods of graphene preparation allowed observation of unique properties including a half-integer quantum Hall effect for both electrons and holes even at room temperature,^{19–22} extraordinarily high carrier mobility, and single-molecule detection.²³ Graphene also exhibits other superior characteristics of electronic, mechanical, optical, and transport nature. These include ambipolar field effect,²² superlative mechanical strength,²⁴ large specific surface area,²⁵ high transparency,^{9,26} and high thermal conductivity.²⁷

Thanks to these extraordinary and superior properties, graphene has already revealed a great number of potential applications with possible uses in touch screens, capacitors, spintronic devices, fuel cells, batteries, sensors, transparent conductive films, high-frequency circuits, toxic material removal, and flexible electronics.^{9,28–32} Once biofunctionalized with biomolecules (proteins, peptides, etc.), the graphene-based nanostructures may open a gateway to new fields in biotechnology.³³ Recently, graphene has been found to be a promising component in the development of fluorescence resonance energy transfer (FRET) biosensors due to its quenching capability toward various organic dyes and quantum dots,^{34–36} as well as fast DNA sequencing.³⁷

Despite the great application potential, it is worth mentioning that graphene itself possesses zero band gap as well as inertness to reaction, which weakens the competitive strength of graphene in the field of semiconductors and sensors. This is one of the reasons for the huge increase in the number of research projects aimed at functionalization of graphene including reactions of graphene (and its derivatives) with organic and inorganic molecules, chemical modification of the large graphene surface, and the general description of various covalent and noncovalent interactions with graphene.^{38–45} Band gap opening of graphene by doping, intercalation, and striping would be useful for functional nanoelectronic devices.^{46,47}

This comprehensive review represents the first complex work covering all modes and methods of graphene functionalization including their classification. The complementary discussion of both experimental and theoretical aspects of graphene functionalization and interaction is presented. The functionalization modes related to chemistry of graphene derivatives (GO, graphane, fluorographene) represent a significant part of the review, which thus considerably exceeds the chemistry of pristine graphene.

As a result we comprehensively discuss both covalent functionalization based on binding of organic functionalities like free radicals and dienophiles on pristine graphene (section 2.1) and attachment through the chemistry of oxygen groups of GO, that is, methods starting from GO (section 2.2). The covalent attachment of hydrogen and halogens and, generally, the chemistry of graphane and fluorographene is described in section 2.3. Section 3 reports noncovalent functionalization and interactions, which do not disrupt the extended π -conjugation on the graphene surface, unlike covalent functionalization. A significant part of this section is devoted to the theory of graphene–ligand noncovalent interactions, while various interaction modes (π interactions) are analyzed from both theoretical

and experimental viewpoints. In section 4, we discuss the methods of deposition of various nanostructures on graphene including a great variety of nanoparticles like noble metals, metal oxides, quantum dots, polymers, and others. The superior properties and applicability of these graphene–nanoparticle composites are extensively analyzed. The specific methods of graphene doping to control the type and concentration of charged carriers are summarized in section 5. A recent number of reviews have dealt with graphene application in biosensors, energy storage and production, and photocatalysis.^{48–51} As such section 6 addresses selected applications of functionalized graphene, including doped graphene electronic devices, magnetic bilayer intercalates, electronic/spintronic devices and DNA sequencing devices, green chemistry, and bio-imaging.

2. FUNCTIONALIZATION BY COVALENT BONDING

2.1. Covalent Attachment of Organic Functionalities to Pristine Graphene

Several chemical procedures have been developed to afford dispersible graphene; in principle they are based on the exfoliation of graphite, chemical or thermal reduction of GO, intercalative expansion of graphite, chemical vapor deposition, and epitaxial growth.^{4,52–61} Pristine graphene has been isolated by sonication of graphite in organic solvents.⁵ Similarly, Tour and co-workers described isolation of graphene monolayers with graphite dispersed in *ortho*-dichlorobenzene (*o*-DCB).⁶² Bourlino et al.⁶³ achieved dispersion of graphite in a variety of organic solvents, including perfluorinated aromatic molecules, pyridine, and chloroacetate, in noticeable yield using a combination of extended bath sonication and careful centrifugation. The dispersible material includes mainly monolayer and few-layer graphenes, as well as ultrathin layered graphitic sheets, which have limited defects. This means that the extended aromatic system of the graphene monolayer is not disrupted and thus the electrical conductivity of graphene is almost unaffected. The dispersion of graphene in organic solvents helps in functionalization of graphene by several functional groups. Pristine graphene nanoribbons have also been produced by chemical unzipping of carbon nanotubes.^{44,64}

The functionalization of pristine graphene sheets with organic functional groups has been developed for several purposes. The main purpose is the dispersibility of graphene in common organic solvents that is usually obtained after attachment of certain organic groups. The dispersion of graphene sheets in organic solvents is a crucial move toward the formation of nanocomposite materials with graphene. In addition, organic functional groups such as chromophores offer new properties that could be combined with the properties of graphene such as conductivity. In most cases when organic molecules are covalently attached on the graphene surface, its extended aromatic character is perturbed, enabling the control of its electronic properties. The development of a band gap through chemical doping is a powerful method for the use of graphene in nanoelectronic devices.⁶⁵

The organic covalent functionalization reactions of graphene include two general routes: (a) the formation of covalent bonds between free radicals or dienophiles and C=C bonds of pristine graphene and (b) the formation of covalent bonds between organic functional groups and the oxygen groups of GO.

Based on the previous experimental and theoretical experience with fullerene and carbon nanotubes, the most attractive organic species for the reaction with sp^2 carbons of graphene are organic

free radicals and dienophiles. Usually both are intermediate reactive components that are produced under certain conditions in the presence of graphene.

2.1.1. Addition of Free Radicals to sp^2 Carbon Atoms of Graphene. Upon heating of a diazonium salt, a highly reactive free radical is produced, which attacks the sp^2 carbon atoms of graphene forming a covalent bond. This reaction has been used by Tour and co-workers to decorate graphene with nitrophenyls.^{44,64} The graphene sheets in this work were produced through the chemical unzipping of carbon nanotubes. A measurement of the conductivity of a graphene sheet through a simple device (Figure 1) during chemical functionalization with

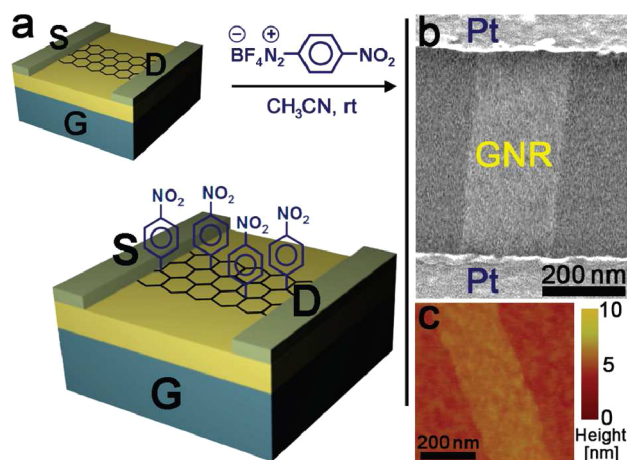


Figure 1. Chemical doping of graphene with 4-nitrophenyl groups: (a) schematic representation; (b) SEM image of a graphene nanoplatelet between Pt electrodes; (c) AFM image of a fragment of a monolayer graphene. Reprinted with permission from ref 64. Copyright 2010 American Chemical Society.

diazonium salts results in a remarkable decrease in conductivity due to disruption of the aromatic system by transformation of carbon atoms from sp^2 to sp^3 hybridization. The conductivity of the graphene sheets was shown to decrease in a controlled manner, showing that conductivity can be controlled by reaction time (Figure 2, left). In a similar approach, Niyogi and co-

workers⁶⁵ showed that the covalent attachment of nitrophenyls to graphene sheets results in the introduction of a band gap, which can be controlled, making the functionalized graphenes potentially useful as semiconducting nanomaterials.

The strong covalent binding of the nitrobenzyl group on graphene was detected by X-ray photoelectron spectroscopy (XPS) (Figure 2, right). The N1s XPS spectrum of the functionalized graphenes exhibits two peaks at 406 and 400 eV that correspond to the nitrogen of NO_2 and the partially reduced nitrogen of the product, respectively. The reactions with diazonium salts have been applied to the functionalization of chemically or thermally converted graphenes, single graphene sheets obtained by micromechanical cleavage from bulk graphite, and epitaxial graphenes.^{64,66–70}

Hydroxylated aryl groups grafted covalently on graphene by the diazonium addition reaction act as initiators for the polymerization of styrene via the atomic transfer radical polymerization (ATRP) method (Figure 3). As a consequence the polymeric chains are covalently grafted on the graphene surface.⁷¹

The ratio between carbon atoms with sp^2 and sp^3 hybridization in the graphitic lattice is an indication of the degree of oxidation or a covalent functionalization reaction. This ratio is estimated using Raman spectroscopy as the I_D/I_G ratio, where I_D and I_G are the intensities of the peaks at ~ 1350 and 1580 cm^{-1} , which correspond to the number of sp^3 and sp^2 C atoms, respectively. Graphene is defined as a pristine two-dimensional sp^2 hybridized carbon sheet; as such the coexistence of sp^3 carbons in the lattice are inherently classified as defects, where these defects can be on the basal edges or inside defects in the plane. For the modification described in Figure 3, the I_D/I_G ratio increased from 1.7 to ~ 2 after functionalization by diazonium addition.

An alternative free radical addition method includes the reaction of benzoyl peroxide with graphene sheets.⁷² Graphene isolated mechanically from Kish graphite was deposited on a silicon substrate and immersed in a benzoyl peroxide/toluene solution. The reaction was initiated photochemically, by focusing an Ar-ion laser beam onto the graphene sheets in the solution. The attachment of the phenyl groups was directly indicated by the appearance of a strong D band at 1343 cm^{-1} . The appearance of this D band is due to the formation of sp^3 carbon atoms in the

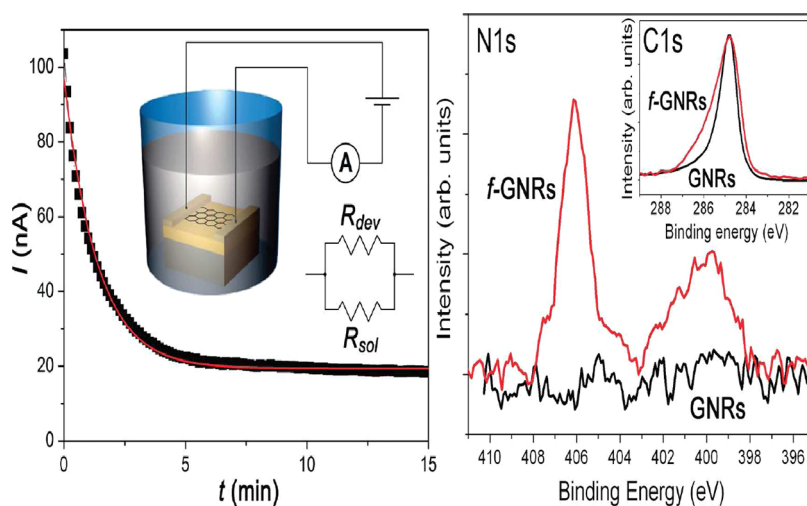


Figure 2. Time dependence of current I : (left) Scheme of the experiment shows the device consisted of two parallel resistances derived from the graphene and the solution, and (right) N1s and C1s XPS spectra of GNRs before and after the functionalization (f-GNRs). Reprinted with permission from ref 64. Copyright 2010 American Chemical Society.

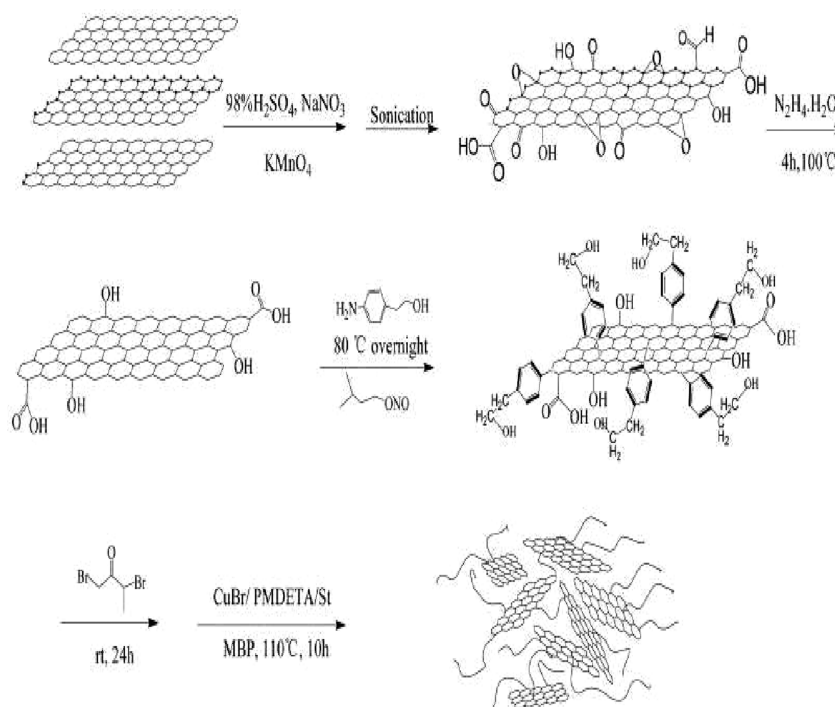


Figure 3. The attachment of aryl groups on graphene nanosheets and the formation of polystyrene chains grafted on graphene nanosheets. Reprinted with permission from ref 71. Copyright 2009 Royal Society of Chemistry.

basal plane of graphene by covalent attachment of phenyl groups (Figure 4). The above reaction was also carried out on a

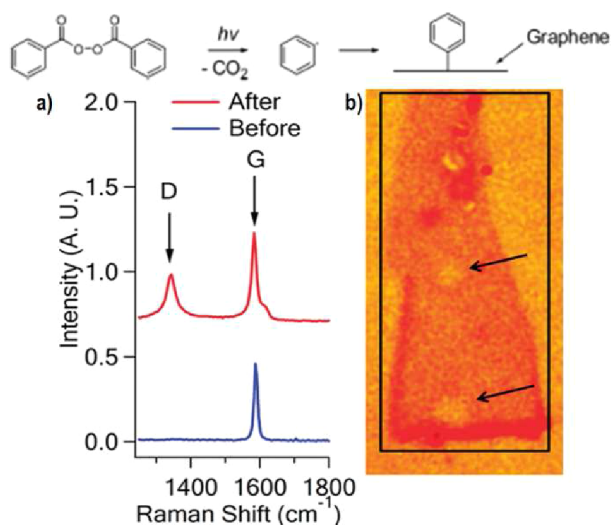


Figure 4. Schematic representation of the radical addition reaction: (a) the appearance of D band in the Raman spectrum of a single layer graphene after the photochemical reaction and (b) optical image of a functionalized single-layer graphene. The arrows indicate holes resulting from prolonged laser exposure. Reprinted with permission from ref 72. Copyright 2009 American Chemical Society.

graphene sheet placed in a field effect transistor (FET) device. In this case, apart from the significant decrease in conductivity due to the increase of sp^3 carbon atoms after the covalent addition of phenyl groups, an increase in the level of hole doping was also observed. The increase in the hole doping was attributed to the physisorbed benzoyl peroxide. Regarding the mechanism of radical generation, Liu et al.⁷² suggest that a hot electron initiates

an electron transfer from photoexcited graphene to the physisorbed benzoyl peroxide. The short-lived benzoyl peroxide radical anion is then decomposed to produce the phenyl radicals, which react with the sp^2 graphene carbon atoms.

2.1.2. Addition of Dienophiles to Carbon–Carbon Bonds. Apart from free radicals, dienophiles also react with sp^2 carbons of graphene. Azomethine ylide, which reacts through a 1,3 dipolar cycloaddition, is one of the most common dienophiles that have been successfully applied in the functionalization of carbon nanostructures: fullerenes, nanotubes, onions, and nanohorns. This type of reaction affords a variety of organic derivatives, which display interesting applications in several areas; these include polymer composites, biotechnology, nanoelectronic devices, drug delivery, and solar cells.^{73–78} After the successful production of graphene sheets directly from graphite dispersed in organic solvents,⁶³ Georgakilas et al.⁷⁹ showed that these graphene sheets could be substituted with pyrrolidine rings via a 1,3 dipolar cycloaddition of azomethine ylide.

The graphene sheets were decorated with dihydroxyl phenyl groups by pyrrolidine rings that were formed perpendicular to the graphene surface by addition of azomethine ylide precursors (Figure 5).⁷⁹ The azomethine ylide was formed by the condensation of 3,4-dihydroxybenzaldehyde and sarcosine. The hydroxyl groups introduced onto a graphene sheet increase its dispersibility in polar solvents such as ethanol and *N,N*-dimethylformamide (DMF). The remarkable increase in the I_D/I_G ratio and peak broadening after the reaction indicates that the functionalization brings about an impressive increase in the sp^3 planar carbon atoms.

The TEM and AFM images reveal the presence of large graphene sheets and few-layer graphitic nanosheets with sizes ranging between 500 nm and 1 μ m (Figure 6). Figure 6, bottom, shows an AFM image of a characteristic graphene sheet with a thickness of 1.5 nm, generally the thickness of unmodified

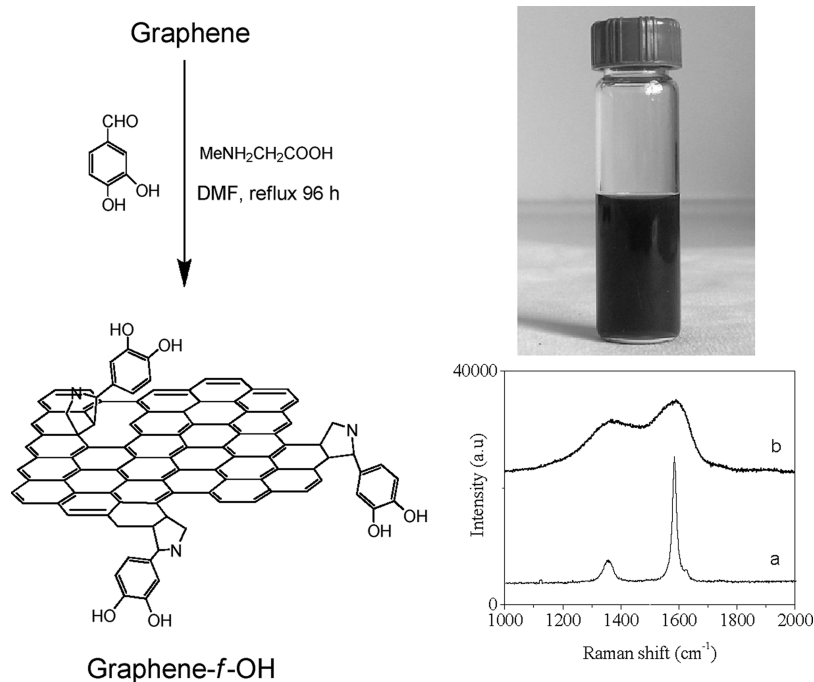


Figure 5. (left) Schematic representation of the 1,3 dipolar cycloaddition of azomethine ylide on graphene. (top, right) Dispersion of functionalized graphene nanoplatelets in ethanol. (bottom, right) Raman spectra of (a) pristine graphene and (b) pyrrolidine functionalized graphene. Reprinted with permission from ref 79. Copyright 2010 Royal Society of Chemistry.

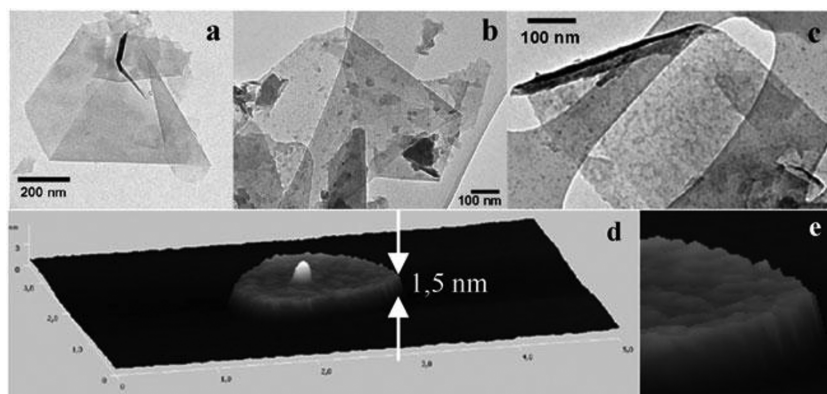


Figure 6. (top) Characteristic TEM and (bottom) AFM images of the graphene-*f*-OH isolated from an ethanol dispersion. Reprinted with permission from ref 15. Copyright 2009 Nature Publishing Group.

monolayer graphene is between 0.6 and 0.9 nm.^{15,80} This increase in graphene layer thickness indicates the existence of functional groups across the graphene surface.

The flexibility of this reaction procedure makes it important because one is able to choose among several aldehydes or substituted α -amino acids as precursors, thus yielding a variety of desirable functional groups. For example, to decorate graphene sheets with tetraphenylporphyrin (TPP) or palladium-TPP, Zhang and co-workers⁸¹ used tetraphenylporphyrin aldehyde (and the Pd analogue) and sarcosine as precursors.

Quintana et al.⁸² utilized 1,3-dipolar cycloaddition to graphene sheets by employing precursors of paraformaldehyde and a specifically designed NH_2 -terminated α -amino acid. These amino groups were shown to selectively bind gold nanorods.

Phenyl and alkyl azides react with the C–C bonds of graphene by the formation of the reactive intermediate nitrene. The reaction of organic azides with graphene has been used successfully by several research groups affording a variety of

organic graphene derivatives. By thermally and photochemically activating a variety of para-substituted perfluorophenylazides (PFPA), Liu et al.⁸³ were able to attach various functionalities to the graphene sheet via a three-membered aziridine ring (Figure 7). These modifications result in varying solubility–dispersibility and surface energy of the modified graphenes.

Nitrene addition has also been used in the functionalization of graphene sheets with phenylalanine. The graphene sheets were reacted with Boc-protected azidophenylalanine in *o*-DCB (Figure 8). The product was determined to have 1 phenylalanine substituent per 13 carbons.⁸⁴

Vadukumpully et al.⁸⁵ reported that graphene sheets can be covalently functionalized with alkylazides, where the alkyl chains include several groups such as hexyl, dodecyl, hydroxyl-undecanyl, and carboxy-undecanyl. The carboxylate groups introduced on the surface facilitated the attachment of Au nanoparticles, which were used as markers to investigate the reactive site distribution. The organically modified graphene

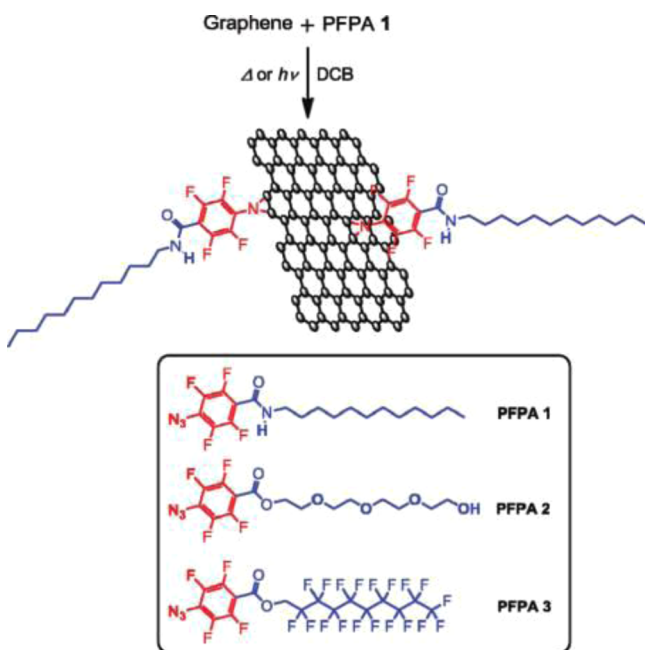


Figure 7. Functionalization of pristine graphene with PFFPA. Reprinted with permission from ref 83. Copyright 2010 American Chemical Society.

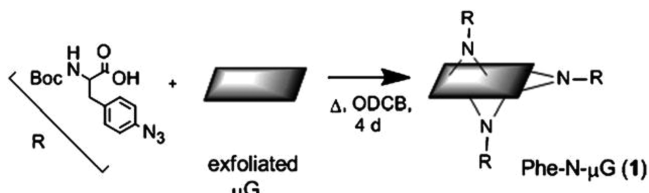


Figure 8. Nitrene addition to graphene sheets using Boc-protected azidophenylalanine. Reprinted with permission from ref 84. Copyright 2010 Royal Society of Chemistry.

sheets showed enhanced dispersibility in common organic solvents such as toluene and acetone. An increase in the I_D/I_G ratio was observed on functionalization, which increased when excess nitrene was added. This indicates that the degree of functionalization is dependent on the amount of nitrene added to the reaction mixture (Figure 9). The appearance of the broad 2D band at 2700 cm^{-1} is characteristic of few layer modified graphene sheets.

He and Gao⁸⁶ developed a facile and versatile method for the introduction of various functional groups and polymeric chains onto graphene sheets via nitrene cycloaddition. This strategy allows various kinds of functional moieties and polymers to be covalently bonded to graphene, resulting in functional graphene sheets and 2-D macromolecular brushes, respectively. The functionalized graphene sheets show enhanced chemical and thermal stabilities compared with GO and can be further modified by different chemical reactions, including amidation, surface-initiated polymerization, and reduction of metal ions. The resulting functionalized graphene sheets are electrically conductive and display excellent dispersibility and processability in solvents.

The formation of covalent bonds between thermally generated nitrene and epitaxial graphene has been demonstrated by Choi et al.⁸⁷ In this case, the formed band gap of the functionalized

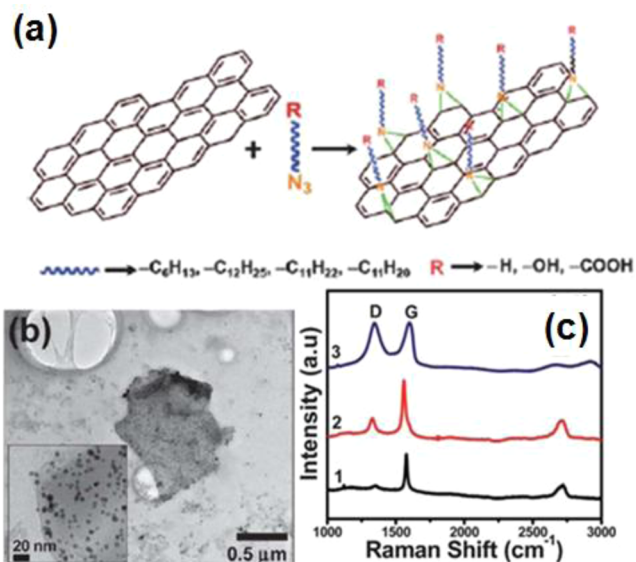


Figure 9. (a) The reaction of alkyl nitrenes with graphene sheets. (b) TEM images of the Au decorated graphene nanoplatelets after organic modification with undecanoic acid groups. (c) Raman spectra of graphene sheet before (1) and after the nitrene addition of azidoundecanoic acid in 1:1 (2) and 10:1 (3) ratios. Reprinted with permission from ref 85. Copyright 2011 Royal Society of Chemistry.

epitaxial graphene can be controlled by the amount of the added nitrene in the reaction.

Zhong et al.⁸⁸ recently described aryne cycloaddition to the graphene surface using 2-(trimethylsilyl)aryl triate as a precursor toward the reactive benzyne intermediate (Figure 10, top). The reaction resulted in the formation of a four-membered ring that connected the aromatic arene rings to the graphene surface. The

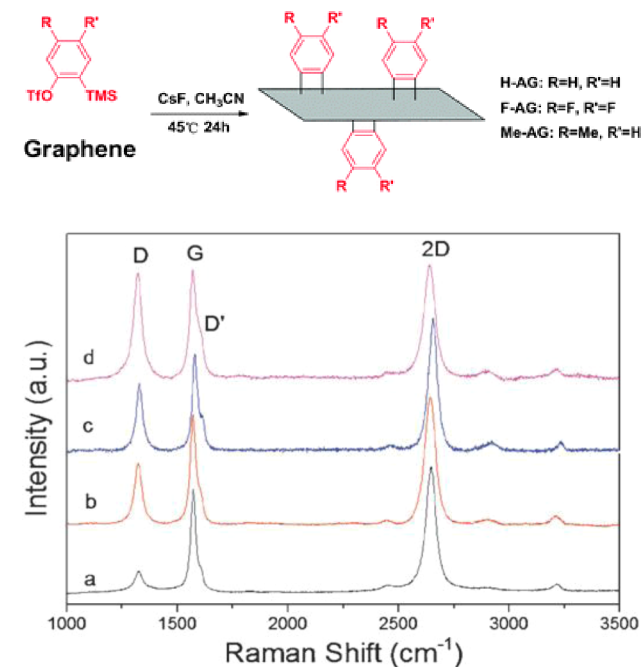


Figure 10. (top) Aryne cycloaddition to graphene sheets. (bottom) Raman spectra of (a) pristine and (d) functionalized graphene nanoplatelets by aryne, (c) methylated aryne, and (b) fluorinated aryne. Reprinted with permission from ref 88. Copyright 2010 Royal Society of Chemistry.

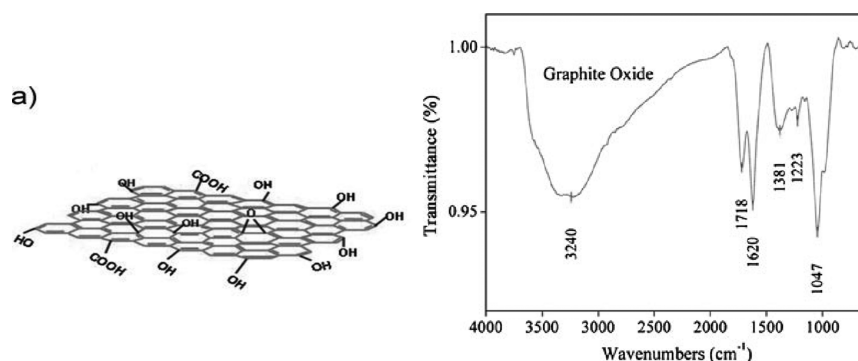


Figure 11. (left) Structure of GO and (right) its FTIR spectrum. Left panel reprinted with permission from ref 101. Copyright 2009 Wiley. Right panel reprinted with permission from ref 102; Copyright 2011 Indian Academy of Sciences.

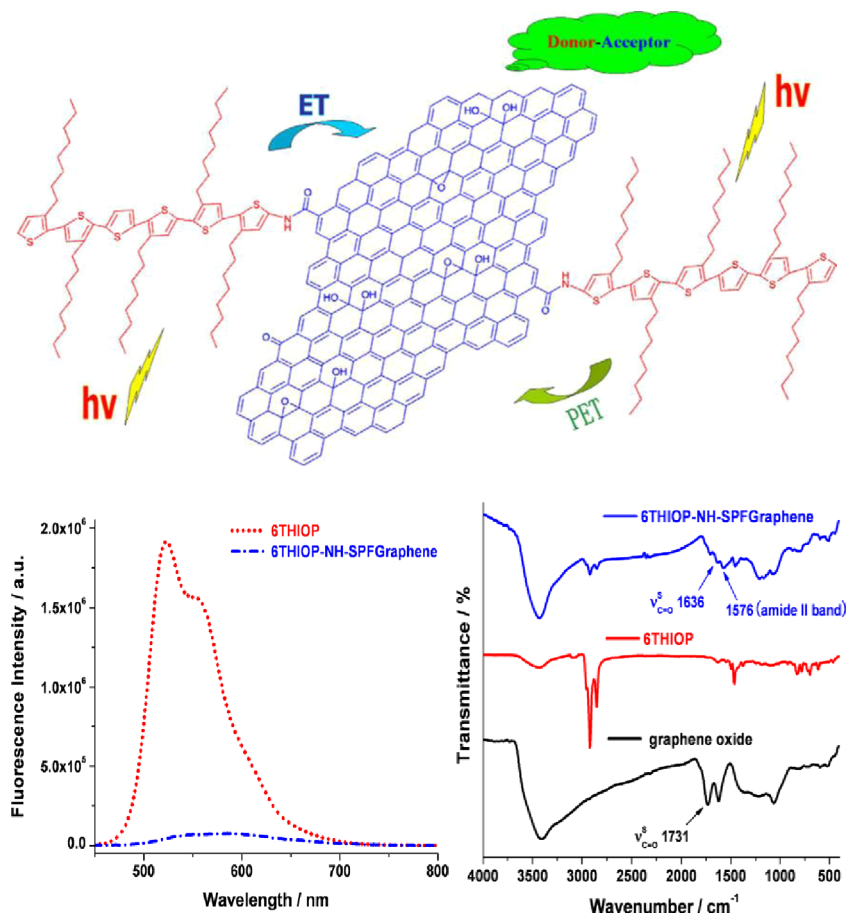


Figure 12. (top) Structure of oligothiophene functionalized GO. (bottom, left) Fluorescence spectra of oligothiophene–GO compared with that of pure oligothiophene. (bottom, right) FTIR spectra of GO, oligothiophene (6Thiop), and the functionalized GO (6Thiop-NH-SPFGraphene). Reprinted with permission from ref 103. Copyright 2009 Elsevier.

aryl-modified graphene sheets were dispersible in DMF, *o*-DCB, ethanol, chloroform, and water. Additionally, the aryl rings can be substituted by several organic groups (i.e., methyl and fluoro), thereby giving a variety of interesting derivatives.

The I_D/I_G ratio of the functionalized graphenes increased from 0.24 for pristine graphene to 0.55 for the fluorinated arylene, 0.69 for the methylated arylene, and 0.97 for the unsubstituted arylene graphene sheets (Figure 10, bottom).

2.2. Covalent Attachment of Functionalities to Graphene Oxides

GO can be characterized as a single graphitic monolayer with randomly distributed aromatic regions (sp^2 carbon atoms) and oxygenated aliphatic regions (sp^3 carbon atoms) containing hydroxyl, epoxy, carbonyl, and carboxyl functional groups. The epoxy and hydroxyl groups lie above and below each graphene layer and the carboxylic groups exist usually at the edges of the layers; however it should be noted that the chemistry and heterogeneity of graphene oxide is still heavily debated. The presence of oxygen groups on the surface of GO provides a remarkable hydrophilic character and analogous chemical



Figure 13. The reaction between GO and CH_2OH -terminated P3HT chains through an esterification reaction. Reprinted with permission from ref 104. Copyright 2010 American Chemical Society.

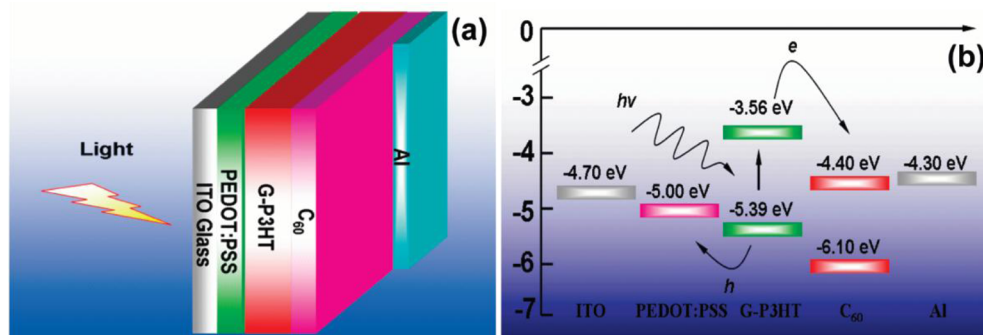


Figure 14. (a) Schematic and (b) energy level diagram of a ITO/PEDOT:PSS/GO–P3HT/C₆₀/Al photovoltaic device. Reprinted with permission from ref 104. Copyright 2010 American Chemical Society.

reactivity. GO is prepared either by methods based on the oxidation of graphite with strong acidic media⁵⁷ or ozone⁵⁸ or the chemical/thermal exfoliation of graphite oxide.^{52–56} GO forms unstable dispersions in water and polar organic solvents such as ethylene glycol, DMF, NMP, and THF, since the exfoliated GO nanoplatelets tend to aggregate through π – π stacking and form large particles of graphite oxide. Several protective agents have been presented for the stabilization of GO nanoplatelets in the solution such as octadecylamine,⁸⁹ 1-octyl-3-methyl-imidazolium,⁹⁰ large aromatic molecules,⁹¹ didodecyldimethyl-ammonium bromide,⁹² polystyrene,⁹³ and poly(sodium 4-styrenesulfonate)⁹⁴ and also elastomeric silicon foams⁹⁵ and DNA.⁹⁶ The presence of these stabilizing groups is not favorable however in terms of use of graphenes in technological applications.

Theoretically, a simple reduction of GO should remove the oxygen groups and rehybridize the effected sp^3 C atoms to sp^2 C, thereby leaving it aromatic and defect free. However experimentally, after any reductive treatment of GO a critical number of oxygen groups and defects remain. The reduction of GO has been extensively researched, and the methods ranging from the traditional hydrazine treatment⁵² to bacterial treatment⁹⁷ have shown to be successful, as well as a variety of other methods.^{56,98–100} These defects affect the properties of the reduced GO (RGO), most importantly its electric conductivity. For this reason, the type of graphene used is usually specified, that is, chemically converted graphene, chemically reduced graphene, RGO, or thermally reduced graphene, in order to discriminate it from pristine graphene.⁴

Thanks to the rich chemistry of hydroxyl, carboxyl, and epoxy groups, GO has been selected very often as the starting material for the formation of graphene derivatives through the covalent attachment of organic groups on its surface. In this type of functionalization where the added groups are linked through the oxygen atoms of GO, the Raman spectra of the functionalized

graphene show no important differences from those of GO, since no further structural perturbation occurred. After the functionalization of GO a large number of oxygen groups remain, as revealed by FTIR analysis of the functionalized GO products in comparison with the starting GO nanoplatelets (Figure 11).^{101,102}

2.2.1. Addition of Chromophores. Polythiophenes and oligothiophenes are well-known conjugated polymeric materials with potential use in various optoelectronic applications, for example, solar cells, due to high charge mobility arising from the large number of π electrons delocalized along their molecular chains.¹⁰³ Amine-terminated oligothiophenes can be grafted on GO nanoplatelets through covalent amide bonds, as described by Liu et al.¹⁰³ (Figure 12). The disappearance of the carboxyl groups and emergence of the amide bonds were recorded in the FTIR spectrum of the functionalized GO (Figure 12, bottom, left). An important observation from the FTIR spectrum is that GO keeps its “oxide” character after functionalization in terms of the presence of hydroxyl groups as confirmed by the absorption band at 3431 cm^{-1} in spectra recorded before and after functionalization. The strong interaction between GO and oligothiophene is indicated by the almost complete fluorescence quenching observed in the functionalized graphene in comparison with pure oligothiophene (Figure 12). The as-synthesized donor–acceptor material displayed a superior optical limiting effect compared with the standard optical limiting material C₆₀ and a control sample consisting of a physical mixture of GO and oligothiophene.

In an analogous approach, Yu et al.¹⁰⁴ reported functionalization of GO with $-\text{CH}_2\text{OH}$ terminated regioregular poly(3-hexylthiophene) (P3HT) through the formation of ester bonds with the carboxyl groups of GO nanoplatelets (Figure 13). Due to the presence of an abundant number of hydroxyl groups in the added polymer, P3HT-GO was soluble in common organic

solvents, facilitating its characterization and device fabrication by solution processing. Yu et al.¹⁰⁴ move a step forward designing and presenting a photovoltaic device using a combination of P₃HT/GO product with C₆₀ as illustrated in the scheme of Figure 14, which recorded a 200% increase in the power conversion efficiency in comparison with a pure P₃HT/C₆₀ analogous system. This remarkable increase is attributed to an extended electron delocalization that occurred after the covalent attachment of P₃HT with GO in comparison to pure P₃HT.

Apart from the classical esterification and amidation reactions, Melucci et al.¹⁰⁵ covalently attached optically active silane-terminated oligothiophene groups to GO substrates. The advantage of this reaction is that the covalent attachment is completed within a few minutes via microwave radiation, thereby affording GO derivatives soluble in water as well as nonpolar solvents.

Apart from conjugated polymers, simple organic chromophores such as porphyrins, phthalocyanines, and azobenzene with very interesting optoelectronic properties have been covalently attached on graphene nanoplatelets.^{106–109} Due to the large visible light extinction coefficients, porphyrins and phthalocyanines are frequently used as antennas for harvesting energy from photons. GO can be functionalized with porphyrins through the formation of amide bonds between amine-functionalized porphyrins and carboxylic groups of GO as shown in Figure 15.¹⁰⁶

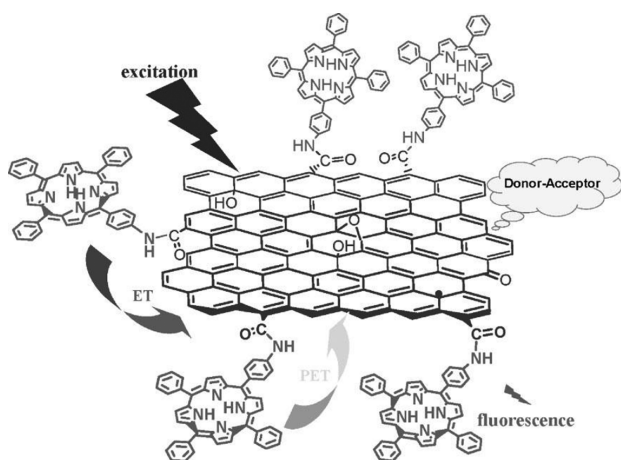


Figure 15. Schematic representation of the product of the reaction between GO and amine-functionalized porphyrin. Reprinted with permission from ref 106. Copyright 2009 Wiley.

The covalent interaction between the porphyrin and the GO surface resulted in an improvement in the dispersibility in organic solvents and an effective fluorescence quenching after the photoexcitation of the porphyrin. Furthermore, the as prepared nanocomposite displayed much better optical limiting properties compared with C₆₀ or a control sample consisting of a physical mixture of GO and the amine-functionalized porphyrin (Figure 16).¹⁰⁶ Liu et al.¹⁰⁸ presented in a related report better nonlinear optical properties for porphyrin or C₆₀ covalently functionalized GO derivatives in comparison with their individual components; this effect is attributed to a photoinduced electron transfer between the porphyrin or C₆₀ and GO.

2.2.2. Covalent Linkage to Polymers. GO can be grafted to polymeric chains that have reactive species like hydroxyls and amines, that is, poly(ethylene glycol), polylysine, polyallylamine, and poly(vinyl alcohol). These materials combine the properties

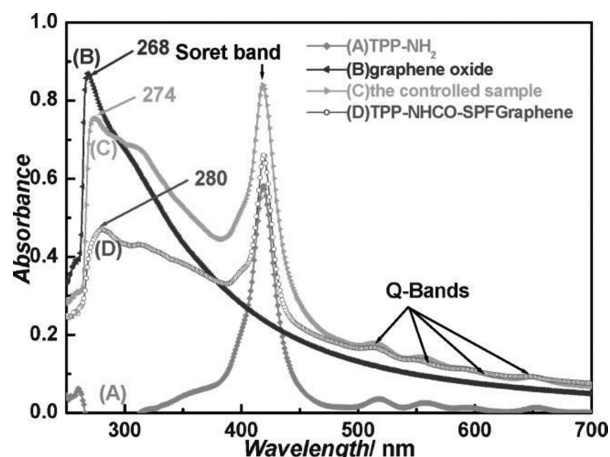


Figure 16. UV-vis absorption spectra of TPP-graphene, TPP-NH₂, GO, and the control sample in DMF. Reprinted with permission from ref 106. Copyright 2009 Wiley.

of their parts; the polymeric part offers dispersibility in certain solvents, mechanical strengthening, and several morphological characteristics, while graphene contributes to the electrical conductivity, chemical reactivity, and reinforcement of the mechanical properties.

Poly(ethylene glycol) (PEG) is a biocompatible super-hydrophilic polymer that has been used to cover nanostructures providing them with these basic characteristics. It has found use as a carrier for drug delivery, that is, metallic nanoparticles or carbon nanotubes. Amine-terminated PEG can be grafted onto GO nanoplatelets through amide bond formation. The PEGylated GO is highly dispersible in water, as well as, in several aquatic biological solutions such as serum or cell medium. This important characteristic makes PEGylated GO an important candidate for the delivery of hydrophobic drugs in biological systems. As an example, a camptothecin analogue named SN38 (Figure 17), which is highly hydrophobic, can be immobilized on the surface of PEGylated GO through van der Waals interactions, forming a nanostructure with excellent stability in biological solutions.¹¹⁰ Camptothecin is an organic aromatic molecule, which displays remarkable anticancer properties. Its main disadvantage in cancer therapy is its low solubility in aqueous media. In further work, Yang et al.¹¹¹ studied the behavior of PEGylated GO nanoplatelets in vivo.

RGO can be made dispersible in biological solution after its functionalization by poly(L-lysine) (PLL) through amidation (Figure 18).¹¹² Poly(L-lysine) is an attractive biocompatible molecule, with uses in promoting cell adhesion, drug delivery, cell labeling, biofuel cells, and DNA electrochemical sensors. The PLL/RGO nanostructure was used as a biosensor for hydrogen peroxide (H₂O₂) detection exhibiting improved sensing of H₂O₂. The detector device was based on the immobilization of horseradish peroxidase onto the PLL/RGO surface and the deposition of the resulting nanocomposite on a gold electrode.

Polyallylamine (PAA) can be reacted with GO; in this reaction the numerous amine groups react successfully with the epoxy groups of GO forming an effective cross-linking of the GO sheets (Figure 19). After filtration of a colloidal suspension of PAA/GO through a filter paper, a thin paper-like membrane was formed.¹¹³ Although the mechanical properties of PAA/GO membrane are not impressively increased in comparison to a GO analogue, the



Figure 17. Immobilization of SN38 camptothecin on PEG-GO. Reprinted with permission from ref 110. Copyright 2008 American Chemical Society.

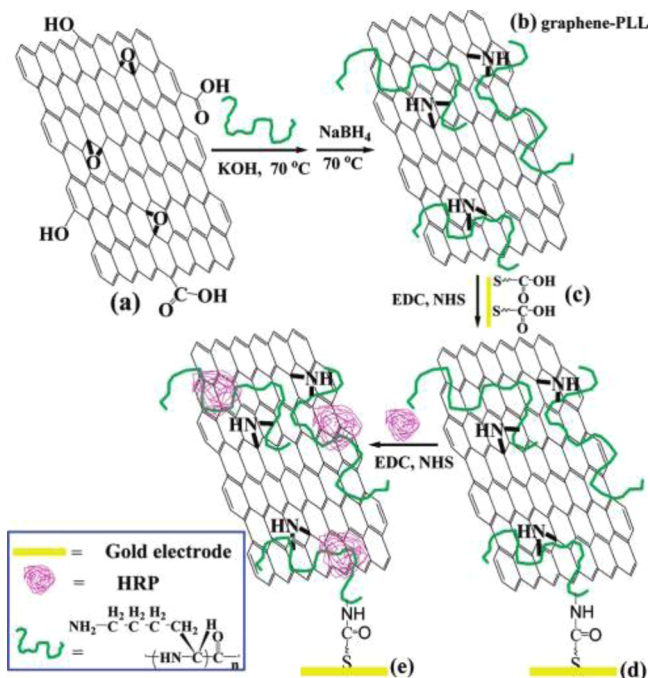


Figure 18. Schematic representation of the formation of the PLL/RGO-horseshoe peroxidase and its subsequent deposition on a gold electrode. Reprinted with permission from ref 112. Copyright 2009 American Chemical Society.

idea of making stiff GO membranes by cross-linking with polymers seems to work successfully.

Poly(vinyl alcohol) (PVA) can be grafted onto GO nanoplatelets via ester bonds between the hydroxyl groups of PVA and the carboxylic groups of GO. These covalent bonds can be

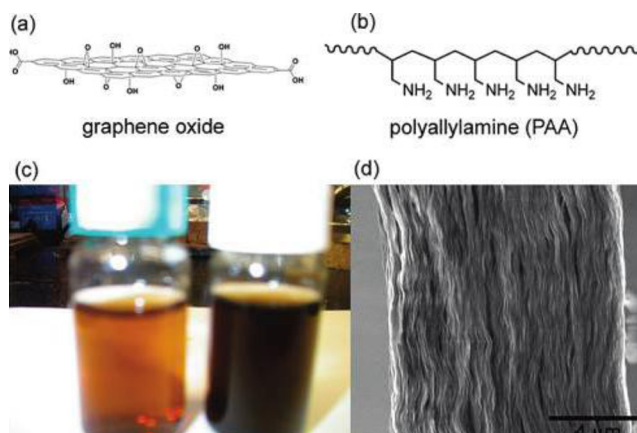


Figure 19. Schematic representation of (a) GO and (b) PAA. (c) Photograph of an aqueous colloidal dispersion of GO (left) and PAA-GO (right). (d) SEM image of the cross section of a PAA-GO paper sample. Reprinted with permission from ref 113. Copyright 2009 American Chemical Society.

formed either by direct formation or after the transformation of carboxylates to the more reactive acyl chlorides. The PVA/GO composite was dispersible in DMSO and hot water. In a further step, the PVA/GO composite was partially reduced by hydrazine, affording the PVA/RGO composite.¹¹⁴ Veca et al.¹¹⁵ also reported covalent functionalization of graphene nanoplatelets with PVA, affording derivatives readily soluble in aqueous and polar organic solvents for further application.^{116,117} Lin et al.¹¹⁸ demonstrated an efficient method to covalently graft polyethylene (PE) chains onto the surface of GO, which resulted in a high polymer grafting efficiency and a 10 °C increase in the crystallization temperature compared with the pure polymer. Furthermore, the polyethylene-functionalized GO (PE/GO) displays a unique encapsulating structure and can be stably dispersed in toluene.

Lee et al.¹¹⁹ reported an atom transfer radical polymerization (ATRP) approach to functionalize GO nanoplatelets with polymers. In this method, polymer chains were directly grown from the surface of GO via living radical polymerization. The technique involves the covalent attachment of the initiator followed by the ATRP of various monomers including styrene, methyl methacrylate, or butyl acrylate without damaging the GO structure.¹²⁰ The obtained nanocomposites showed significant enhancement in thermal and mechanical properties compared with the pure polymers. Poly(methyl methacrylate) PMMA functionalization of GO was carried out by Goncalves et al.¹²¹ Different PMMA/GO composites were synthesized by changing the percentage of PMMA polymer to GO in the reaction. The resulting composites were readily dispersible in organic solvents and used as reinforcement fillers in the preparation of PMMA composite films.

The formation of covalently bonded polymer-GO nanocomposites, where GO was initially functionalized with octadecylamine (ODA) has been reported by Pramoda et al.¹²² These ODA functionalized GO nanoplatelets were subsequently reacted with methacryloyl chloride to incorporate polymerizable $-C=C-$ functionalities at the graphene surfaces. These intermediates were then employed in *in situ* polymerization of methylmethacrylate to obtain covalently bonded PMMA/GO nanocomposites.

Ramanathan et al.¹²³ mixed oxygen and hydroxyl-functionalized high-surface-area graphene nanoplatelets with PMMA to

yield graphene reinforced PMMA nanocomposites with a significant increase of about 30 °C in the glass transition temperature using only 0.5 wt % functionalized graphene nanoplatelets.

Amide-functionalized graphene nanoplatelets (few layer graphene) were prepared by Das et al.¹²⁴ to reinforce PMMA. This functionalization resulted in a significant increase of 70% and 10% in the elastic modulus and the hardness, respectively, of the composites with the addition of 0.6 wt % of graphene nanoplatelets.

Fang et al.⁷¹ demonstrated that polystyrene (PS) chains can be covalently grafted onto the surface of partially RGO nanoplatelets, enhancing the glass transition temperature of the polymer by 15 °C. The initiator molecules were covalently bonded to the RGO surface via a diazonium addition, and the subsequent ATRP of styrene was carried out. With the addition of only 0.9 wt % GO nanoplatelets, the resulting PS/RGO composite film exhibited a prominent reinforcement effect, showing a 57.2% and 69.5% increase in Young's modulus and tensile strength, respectively. The synthesis of PS grafted GO nanoplatelets at room temperature was reported by Sun et al.¹²⁵ The obtained functionalized nanoplatelets exhibited good dispersibility in organic solvents. The covalent grafting of polyglycerol onto the surface of GO was reported by Pham et al.,¹²⁶ while Zhang et al.¹²⁷ reported that GO can be functionalized with poly(*N*-vinylcarbazole) (PVK), where GO acts as an electron acceptor, while PVK acts as the electron donor. This material was characterized by IR, DSC, TGA, UV-vis, CV, XRD, and AFM. A nanocomposite of waterborne polyurethane (WPU) with covalent functionalized graphene nanoplatelets finely dispersed in the polymer matrix improves the conductivity of the WPU.¹²⁸

2.2.3. Addition of Other Organic Molecules. One of the earliest reports of the functionalization of GO was the formation of amide bonds between octadecylamine (ODA) and the carboxylic groups of GO.^{62,129} The functionalized GO product was characterized by Raman, FTIR, UV spectroscopy, AFM microscopy, and thermogravimetric analysis and was found to be dispersible in THF (0.5 mg/mL), CCl₄, and 1,2-dichloroethane. Water-dispersible GO derivatives have been produced by the attachment of allylamine, *p*-phenyl sulfonate, and phenylene diamine groups on the graphene surface.^{39,130}

GO can also be used as support for the immobilization of enzymes in the preparation of biosensors. As an example, glucose oxidase (GO_x) can be immobilized on GO nanoplatelets through amide bonds (Figure 20).¹³¹ The GO/GO_x composite has been examined as a biosensor for the determination of glucose and was shown to give a linear response over a broad concentration range and exhibit high sensitivity, reproducibility in measurements, and biocompatibility with human cells.

Zhang et al.¹³² have reported on the formation of a hybrid material by covalent linking of C₆₀ with GO (Figure 21). In this synthesis an amide bond was formed between a pyrrolidine ring modified C₆₀ and the carboxyl groups on the GO surface. Analogously to the fullerene derivatives of carbon nanotubes,^{133,134} GO-C₆₀ hybrids could be useful in many optoelectronic applications due to their remarkable electronic and optical properties.

Another interesting modification of partially RGO with imidazolium derivatives was presented by Yang et al.;¹³⁵ they showed that 1-(3-aminopropyl)-imidazolium bromide can be attached to the epoxy groups of GO nanoplatelets (Figure 22).

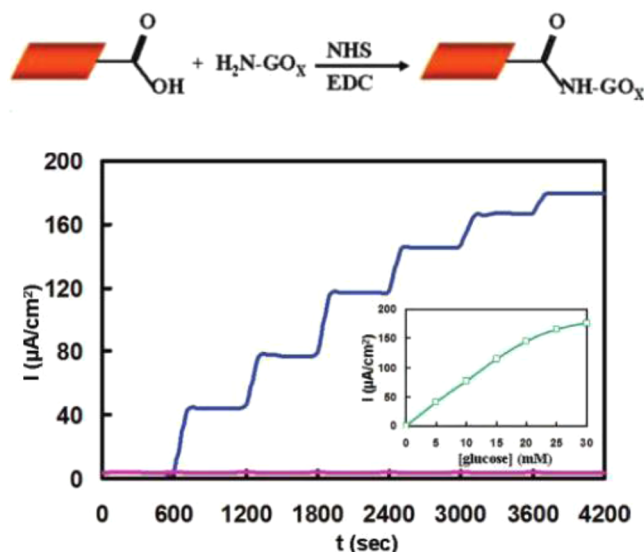


Figure 20. (top) Immobilization of glucose oxidase (H₂N-GO_x) onto GO nanoplatelets. (bottom) Typical amperometric response of the GO_x-GO electrode (blue line) and the pristine graphene electrode (pink line). Inset shows calibration curve obtained for glucose determination at 0.4 V vs Ag/AgCl. Reprinted with permission from ref 131. Copyright 2010 American Chemical Society.

The imidazolium-modified GO was easily dispersed in water, *N,N*-dimethylformamide, and dimethyl sulfoxide.

Functionalization of GO by imidazolium derivatives has also been reported by Karousis et al.¹³⁶ In this case, 1-(3-aminopropyl)-imidazole was attached to the carboxylic groups of GO through amide bonds. Subsequently, the heterocyclic ring was transformed through *N*-methylation to its ionic imidazolium analogue. The counterion of the imidazolium ring can be substituted by other ions, providing new composite materials with interesting properties. As an example, bromine was exchanged by lipophilic hexafluorophosphate (PF₆⁻) making the product dispersible in organic solvents such as dichloromethane, dimethylformamide, and methanol. Bromine can also be substituted by a photoactive porphyrin molecule (Figure 23).

Graphene sheet seems to be a suitable material for transparent conductive electrodes in polymer solar cells due to its 98% transparency and 6 KΩ·sq⁻¹ sheet resistance. The chemical modification of graphene sheets remarkably improves their dispersibility in organic solvents and polymers that are used in polymer solar cells. As an example, the introduction of butylamine groups to GO nanoplatelets improves their dispersibility in organic solvents and polystyrene sulfonate, which makes it possible to fabricate the transparent poly(3,4-ethylene-dioxythiophene)/PS-sulfonate/GO composite film. This film was deposited on an indium tin oxide (ITO) electrode, which was then used as an anode in a polymer bulk heterojunction solar cell. The use of butylamine-functionalized GO nanoplatelets resulted in an increase of the overall power conversion efficiency to 0.75% in comparison with the value of 0.38% based on simple GO.¹³⁷

To introduce butyl amine onto graphene sheets, RGO nanoplatelets were first functionalized by fluorine using plasma-assisted decomposition of CF₄.¹³⁸ The fluorinated GO was then transformed to butylamine-functionalized GO by exchanging fluorine atoms with butylamine groups (Figure 24).

Very often, carbon nanostructures have been used to reinforce polymers, ceramics, and other matrices, which affords the

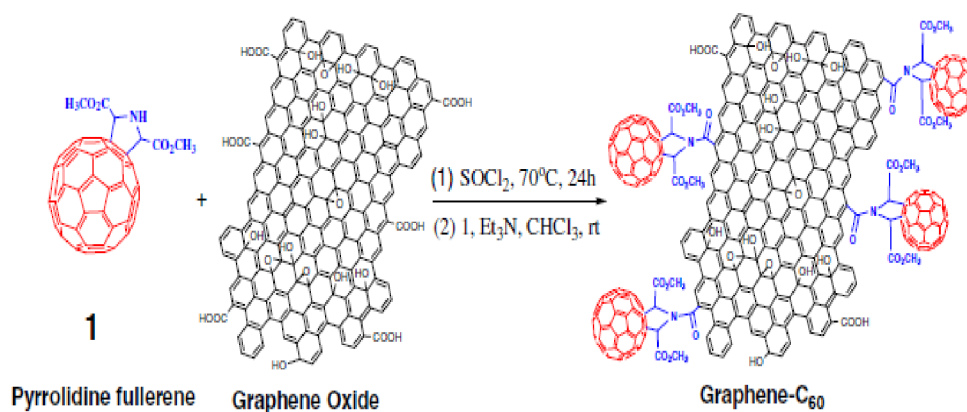


Figure 21. Representation of the formation of the C₆₀-GO composite. Reprinted with permission from ref 132. Copyright 2008 Elsevier.

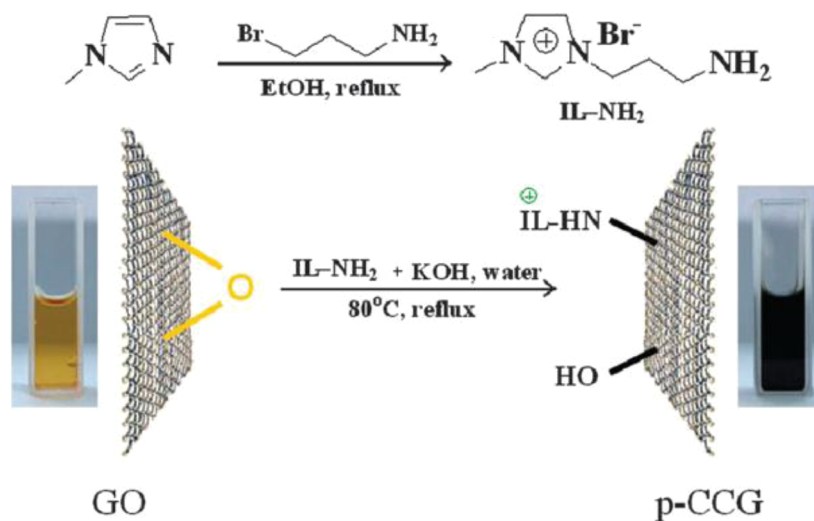


Figure 22. Illustration of the preparation of imidazolium-modified GO. Reprinted with permission from ref 135. Copyright 2009 Royal Society of Chemistry.

polymers with interesting mechanical, optical, and electrical properties.^{139–142} The effect of the dispersion of carbon nanostructures in such matrices is greatest when the dispersion is fine and interfacial interactions between the nanostructures and the matrix are present. These two factors, fine dispersion and interfacial interaction, are important for chemical functionalization of carbon nanostructures. As an example, in order to enhance the silica monolith structure, Yang et al.¹⁴³ presented the functionalization of GO with 3-aminopropyl triethoxysilane (APTS). The APTS was grafted onto the GO surface through covalent bonds with the epoxy groups as represented in Figure 25. The silicon-functionalized GO (Si-GO) was incorporated into a silica matrix by hydrolytic condensation of an excess of APTS in the presence of Si-GO.

The functionalized GO was easily dispersed in water, ethanol, DMF, dimethyl sulfoxide (DMSO), and APTS. The GO reinforced Si monolith showed better mechanical properties in comparison with the pure Si monolith (Figure 26); the compressive failure strength and toughness were improved by 20% and 92%, respectively, compared with the pure Si monolith.

An organic GO derivative obtained from the covalent attachment of phenyl isocyanate to GO through the formation of an ester bond with the epoxy group has been used in several diverse applications. After this chemical modification, GO nanoplatelets were easily dispersible in organic solvents such as

o-DBC and DMF; additionally the incorporation of these organically modified GO nanoplatelets into polymers and conjugated polymers for photovoltaics was facilitated. This procedure was initially developed by Stankovich et al.³ as a general approach for preparation of GO-polymer composites. Phenyl isocyanate-treated GO nanoplatelets were dispersed in PS and other styrenic copolymers, such as acrylonitrile-butadiene-styrene or styrene-butadiene, through solution phase mixing. The modified GO was then chemically reduced in order to improve the electrical conductivity of composites.

This functionalization procedure has been further used by Liu and co-workers^{144–146} in the fabrication of organic photovoltaic cells. The phenyl isocyanate functionalized graphene was easily dispersed into *o*-DBC, and this was further dispersed in P3HT to form a donor/acceptor system. After the insertion of modified GO into P3HT, a remarkable quenching of the photoluminescence was observed, indicating a strong interaction and electron transfer from P3HT to GO nanoplatelets. This function makes the formed composite suitable as an active layer in bulk heterojunction photovoltaic cells as represented in Figure 27. A photovoltaic cell containing the P3HT/GO composite showed a power conversion efficiency of 1.1%.¹⁴⁶

Finally, Avinash et al.¹⁴⁷ obtained covalently functionalized GO with ferrocene via a green chemistry approach at room temperature on solid phase alumina. The ferrocene/GO

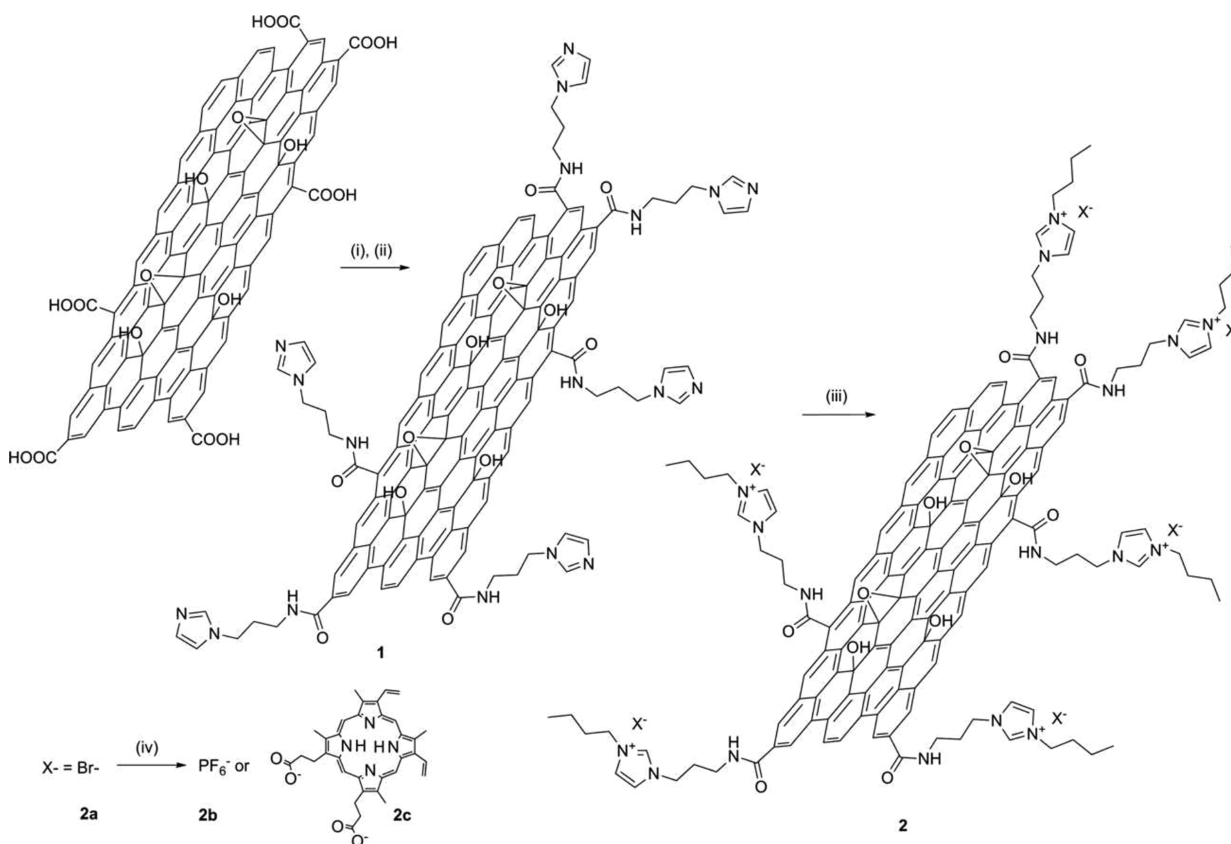


Figure 23. Preparation of imidazolium-modified GO hybrid materials and anion-exchange reactions: (i) $(\text{COCl})_2$, 80 °C, 18 h; (ii) 1-(3-aminopropyl)imidazole, 100 °C, 18 h; (iii) 1-bromobutane, 90 °C, 18 h; (iv) H_2O , NaPF_6 or protoporphyrin IX disodium salt, 25 °C, 18 h. Reprinted with permission from ref 136. Copyright 2010 Elsevier.

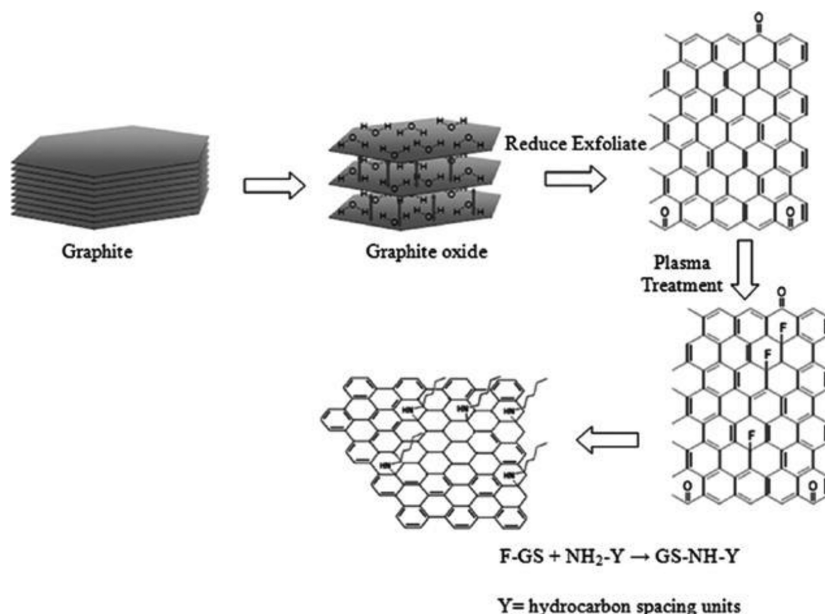


Figure 24. Preparation of butylamine-functionalized RGO nanoplatelets. Reprinted with permission from ref 138. Copyright 2009 American Chemical Society.

composite material exhibited interesting magnetic properties, with the magnetization of the composite material found to be more than that of both GO and ferrocene.

2.2.4. Starting from Partially Reduced Graphene Oxide. As referred in the introduction of this chapter the complete reduction of GO to graphene via different routes has

not been achieved yet. There are always epoxy and hydroxyl functional groups on the basal plane of the RGO.¹⁴⁸ Density functional theory (DFT) investigations of the structure of graphene after deoxygenation confirm that it is impossible to completely remove the oxygen-containing functional groups from the graphene surface using chemical or thermal reduction

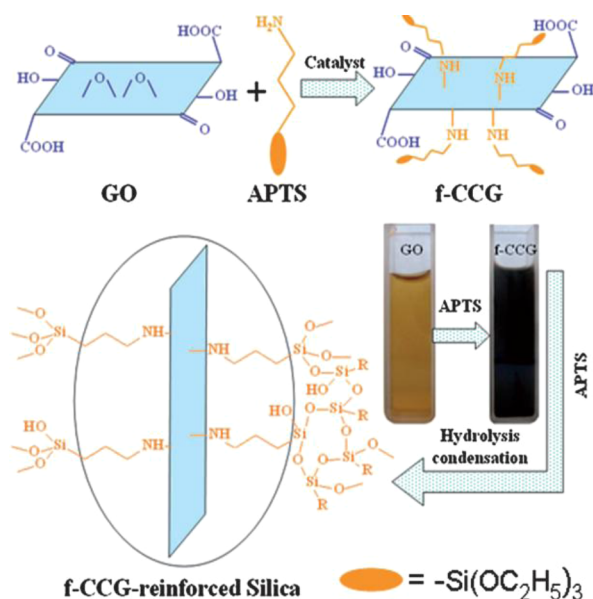


Figure 25. Illustration of the reaction between GO and APTS and incorporation of Si-*f*-GO nanoplatelets into the silica matrix. R = –OH or –CH₂(CH₂)₂NH₂. Reprinted with permission from ref 143. Copyright 2009 Royal Society of Chemistry.

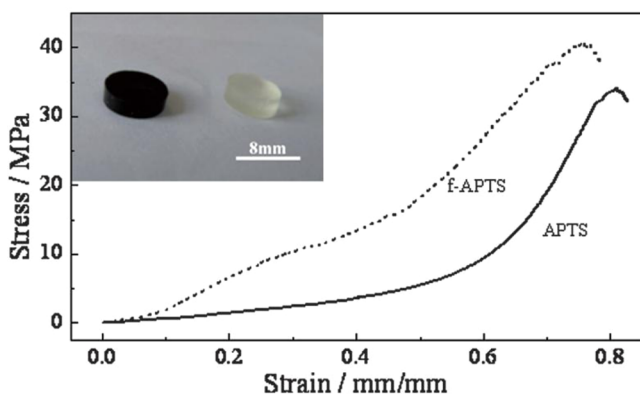


Figure 26. Stress–strain plots of neat APTS monolith (solid) and Si-*f*-GO reinforced APTS monolith (dotted). Inset: photographs of monolith disks for the compressive tests. From left to right: Si-*f*-GO reinforced APTS monolith and neat APTS monolith. Reprinted with permission from ref 143. Copyright 2009 Royal Society of Chemistry.

or even a combination of these two.^{149,150} In a subsequent DFT study, Ghaderi and Peressi¹⁵¹ confirmed the presence of hydroxyl groups after reduction.

The residual oxygen-containing groups give the RGO a weaker chemical reactivity as regards organic groups that can be grafted onto the graphene surface through oxygen linkers. The chemical functionalization of RGO using residual oxygen groups has been presented by Hsiao et al.¹⁵² This procedure has the advantage that it does not create additional defects on the graphene surface compared with the reaction with C=C bonds. They used a specific polymeric molecule (MA-POA2000), which was grafted onto RGO by two different methods, radical addition and condensation using residual epoxy groups (Figure 28). In the free radical grafting method, initiated by benzoyl peroxide, the radical attacked the sp² carbon atoms on the RGO surface. In the second method, the free amine groups reacted with the residual epoxy groups of RGO.

Comparing the two methods in terms of the thermal stability of the derivatives (Figure 29), after the removal of the organic addends near 400 °C for the derivative obtained via the epoxy reaction (D-graphene/MA-POA2000), the RGO remained nearly stable even at 800 °C. In contrast the free radical addition product (F-graphene/MA-POA2000) was continuously oxidized from 400 to 800 °C. Derivatives of RGO with poly(oxyalkyne)-amine are dispersible in THF (0.25 mg/mL), and the dispersions remain stable for at least two months.

RGO was also used by Shen et al.¹⁵³ for the preparation of “amphiphilic” graphenes. Here GO was reduced by sodium boron hydride (NaBH₄) affording RGO nanoplatelets, which were decorated with PS–polyacrylamide copolymer (PS–PAM) by in situ free radical polymerization, initiated by benzoyl peroxide (Figure 30).

The polymerized GO is dispersible in water, due to its hydrophilic PAM component, and simultaneously in xylene due to the hydrophobic PS component. Additionally, by controlling the ratio between the two polymeric components, the hydrophilic–hydrophobic balance of the functionalized graphene can also be controlled.

2.3. Covalent Attachments of Hydrogen and Halogens toward Graphene Derivatives

2.3.1. Graphane. Covalently modified graphene derivatives can be prepared by attachment of atoms or molecular groups to sp² carbons. Such modification maintains the graphene 2D lattice; however, due to the loss of the π-conjugated electron cloud present above and below the graphene plane, there are dramatic changes to its properties. The idea to modify graphene was introduced by Sofo et al.,¹⁵⁴ who theoretically predicted the existence of graphane, fully hydrogenated graphene, as well as its fluorinated counterpart. Graphane was synthesized by the exposure of graphene to cold hydrogen plasma.^{42,155} The attachment of hydrogen atoms to sp² carbons changes their hybridization state to sp³ (Figure 31), thus graphene while maintaining the graphene hexagonal symmetry, has altered electronic properties and local structure. The charge carrier mobility of graphane is 3 orders of magnitude smaller than that of graphene; as a consequence graphane behaves as an insulator.^{42,156} The locally flat graphene structure becomes buckled in graphane, the C–C–C angle decreases from 120° (in graphene) to 109.5° and the C–C bond increases from 1.42 Å (in graphene) to 1.52–1.56 Å.^{157,158} Besides the typical G (1580 cm⁻¹) and 2D (2680 cm⁻¹) Raman peaks observed for graphene, two additional peaks are observed in the graphane spectrum at 1620 cm⁻¹ (D′) and 1350 cm⁻¹ (D, the defect peak) (Figure 32).^{42,159} It was shown that the hydrogenation of graphene is reversible, and graphane can be dehydrogenated by annealing to give graphene (450 °C in Ar atmosphere).⁴²

The graphene conduction band formed by π-conjugated p_z orbitals is missing in graphane, and consequently, the graphene zero band gap opens. The initial DFT calculations, using a generalized gradient approximation (GGA), of the band gap identified graphane as a direct band gap material and estimated a band gap value of about 3.5 eV at the Γ point.¹⁵⁴ However, it is well-known that GGA DFT underestimates band gap values,¹⁶⁰ and more rigorous methods including, for example, screened hybrid functional or involvement of increased electron correlation (e.g., GW) should be used. The GW calculation suggests the band gap values should be 5.4 eV (refs 161 and 162) and 5.7 eV (ref 163.), while screened hybrid functional calculations give a value of 4.5 eV. Recent high-level theoretical

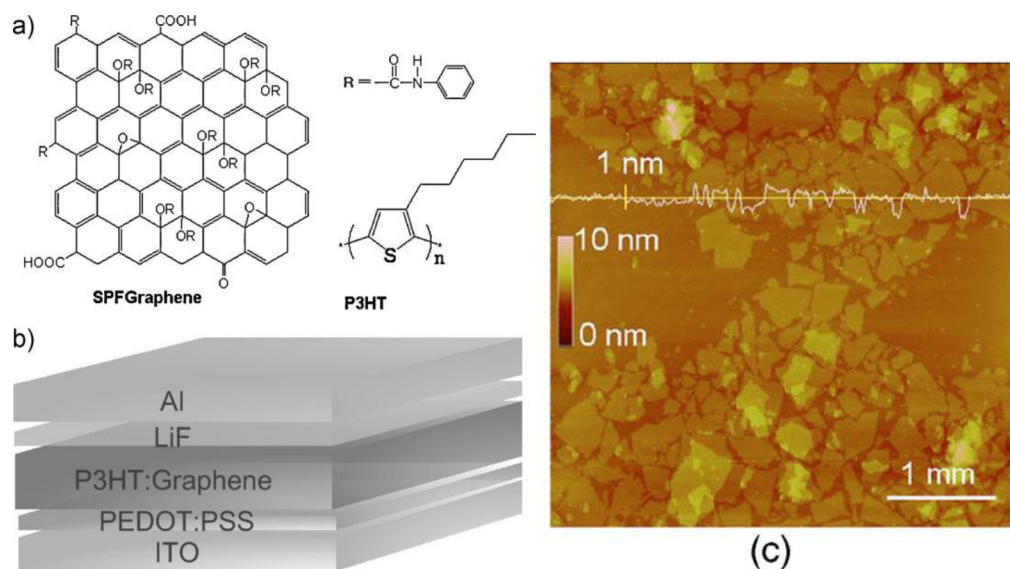


Figure 27. (a) Graphical representation of the modified graphene and P3HT, (b) schematic representation of the bulk heterojunction photovoltaic cells, and (c) an AFM image of the modified graphene. Reprinted with permission from ref 146. Copyright 2009 Wiley.

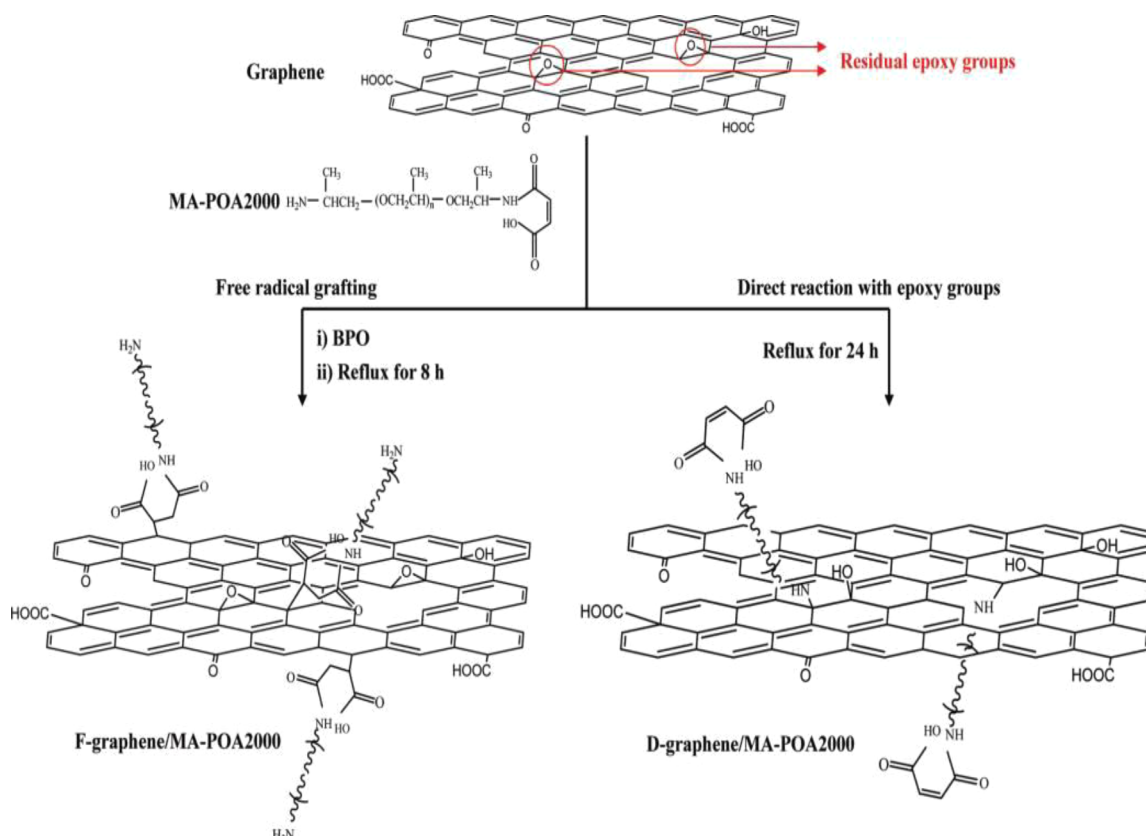


Figure 28. Two different grafting methods from the same organic molecule. Reprinted with permission from ref 152. Copyright 2010 American Chemical Society.

calculations of the optical properties of graphene, which were carried out with the Bethe–Salpeter equation (BSE), which accounts for electron–electron and electron–hole correlations as well as excitonic effects,¹⁶⁴ show an absorption spectra with the first exciton peak at 3.8 eV (for x or y polarized light, while the transition is dipole forbidden for z polarized light, Figure 33).¹⁶²

When one considers the electronic properties of graphene and graphene two sharply differing materials are represented, one is a

semimetal and the other an insulator. It should be noted that opening of the graphene zero band gap still represents a challenge in the manufacture of field effect transistors.¹⁶⁵ In this respect, the electronic properties of graphene can be relatively finely tuned by its partial hydrogenation.¹⁶⁶ Well structured partially hydrogenated graphene derivatives represent very interesting materials with magnetic, metallic, and semiconducting properties, which can be designed by the degree of

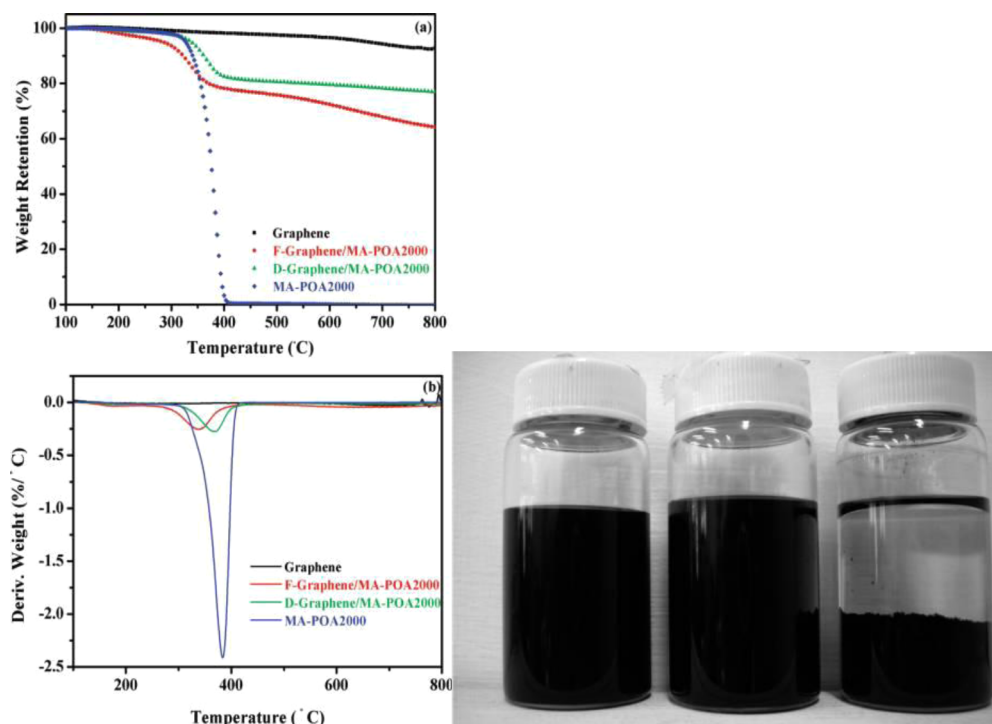


Figure 29. (a) Thermogravimetric curves and (b) corresponding derivative curves of the starting materials and the derivatives. Photograph showing the dispersion of graphene, F-graphene/MA-POA2000 and D-graphene/MA-POA2000 in THF (from right to left). Reprinted with permission from ref 152. Copyright 2010 American Chemical Society.

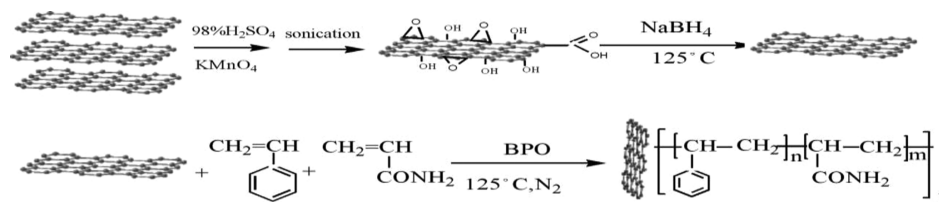


Figure 30. Schematic representation of covalent attachment of PS/PAM copolymer to RGO. Reprinted with permission from ref 153. Copyright 2009 Wiley.

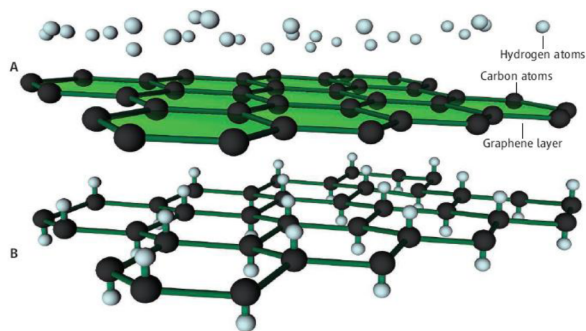


Figure 31. Graphene layer (in green) that is attacked by cold plasma hydrogen atoms to produce graphane. Reprinted with permission from ref 159. Copyright 2009 American Association for the Advancement of Science.

hydrogenation. Properties of graphene nanoroads (Figure 34) and hexagonal nanodots have been studied theoretically. It has been shown that the zigzag and armchair orientation, as well as width, of graphene nanoroads affect its inherent properties, for example, band gap (Figure 35). Wide zigzag roads (involving more than two zigzag chains, $N_z > 2$, Figure 34) are magnetic with energetically similar ferromagnetic and antiferromagnetic

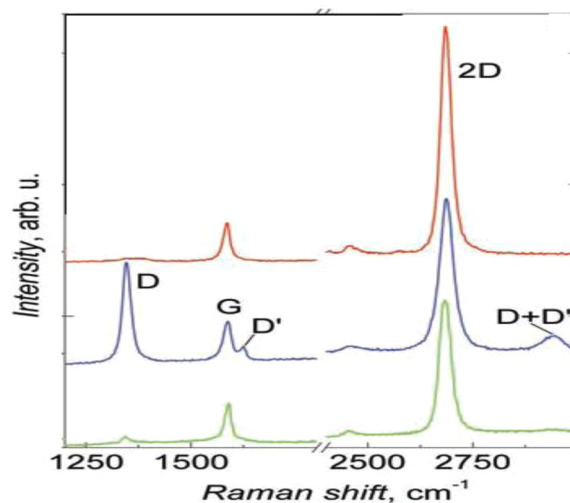


Figure 32. Raman spectra of pristine graphene (red), graphane (blue), and graphane after annealing (green). In the Raman spectrum of graphane the D defect peak becomes active, as well as the appearance of D' and D+D' peaks. Reprinted with permission from ref 42. Copyright 2009 American Association for the Advancement of Science.

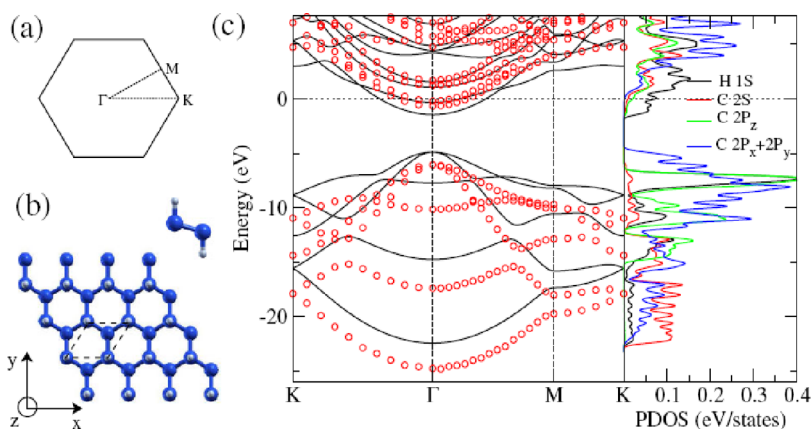


Figure 33. (a) First Brillouin zone and (b) unit cell and bases of graphane in the chair conformation. Blue and white balls represent carbon and hydrogen atoms, respectively. (c) Band structure in local-density approximation (LDA, full line) and GW approximation (circles) and projected density of states of graphane. The zero level indicates the vacuum level position. Reprinted with permission from ref 162. Copyright 2010 American Physical Society.

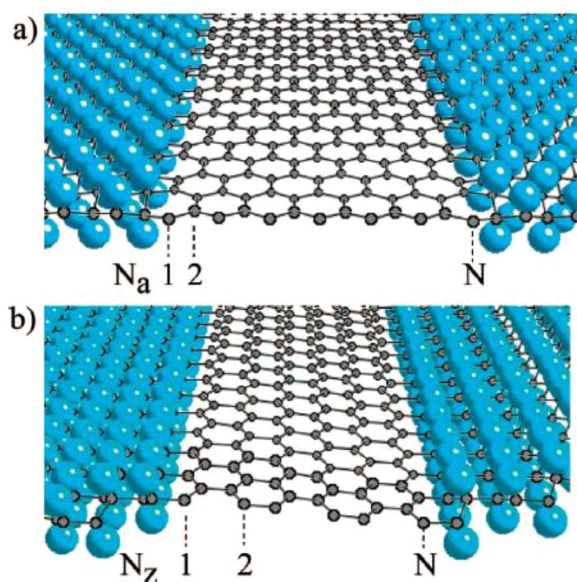


Figure 34. Structures of (a) armchair and (b) zigzag graphene nanoroads in graphane. N_a denotes width of sp^2 carbon lines in armchair and N_z in zigzag roads. Reprinted with permission from ref 167. Copyright 2009 American Chemical Society.

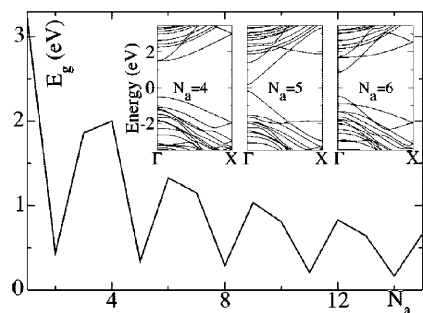


Figure 35. Dependence of band gap (E_g in eV) of armchair nanoroads on nanoroad width (N_a). The insets show band structures of armchair nanoroads of width (N_a) 4, 5, and 6. Reprinted with permission from ref 167. Copyright 2009 American Chemical Society.

states.¹⁶⁷ Thus, the graphene nanoroads behave like graphene ribbons, while the hexagonal patterned vacancies in graphane structure are shown to behave like quantum dots.¹⁶⁸

2.3.2. Fluorographene (Graphene Fluoride). Fluorographene (also known as graphene fluoride) was synthesized by fluorination of graphene using XeF₂ at room temperature (30 °C).¹⁶⁹ Fluorination of CVD grown graphene on a copper support leads to single side fluorination with preferred C₄F stoichiometry, while fluorination of graphene on a silicon-on-insulator support leads to fluorination on both sides of the surface with a dominant C₁F₁ stoichiometry. Due to the presence of defects in the CVD graphene structure (vacancies, free edges, and grain boundaries), a small fraction of C–F₂ (12%) and C–F₃ (2%) besides the majority C–F (86%) bonds were also identified in fluorinated samples using XPS.¹⁶⁹ Single side fluorination leads to the appearance of a D peak at 1350 cm⁻¹ and broadening of the G (1580 cm⁻¹) and D' peaks (1620 cm⁻¹), as well as a decrease in the 2D Raman peaks, while fluorination on both sides of the surface cancels the Raman signal (Figure 36). Graphene fluoride was also prepared from pristine graphite fluoride by mechanical exfoliation,^{170,171} that is, by an analogous approach to that for the preparation of graphene. The chemical exfoliation of graphite fluoride, prepared by fluorination of highly ordered pyrolytic graphite at 600 °C and 1 atm of fluorine, provides graphene fluoride with stoichiometry C_{0.7}F₁.¹⁷² However, high-temperature synthesis leads to highly defective graphene fluoride.¹⁶⁹ Chemical etching of graphite fluoride by sulfolane (at 80 °C) was also successful in producing a colloidal solution of graphene fluoride.¹⁵⁸

Fluorination of graphene dramatically changes its structure and electronic and optical properties (Figure 36). The graphene sp² carbon atoms rehybridize to sp³ carbons in fluorographene, and consequently the fluorographene structure is buckled; C–C and C–F bonds are 1.57–1.59 Å and 1.41–1.45 Å long, respectively. The zero band gap of pristine graphene opens, and fluorographene behaves like an insulator with a resistivity higher than 10¹² Ω.¹⁷¹ An anisotropic negative magnetoresistance and unusual staircaselike magnetic-field dependence at low temperature of diluted fluorographene has been reported recently.¹⁷³ A high third-order nonlinear optical response of fluorographene dispersion has been recently observed.¹⁷⁴ Photoluminescence measurements of a fluorographene dispersion in acetone identify an emission peak at 3.8 eV (Figure 37), which has been assigned to band-to-band recombination of free electrons and holes.¹⁷⁵ Theoretical calculations of the fluorographene band gap by GGA DFT method provides values around 3.1 eV,^{158,176,177} not very different from the value for graphite fluoride.^{178,179} The

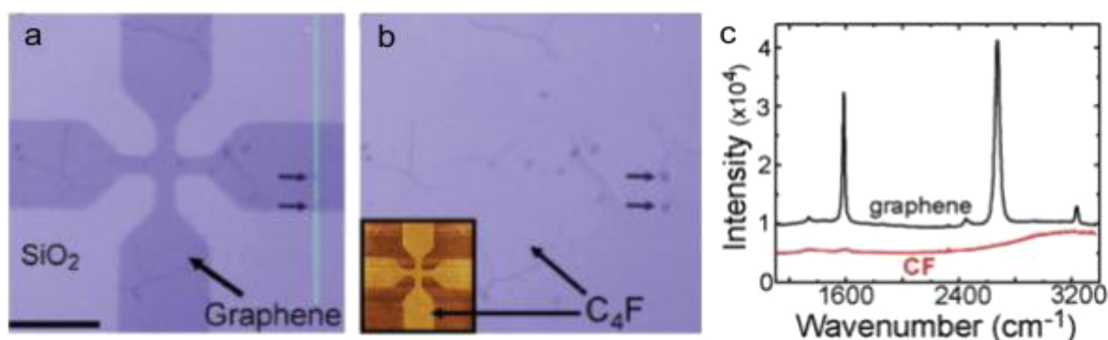


Figure 36. One side fluorination (one side fluorinated graphene C_4F , panel b) changes the optical properties of graphene (panel a). Raman signal of stoichiometric fluorographene (CF, panel c) disappears. The spectra of graphene and fluorographene are offset for clarity. Reprinted with permission from ref 169. Copyright 2010 American Chemical Society.

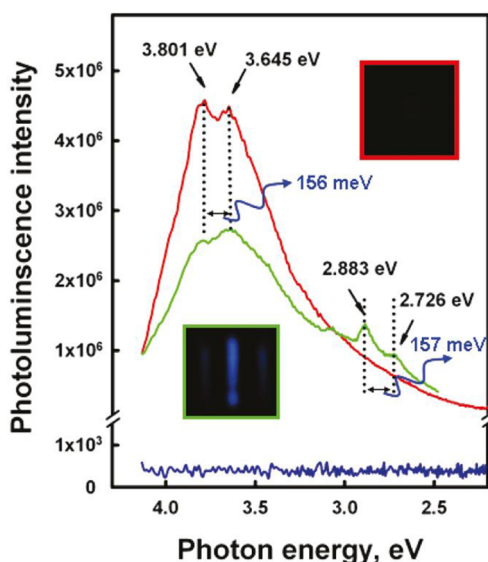


Figure 37. Photoluminescence emission spectra at room temperature (excitation at 290 nm, 4.275 eV) of graphene (blue) and fluorographene (green, 1 day fluorination; red, 5 days). The difference between the main emission peaks is 156 meV (1260 cm^{-1}); this corresponds to the energy of a C–F vibration. The blue emission (at 2.88 eV) lasts ca. 30 s after excitation, and its exact origin is uncertain. Reprinted with permission from ref 175. Copyright 2011 American Chemical Society.

agreement between theoretical and experimental band gap is accidental, because high-level theoretical calculations by GW predict a band gap of 7.5 eV.^{176,177,180} It is worth noting that screened hybrid functional HSE06 calculations^{181,182} provide higher band gap values than GGA DFT. This screened hybrid functional method gives band gap values closer to the GW method for graphane (GGA 3.5 eV, HSE06 4.5 eV, GW 5.4 eV) and for fluorographene (GGA 3.1 eV, HSE06 5.1 eV, GW 7.5 eV). The calculation of the optical spectra by BSE on the top of the GW calculations predicts a spectral onset around 5.4 eV, which is in good agreement with the experimental value (3.8 eV) when taking into account effects of corrugation and defects.¹⁷⁷

Graphene nanoroads and nanodots have also been theoretically analyzed in the fluorographene matrix. Their electronic properties depend on their orientation, structure, and width.¹⁸³ It was shown that fluorographene is rather inert and thermostable (up to 400 °C) like Teflon.¹⁷¹ Thermal defluorination (400–600 °C) leads to the removal of carbons and evolution of C–F products (e.g., CF_4 , C_2F_4 , C_2F_6) from the graphene fluoride structure. On the other hand, defluorination of fluorographene

by hydrazine vapor (under relatively mild thermal conditions 100–200 °C)¹⁶⁹ or the action of KI on a fluorographene colloidal dispersion in sulfolane (at 240 °C) leads to graphene. It was suggested that defluorination by KI proceeds via unstable, spontaneously decomposing graphene iodine. This finding is supported by the transient appearance of C–I vibrations in IR spectra and theoretical DFT calculations, which identify graphene iodine as an unstable compound.¹⁵⁸ Generally the stability of stoichiometric graphene halides (C_1X_1) decreases in the order $F > Cl > Br > I$, and fluorographene (CF) seems to be more stable than graphane (CH).¹⁵⁸ The future preparation of stoichiometric chlorographene (graphene chloride, CCl) is improbable, because the potential pristine material graphite chloride is unstable above 0 °C.¹⁸⁴

Recent photochemical chlorination of graphene produces partially chlorinated graphene of uniform 8% coverage with stoichiometry $C_{16}Cl$. Typically, the partially chlorinated graphene has a nonzero band gap and displays a higher sheet resistance than graphene. Raman spectrum shows the appearance of the D peak (1330 cm^{-1}), while the 2D peak (2654 cm^{-1}) disappears and the G peak (1587 cm^{-1}) broadens.¹⁸⁵ Very recently, preparation of few-layered graphene chlorinated up to 30 at.% and brominated up to 4.8 at.% by UV irradiation in liquid-chlorine medium has been reported.¹⁸⁶ The mixed graphene halides have not been yet prepared and seem to be promising materials with controlled electric properties.

3. NONCOVALENT FUNCTIONALIZATION OF GRAPHENES

Graphite is a natural and inexpensive source for large scale production of graphene sheets. However, the π – π stacking between graphene sheets results in the formation of multilayers. Pristine graphene sheets are hydrophobic in nature, so they cannot be dissolved in polar solvents. This makes functionalization of graphene sheets important for their future applications. To make graphene soluble in common solvents, and thereby avoid stacking, noncovalent functionalization with different organic compounds is essential. Noncovalent functionalization by π -interactions (as in the case of carbon nanotubes) is an attractive synthetic method, because it offers the possibility of attaching functional groups to graphene without disturbing the electronic network.^{187,188}

3.1. Graphene–Ligand Noncovalent Interactions: Theory

Graphene is a π -system. The structure and electronic properties of graphene, as well as the interaction of graphene with atoms and molecules, have been studied extensively. Noncovalent

intermolecular interactions involving π -systems are pivotal to the stabilization of proteins, enzyme–drug complexes, DNA–protein complexes, organic supramolecules, and functional nanomaterials.^{189–193} These interactions involving π systems are most relevant in the context of nanomaterial design and fabrication of nanodevices, because subtle changes in the electronic characteristics of the π systems can lead to dramatic effects in the structure and properties of the nanosystem.^{193–195}

In the last two decades, extensive studies have been conducted to understand the nature of π -complexes including the nonpolar gas– π interaction, H– π interaction, π – π interaction, cation– π interaction, and anion– π interaction.^{196,197} These π -interactions are of importance in device and sensing applications of carbon nanotubes and graphene sheets.¹⁹⁸ Extensive investigations have been made regarding the energetic and geometrical significance of π -interactions. Theoretical interpretations based on high-level *ab initio* calculations have been instrumental in understanding the nature of π -interactions. The strength of the π -interactions is determined by the combined effect of attractive forces (electrostatic, dispersive, and inductive interactions) and repulsive forces (exchange repulsion). Each of these components shows characteristic differences in physical origin, magnitude, and directionality.

3.1.1. Nonpolar Gas– π Interaction. In π -interactions, when the countermolecule is either a rare gas atom or a nonpolar molecule (gas dimers, hydrocarbons), dispersion energies predominate,^{199,200} while when the countermolecule is either a polar molecule or Lewis acid, both electrostatic and dispersion energies govern the interaction.

3.1.2. H– π Interaction. Complexes exhibiting the H– π interaction^{190,201–207} are of interest, because this interaction is also one of hydrogen bonds. In going from CH₄ to NH₃ to H₂O to HF, the increase in the repulsive exchange energies is more pronounced in ethene complexes than in benzene complexes.²⁰¹ However, this increase is almost canceled out by both the electrostatic and dispersion energies in the case of the ethene complexes. Consequently, the induction energies become more important in the case of the ethene complexes. On the other hand, electrostatic, induction, and dispersion energies seem to be significant in the description of the benzene complexes. The polarizabilities of the π -electron systems play a key role in governing the nature and geometry of the H– π interaction. The magnitude of the dispersion energies tends to be proportional to the number of electrons participating in the interaction. In the case of extended π -systems, like those found in poly complexes, involving several hydrogen bonds, the multidentate H– π complexes are additionally stabilized by a substantial contribution from the dispersion energy.

3.1.3. π – π Interaction. The π – π interactions^{197,198,208–213} are one of the most intriguing noncovalent interactions, in the sense that the negatively charged and diffuse electron clouds of the π systems exhibit an attractive interaction. This interaction is predominated by dispersion interactions when both π systems possess very similar electron densities. However, when one of the systems is electron-rich and the other electron-deficient, the resulting complexes are bound by induction interactions as is the case when the negative charge gets transferred from benzene to hexafluorobenzene.^{214–219} The interaction of two benzene rings has been widely investigated both experimentally and theoretically. Experimental estimates of the interaction energy give a value of ~ 2 kcal/mol,²²⁰ which indicates that the attraction is appreciable and this attraction significantly influences the interaction of phenyl rings in solution or other environments,

in addition to other factors such as solvophobic effects. For the benzene dimer the edge-to-face conformer is the most stable but is nearly isoenergetic to the parallel displaced conformation. Due to this the isolated benzene dimer is extremely flexible and could coexist in both forms. On the other hand, when considering the facial or axial substitution effect on the edge-to-face aromatic interaction, we observe that for the axially substituted aromatic systems, the electron density at the para position is an important stabilizing factor. Thus, the stabilization/destabilization by substitution of an aromatic ring is significantly affected by the electrostatic energy,²¹³ while the dispersion energy is mostly canceled out by the exchange repulsion. This leads to the conclusion that stabilization/destabilization by substitution is governed mainly by electrostatic energies. However, the facially substituted aromatic system depends not only on the electron-donating ability responsible for the electrostatic energy but also on the dispersion interaction and exchange repulsion. The dispersion energy, together with the exchange repulsion, augments the electrostatic energy in the facially substituted aromatic systems. Using the flipping/flapping motion due to the changes of edge-to-face and face-to-face aromatic interactions, Kim et al.²¹⁶ designed a molecular flipper. In order to have maximum control of this interconversion, electrochemically and photochemically active π systems can be utilized. The π – π interaction is one of the most important driving forces for supramolecular self-assembly; thus by controlling the relationships of several noncovalent interactions, we could design and synthesize novel organic nanostructures.²¹⁷ While both T-shaped and stacked structures of the benzene dimer are almost isoenergetic, (displaced) π -stacked structures tend to be more favored when they involve N-heterocyclic aromatic rings except for the tetraazine dimer.^{218,219}

3.1.4. Cation– π Interaction. When the countermolecule is a metal cation in the π -interactions, a combination of electrostatic and induction energies dominate the cation– π interaction.^{220,221} For the interaction of a positively charged organic cation with the negatively charged π electron cloud, an accurate estimate of the interaction energies requires the inclusion of the polarizability of the π system.^{222,223} The characteristics of transition metal complexes with π complexes are different from the typical cation– π interactions involving alkali metal cations. While the complexes of Na⁺, Cu⁺, and Ag⁺ favor the conformation of C_{6v} symmetry with the cation above the π centroid, those of Au⁺, Pd²⁺, Pt²⁺, and Hg²⁺ prefer the off-centered π coordination to the π centroid because of the TMⁿ⁺ \leftarrow π donation.^{224–229} Various kinds of receptors with strong binding energies and high selectivities for metal cations utilizing the cation– π interactions have been designed.^{226–228} When the cation–water interactions are compared with cation– π interactions, it is found that the distinct difference between them is the magnitude of the electrostatic energy, which is in general the dominant contributor to the total interaction energy in the case of the cation–water interactions. In the context of nanomaterial design, these findings are significant because a greater electrostatic contribution implies that the magnitudes of the interaction energies are more susceptible to the dielectric of the environment. Very similar interaction energies of benzene with ammonium and potassium cations result from a balance of dispersion and induction energies because the electrostatic and exchange energies are very similar and hence mostly cancel out. However, the ammonium cation complexes exhibit a larger contribution of dispersion energies.

3.1.5. π_{cation} – π Interaction. It should be noted foremost that the magnitudes of the electrostatic and induction energies in

the case of the organic cation complexes of these π systems are much smaller than those observed in the case of the π -alkali metal cation complexes, while the contribution of dispersion energies becomes significant. If the counterion is an aromatic cation, the contribution of dispersion energy becomes vital. The $\pi_{\text{cation}}-\pi$ interaction^{229–231} is different from the normal metal cation- π interaction and normal $\pi-\pi$ interaction in terms of binding energies. In terms of total binding energy, the $\pi_{\text{cation}}-\pi$ interaction is weaker than the cation- π interaction but much stronger than the $\pi-\pi$ interaction. On the other hand, for anion templated $\pi^+-\pi^+$ interactions,²³² the binding energies are much larger than those of $\pi-\pi$ and $\pi^+-\pi$. The stabilization is attributed to the attractive electrostatic interaction due to antiparallel displaced geometry with a significant dispersion contribution. In general, when the $\pi^+-\pi^+$ stacking is in an energetically favored configuration the electrostatic interaction is large, similar in magnitude to the large exchange repulsion and much larger than the dispersion interaction, unlike the case of stacked-displaced $\pi^+-\pi$ and $\pi-\pi$ complexes.

3.1.6. Anion- π Interaction. Compared with $\pi-\pi$, cation- π , and H- π interactions, the lone pair- π and anion- π interactions^{233–235} have only recently been investigated, because aromatic rings are considered as electron sources, which give repulsive interactions with anions. Recently, anion- π interactions have been extensively investigated as a strategy toward a new type of anion recognition, host architecture, and supramolecular self-assembly.^{192,236,237} The total interaction energies of anion- π complexes are comparable to those of the corresponding cation- π complexes. While the largest contributions to the total interaction energy in the cation- π complexes are the electrostatic and induction energies, the contribution of the dispersion energies is substantial in the anion- π complexes. Apart from the increase in dispersion energy, the anion- π interactions are also characterized by a substantial increase in the magnitude of the exchange-repulsion energy. Anions can interact with the π rings in two different complexation forms: covalent bonding type and noncovalent anion- π type. The covalent type complexes generally referred to as “Meisenheimer” complexes are found to be the key intermediates in nucleophilic aromatic substitution (S_NAr) and usually the global minima structures in the gas phase. However, in the solution phase, the covalent bonding type complexes merge into the solvent-mediated anion- π type or displaced anion- π type complexes. It is this reason that the displaced anion- π type complexes with some flexible orientations are most common in many crystal structures.²³⁸

3.1.7. Graphene-Ligand Noncovalent Interaction. Various studies involving molecules adsorbed on a graphene or graphite surface have been conducted. Hydrogen physisorption on the graphene surface has been studied for possible applications toward hydrogen storage.²³⁹ Tkatchenko and von Lilienfeld²⁴⁰ have studied the adsorption of Ar on graphite by comparing various density functionals. Umadevi and Sastry²⁴¹ also employed DFT methods to study CO_2 , H_2O , Li, Mg, Li^+ , and Mg^{2+} on polycyclic aromatic hydrocarbons. $\pi-\pi$ stacking interactions are of a special interest due to the extended π orbitals of graphene. Adsorption of benzene and naphthalene on graphite was studied by using the nonlocal vdW-DF method to compute accurate binding energy curves.^{242,243} The vdW-DF method was also shown to provide binding energies for Ag, Au, and Pd atoms adsorbed on graphene surface in good agreement with the reference CCSD(T) method.²⁴⁴ Functional groups attached to an aromatic molecule are shown to affect the nature and

magnitude of interactions between the molecule and graphene.²⁴⁵ Nucleobases receive special attention due to a biological importance of those molecules. Adsorption of adenine on graphite was studied by using DFT taking into account van der Waals interactions.²⁴⁶ A similar study compared the binding energies of nucleobases by using LDA and MP2.²⁴⁷ Umadevi and Sastry²⁴⁸ employed newly developed density functionals to deal with similar systems, while Antony and Grimme²⁴⁹ reported DFT-D/GGA, B2PLYP-D, and SCS-MP2 results for these systems. Berland et al.²⁵⁰ used the vdW-DF method to accurately calculate the binding energy curve for an adenine molecule approaching graphene surface. The interaction of several amino acids with the graphene surface has been studied using GGA and MP2 methods.²⁵¹ The planar nature of graphene can be exploited to tune its electric properties. The benzene-metal ($M = Ni, K, Pd, Al, Ag, Cu, Au,$ and Pt) and graphene-metal interface has been studied.^{244,252–255} It has been shown that a SiC substrate is able to induce a band gap in graphene.^{256,257} Organic molecules can also be used to achieve electronic tuning of graphene,²⁵⁸ in this sense the interactions of diverse molecules with graphene and carbon nanotubes have been utilized in designing devices and sensors that recognize molecular characteristics.^{259–263} The interaction of nucleobases with graphene has been utilized to design a two-dimensional conductance device toward fast DNA sequencing.^{37,264,265}

3.2. Graphene-Ligand Noncovalent Interactions: Experiment

The noncovalent functionalization of graphene (G) exploits van der Waals and ionic interactions between graphene and a functionalized molecule. The pyrene moiety has been reported to have a strong affinity toward the basal plane of graphite via π -stacking.²⁶⁶ Xu et al.²⁶⁷ prepared stable aqueous dispersions of graphene nanoplatelets using a water-soluble pyrene derivative, 1-pyrenebutyrate (PB^-), as a stabilizer. GO was functionalized with pyrenebutyric acid in the presence of a base, and the resulting product was reduced with hydrazine. Figure 38 shows

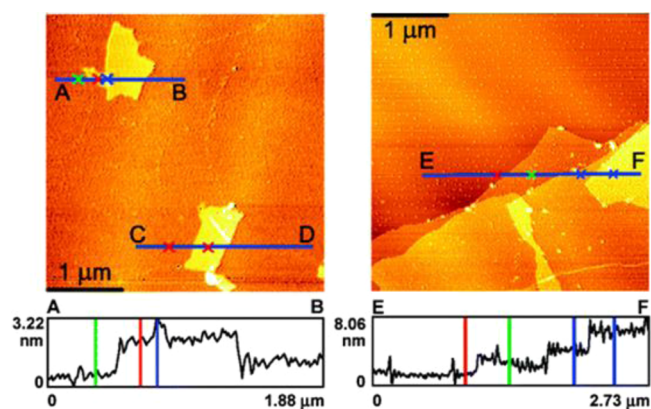


Figure 38. (left) Tapping mode AFM images of exfoliated GO and (right) PB^- functionalized graphene on mica. Reprinted with permission from ref 267. Copyright 2008 American Chemical Society.

AFM images of GO and PB^- graphene nanoplatelets with thickness 1.3 and 1.7 nm, respectively. The flexible graphene film showed conductivity 7 orders of magnitude larger than that of the GO precursor.

Graphene is much more flexible and less expensive than ITO since its precursor is hydrocarbon gas/graphite. To improve the power conversion efficiency of graphene, Wang et al.²⁶⁸

noncovalently modified a graphene film with pyrene butanoic acid succinimidyl ester (PBSA). The π - π interactions between graphene and PBSA have a negligible effect on the optical adsorption of the graphene film in the visible region. This improved the power conversion efficiency to 1.71% for functionalized graphene compared with pristine graphene (0.21%) (Figure 39).

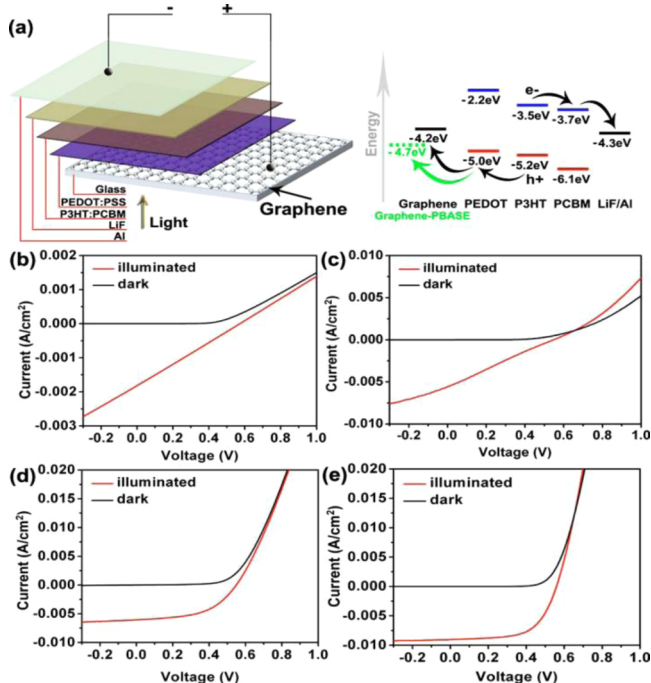


Figure 39. (a) Energy diagram of the fabricated device structure graphene/PEDOT:PSS/P3HT:PCBM/LiF/Al. (b–e) Current–voltage characteristics of the photovoltaic devices based on graphene films in the dark and under illumination: (b) pristine graphene film, (c) graphene film treated by UV light, (d) graphene film modified by PBSA, and (e) ITO anode for comparison. Reprinted with permission from ref 268. Copyright 2009 American Institute of Physics.

An et al.²⁶⁹ presented the functionalization of graphene films with 1-pyrenecarboxylic acid (PCA), which were laminated onto flexible and transparent polydimethylsiloxane (PDMS) membranes. The noncovalent (π -stacked) PCA graphene films display a number of unique optical and molecular sensing properties that are absent in pristine graphene films, while the conducting nature of graphene is maintained. The flexible PCA–graphene–PDMS hybrid structure blocks 70–95% of ultraviolet (UV) light, while allowing 65% or higher transmittance in the visible region, rendering them potentially useful for a number of flexible UV absorbing/filtering applications. In addition, the electrical resistance of these structures is found to be sensitive to visible light illumination, atmospheric pressure change, and the presence of different types of molecular analytes. Owing to their multifunctionality, these hybrid structures have immense potential in the development of versatile, low-cost, flexible, portable electronic and optoelectronic devices for diverse applications.

Stable aqueous suspensions of graphene nanoplatelets with a high concentration (0.6–2 mg/mL) have been prepared by the chemical reduction of exfoliated graphite oxide (EGO) using sodium lignosulfonate (SLS), sodium carboxymethyl cellulose (SCMC), and pyrene-containing hydroxypropyl cellulose

(HPC-Py).²⁷⁰ The functionalized graphene nanoplatelets with a 3.3 ± 1.4 nm average thickness were characterized using UV–vis spectroscopy, fluorescence spectroscopy, atomic force microscopy, attenuated total reflectance micro-Fourier transform infrared spectroscopy, and Raman spectroscopy.

Kodali et al.²⁷¹ have shown that noncovalently functionalized epitaxial graphene with pyrenebutanoic acid-succinimidyl ester (PYR-NHS) can be prepared without disrupting graphene’s electronic structure. The grafting of pyrene-substituted TbPc2 single molecule magnets on graphene has been reported by Lopes et al.²⁷² The enhanced Raman intensity of TbPc2 on graphene allows the detection of a few molecules per laser spot. van der Waals interactions were responsible for the coupling between the substituted pyrene and graphene.

Su et al.⁹¹ presented a unique approach to functionalize graphene sheets with pyrene and perylenediimide as electronic donor and acceptor molecules, respectively. The resulting aqueous graphene dispersion yields single and double layer graphene sheets. A solar cell based on these functionalized graphene nanoplatelets showed an increase in conductivity (Figure 40).

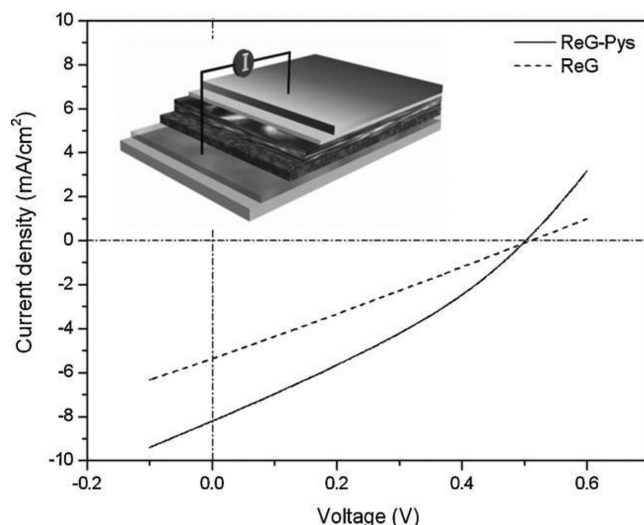


Figure 40. Current density vs voltage (I – V) curves of P3HT/PCBM heterojunction solar cells with 10 nm thick thermally reduced ReG and ReG–PyS films as the transparent electrodes, respectively. Inset is a schematic illustration of the solar cell; the five layers from top to bottom are Al, ZnO, a blend of P3HT and PCMB, PEDOT:PSS, graphene, and quartz, respectively. Reprinted with permission from ref 91. Copyright 2009 Wiley.

It has been shown by Cheng et al.²⁷³ that graphene can be functionalized with 1,5-diaminonaphthalene (DAN) and 1-nitropyrene (NP) as electron-donating and electron-withdrawing molecules, respectively. The chemically modified samples were systematically characterized by optical microscopy, surface topography and potential measurements, and spatially resolved Raman spectroscopic imaging.

Wang et al.²⁷⁴ reported the noncovalent functionalization of graphene with carboxylate-terminated perylene molecules. These functionalized graphene nanoplatelets were used to grow metal oxide via ALD methods (Figure 41). The ultrathin high dielectric integrated graphene is very useful to achieve high currents and ideal subthreshold swing without substantial gate leakage.

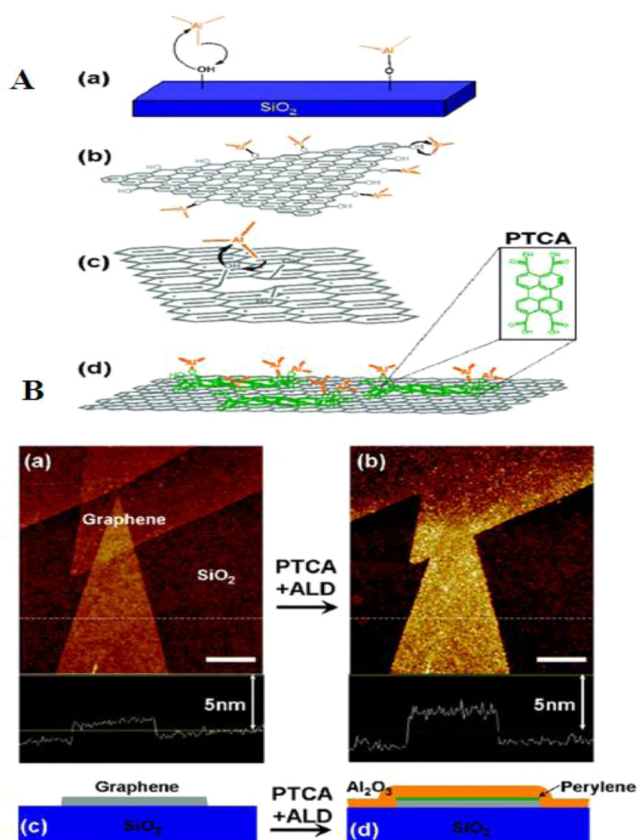


Figure 41. (A) Schematics of atomic layer deposition of aluminum oxide via trimethylaluminum (TMA) precursor on (a) bare SiO₂ substrate, (b) a single layer graphene sheet with edges, (c) graphene containing a defect site, and (d) perylene tetracarboxylic acid (PTCA)-coated graphene. PTCA selectively adheres to graphene on SiO₂ surfaces, providing binding sites for TMA deposition. Inset is a top view of the PTCA structure. (B) ALD of Al₂O₃ on PTCA-coated graphene. (a) AFM image of graphene on SiO₂ before ALD. The height of the triangular shaped graphene is ~1.6 nm as shown in the height profile along the dashed line. Scale bar is 500 nm. (b) AFM image of the same area as panel a after ~2 nm Al₂O₃ ALD deposition. The height of the triangular shaped graphene becomes 3.0 nm as shown in the height profile along the dashed line. Scale bar is 500 nm. (c,d) Schematics of graphene on SiO₂ before and after ALD. The Al₂O₃ grows uniformly on the noncovalently PTCA-coated graphene. Reprinted with permission from ref 274. Copyright 2008 American Chemical Society.

In subsequent work, Wang and Hersam³⁸ reported the room-temperature molecular resolution of a self-assembled perylene-3,4,9,10-tetracarboxylic dianhydride (PTCDA) monolayer on epitaxial graphene using STM. The PTCDA molecular structure is shown in Figure 42a. PTCDA is a planar molecule based on a perylene backbone with a conjugated π -electron system and carboxylic acid anhydride side groups. After gas-phase deposition in ultrahigh vacuum (UHV), the resultant monolayer of PTCDA on graphene is observed at room-temperature using STM (Figure 42b). The molecule forms a well-ordered, self-assembled monolayer with large domains that span hundreds of nanometers. At higher resolution, the herringbone pattern formed by the molecules in the PTCDA monolayer is visible (Figure 42c). This structure closely resembles the (102) plane of the PTCDA bulk crystal structure. Molecular structure diagrams are drawn over the STM image in Figure 42c to indicate the locations of molecules in the monolayer, and the outline of one unit cell is shown with the lattice vectors (**a** and **b**) specified. A larger

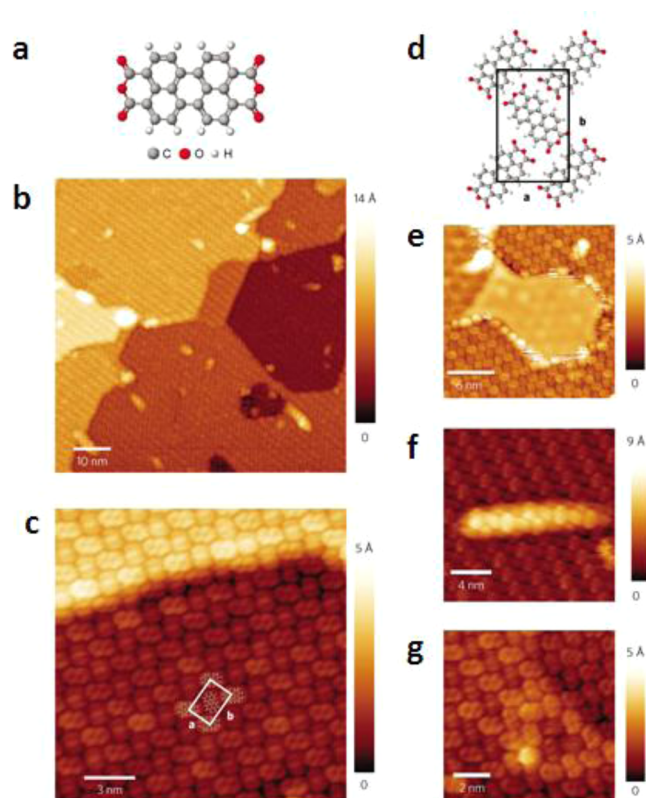


Figure 42. (a) Molecular structure of PTCDA. (b) Monolayer coverage of PTCDA on epitaxial graphene. (c) Molecular-resolution STM image of the PTCDA monolayer. (d) PTCDA herringbone unit cell, with the lattice vectors (**a** and **b**). (e) PTCDA surrounding a step edge where the graphene sheet is not continuous. (f) PTCDA continuously covers a graphene-subsurface nanotube defect. (g) A bright protrusion that does not disrupt the PTCDA monolayer and that is potentially attributed to a 6-fold scattering-center defect ($V_s = -2.0$ V, $I = 0.05$ nA for all five STM images). Reprinted with permission from ref 38. Copyright 2009 Nature Publishing Group.

schematic of the monolayer unit cell is shown in Figure 42d. Interactions of the PTCDA monolayer with various types of epitaxial graphene defects are shown in Figure 42c,e-g. These results demonstrate that organic functionalization of epitaxial graphene possesses wide tolerance and can be readily achieved at room temperature using surface chemistry analogous to that on bulk graphite. This well-ordered, stable, robust, nearly defect-free monolayer presents opportunities to explore self-assembly chemistry on graphene. It allows chemical functionality tailoring of graphene, as well as template growth and deposition of other materials, as a potential route toward realizing graphene-based molecular electronic and sensing devices.

Noncovalent functionalization of graphene nanoplatelets with single-stranded DNA (ssDNA) was obtained by chemical oxidation of graphite to GO, followed by hydrazine reduction in the presence of ssDNA.⁹² This composite material is soluble in water with concentrations as high as 2.5 mg/L.

In subsequent work, Liu et al.²⁷⁵ reported the deposition of gold nanoparticles on DNA-functionalized graphene nanoplatelets. First thiolated DNA oligonucleotides were allowed to adsorb on GO nanoplatelets (Figure 43), with the resulting DNA-coated GO reduced by hydrazine to DNA-RGO. Gold nanoparticles were then added to aqueous solutions of DNA-RGO and DNA-GO to form the related composites. These gold-decorated DNA-functionalized graphene nanoplatelets

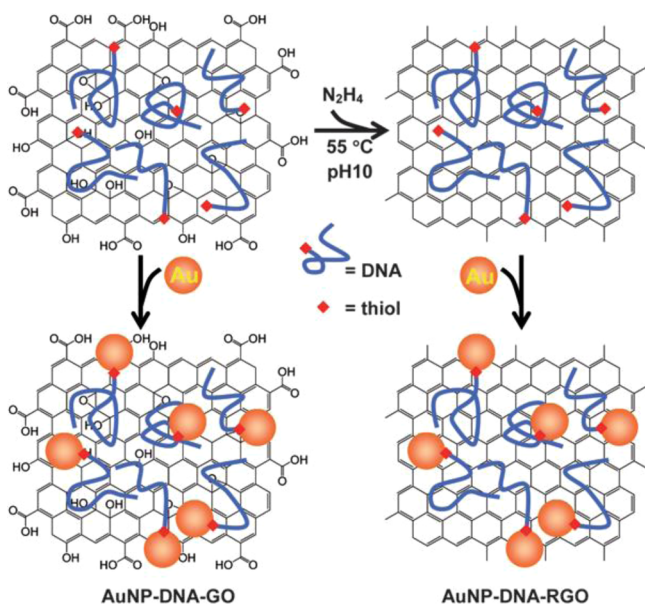


Figure 43. DNA coating and aqueous dispersion of GO and RGO, which were then used as two-dimensional bio–nano-interfaces for homogeneous assembly of metal–carbon heteronanostructures. Reprinted with permission from ref 275. Copyright 2010 Royal Society Chemistry.

have potential application in catalysis, magnetism, battery materials, optoelectronics, field effect devices, and biodetection platforms.

Xu et al.²⁷⁶ developed a novel and facile 3D self-assembly method to prepare GO/DNA composite hydrogels with high mechanical strength, excellent environmental stability, high dye-adsorption capacity, and self-healing function. The multifunctionality of the self-assembled hydrogel can be attributed to the unique structures, properties, and self-assembly behavior of the GO and DNA building blocks.

Methyl green is a water-soluble molecule with a positive charge, so it can be adsorbed on the surface of CRG through π – π stacking, thus weakening the strong van der Waals interactions between CRG nanoplatelets obtained when GO is reduced by

hydrazine. The adsorption of MG onto CRG not only greatly improves the dispersity of CRG in water but also enhances the electrocatalytic activity of the CRG–MG nanocomposite toward the oxidation of nicotinamide adenine dinucleotide (NADH).

Tu and co-workers²⁷⁷ noncovalently functionalized graphene nanoplatelets with water-soluble picket-fence iron porphyrin. An ITO electrode modified with the porphyrin-functionalized graphene showed excellent detection of chlorite. Geng and Jung²⁷⁸ have synthesized porphyrin-functionalized chemically converted graphene (CCG) nanoplatelets by hydrazine reduction of GO with water-soluble porphyrins. The resulting porphyrin-functionalized CCG nanoplatelets have been employed in the preparation of CCG films that have a low sheet resistance of ca. $5 \text{ K}\Omega\cdot\text{sq}^{-1}$ with 80% transparency at 550 nm. The functionalization of graphene nanoribbons with water-soluble iron(III) meso-tetrakis(*N*-methylpyridinium-4-yl) porphyrin (FeTMPyP) via π – π noncovalent interactions on an electrode surface has been demonstrated by Zhang et al.²⁷⁹ The resulting FeTMPyP/RGNRs composite film showed excellent electrocatalysis toward the reduction of dissolved oxygen, and it was subsequently used as a biosensor for the detection of glucose in human serum.

Noncovalent functionalization of graphene nanoplatelets by sulfonated polyaniline (SPANI) to produce a water-soluble composite has been reported by Bai et al.²⁸⁰ A dispersion of the composite was stable even after storage for two weeks; additionally it displayed stability at pH 1–2 due to strong π – π stacking between the backbones of SPANI and the graphene basal planes, as well as the electrostatic repulsion between the resulting negatively charged SPANI/r-G nanoplatelets.

In subsequent work, graphene functionalized with polyaniline was used as a high-performance flexible electrode.²⁸¹ The functionalized material offers enhanced electron transfer from graphene to the polyaniline film and acts as a tensile backbone to maintain a desirable mechanical flexibility. The gravimetric and volumetric capacitances of the GPCP-900s reach 233 F g^{-1} and 135 F cm^{-3} , respectively, much larger than those of graphene–paper (147 F g^{-1} and 64 F cm^{-3}) and many other currently available carbon-based flexible electrodes.

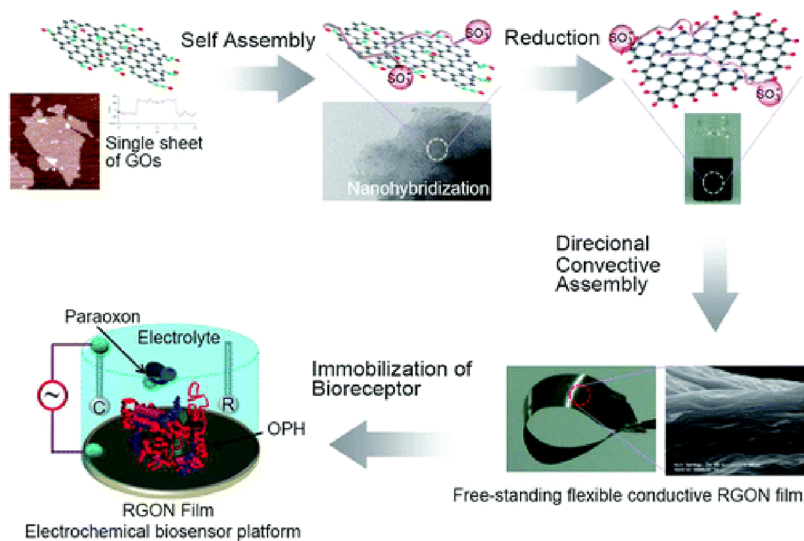


Figure 44. Illustration of a procedure to design RGON hybrids and the RGON platform used as an electrochemical biosensor. Reprinted with permission from ref 283. Copyright 2010 American Chemical Society.

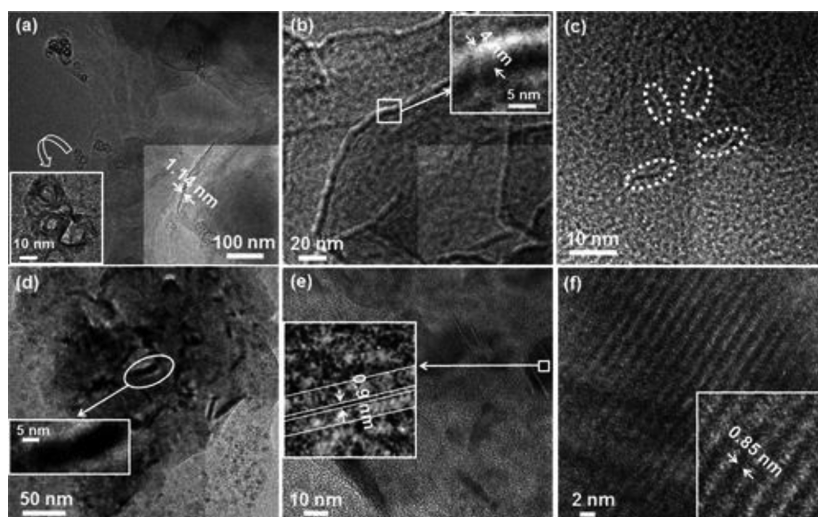


Figure 45. HRTEM micrographs of (a) neat ILFG showing the crumpled sheet like texture (inset on right-hand side shows the thickness of the nanosheet), (b) neat RGO with the inset showing a blown up view of a fold on the nanoplatelet, (c) the PEDOT–RGO nanocomposite; the ellipses encircle the streak like structures typical of RGO and are surrounded by the amorphous polymer, (d) PEDOT–ILFG nanocomposite, the elongated shapes (as in the inset) are characteristic of ILFG, (e) coexisting crystalline and amorphous phases in PEDOT–ILFG (inset is a magnified view of a quasi-ordered arrangement of lattice fringes), and (f) a relatively defect free crystallite of ILFG in PEDOT–ILFG (the inset shows the fringe separation of 0.85 nm). Reprinted with permission from ref 287. Copyright 2011 American Chemical Society.

Wu et al.²⁸² employed a one-step method for the preparation of polystyrene (PS)-functionalized graphene nanoplatelets. The graphene is homogeneously dispersed in the PS matrix, thereby creating electrically conductive graphene/PS nanocomposites. The synthesis of the composite was achieved via in situ peeling of graphite nanoplatelets into graphene nanoplatelets in the presence of a PS solution. The resulting PS-functionalized graphene nanoplatelets displayed a fluffy nanostructure. The backbones of PS were stacked onto the basal plane of graphene nanoplatelets by strong π – π interactions with a graft ratio up to 85 wt. %. The PS chains effectively prevent the graphene nanoplatelets from aggregating and the prepared graphene/PS nanocomposites, with homogeneously dispersed single- and few-layer graphene, exhibited extraordinary electrical properties and a percolation threshold of about 2.7 wt. %, which outperforms that of the starting graphite or carbon black material.

Functionalization of graphene through self-assembly of a hydrophobic backbone of Nafion has been reported by Choi et al.²⁸³ (Figure 44). The resulting graphene nanoplatelets were readily dispersible and displayed high conductivity and electrochemical biosensing properties for organophosphates. Ansari et al.²⁸⁴ reported that a Nafion/graphene nanocomposite can be produced by dispersion of Nafion in a GO aqueous solution and subsequent reduction with hydrazine. In their report, they showed that the presence of Nafion nanochannels dramatically increases the conductivity of graphene.

The widely soluble graphene nanoplatelet/congo red (GSCR) composite was synthesized by noncovalent interaction coupling.²⁸⁵ The resulting graphene nanoplatelets were completely dispersed in DMF, methanol, DMSO, ethanol, and water and partially dispersed in many other organic solvents. The mechanism of GSCR's good solubility was successfully explained by Hansen solubility parameters. These functionalized nanoplatelets were used to prepare GSCR/Au hybrid materials through electrostatic interactions. UV–vis absorption, Fourier transform infrared, Raman, and X-ray photoelectron spectra revealed that congo red (CR) is successfully coupled to the graphene nanoplatelets.

Liu et al.²⁸⁶ functionalized graphene with a water-soluble aromatic electroactive dye, methylene green (MG), during the chemical reduction of GO with hydrazine. Atomic force microscopy and UV–vis spectrophotometric results demonstrate that CRG functionalized with MG (CRG–MG) is well-dispersed in water through coulomb repulsion between MG-adsorbed CRG nanoplatelets. The electrochemical properties of the CRG–MG composite were investigated, and the results demonstrate that CRG–MG confined onto a glassy carbon electrode has lower charge-transfer resistance and better electrocatalytic activity toward the oxidation of NADH than pristine CRG. This method not only offers a facile approach to dispersing graphene in water but also is envisaged to be useful for graphene-based electrochemistry investigations.

Nanocomposite assemblies of poly(3,4-ethylenedioxythiophene) (PEDOT), embedded with (a) fluoro alkyl phosphate based ionic liquid functionalized graphene (ILFG) and (b) RGO prepared from a modified Hummers' method, have been synthesized (Figure 45).²⁸⁷ Defect-free graphene nanoplatelets within the size of a few nanometers were achieved in the PEDOT–ILFG nanocomposite. In contrast, structures comprising GO wrinkles interspersed with the amorphous polymer were obtained in the PEDOT–RGO nanocomposite. X-ray photoelectron spectroscopy showed that ILFG was considerably less oxidized compared with the pure RGO, which ratified the superiority of the ionic liquid functionalization strategy over the conventional chemical approach for exfoliating graphite. Substantially higher electrochemical activity, improved ionic/electronic conductivity, much faster switching rates, and an almost ballistic enhancement in the electrochromic coloration efficiency were attained for the PEDOT–ILFG nanocomposite in comparison to the PEDOT–RGO film. This demonstrated the ability of the ionic liquid to not only fortify the structure of graphene but also facilitate charge transport through the bulk of the film, by providing less impeded pathways. Since PEDOT–ILFG/–RGO nanocomposites of good uniformity achieved this, to some extent, the challenges associated with the processing of

graphene-based high performance materials for practical applications have been overcome.

The site-dependent and spontaneous functionalization of 4-bromobenzene diazonium tetrafluoroborate (4-BBDT) and its doping effect on mechanically exfoliated graphene (MEG) has been investigated by Lim et al. (Figure 46).²⁸⁸ The spatially

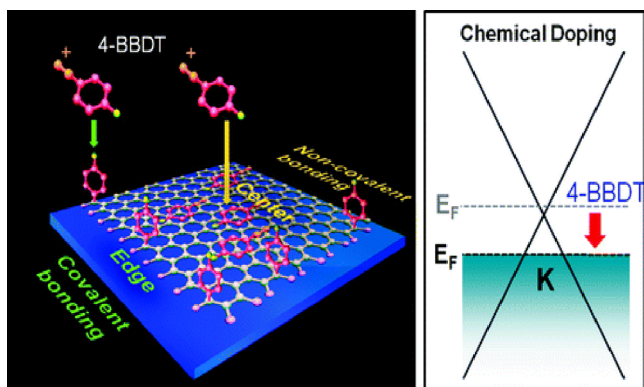


Figure 46. Noncovalent functionalization occurs on the basal plane of defect-free graphene, as opposed to covalent bonding formed on the edge of the graphene. Doping induces modulation of the Fermi level of graphene. Reprinted with permission from ref 288. Copyright 2010 American Chemical Society.

resolved Raman spectra obtained from both edge and basal regions of MEG revealed that 4-BBDT molecules were noncovalently functionalized on the basal region of MEG, while they were covalently bonded to the edge of MEG. The chemical doping effect induced by noncovalently functionalized 4-BBDT molecules on the basal plane region of MEG was explained by using Raman spectroscopy. The position of the Fermi level of MEG and the type of doping charge carrier induced by the noncovalently adsorbed 4-BBDT molecules were determined from systematic G band and 2D band changes.

Noncovalent functionalization of RGO with chitosan by chemical reduction of GO has been demonstrated by Fang et al.²⁸⁹ The graphene captures the amino and hydroxyl groups of chitosan via zwitterionic interactions and hydrogen bonding, resulting in dispersibility of the composite in water. The graphene suspension is highly biocompatible, which makes the system highly desirable for potential biological and medicinal applications. Jo et al.²⁹⁰ prepared RGO nanoplatelets via noncovalent functionalization with a conducting polymer dispersant, PEDOT:PSS. The resulting RGO/PEDOT suspension retains a fairly good colloidal stability in aqueous medium. A large-scale flexible thin film of RGO/PEDOT hybrid material can be prepared by filtration, followed by transfer onto a receiving substrate, such as a flexible PET or a quartz slide. The hybrid RGO/PEDOT film exhibits high conductivity with a controllable transmittance, leading to its potential application as a large scale transparent conducting thin film.

Ghosh and co-workers²⁹¹ demonstrated a simple and efficient methodology to make stable aqueous solutions of single- and few-layer graphenes by exploiting noncovalent interactions with a coronene carboxylate acceptor molecule (Figure 47). Optical and Raman spectroscopy unambiguously shows the strong molecular charge-transfer interactions with the graphene. The fluorescent sheets of the composite with strongly bound electron-deficient fluorescent coronene molecules could be of use in nanoelectronics.

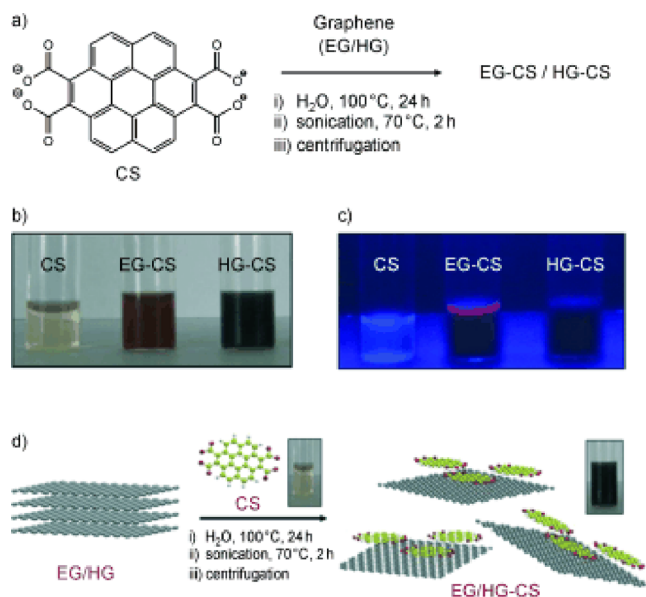


Figure 47. (a) Synthetic scheme for the preparation of graphene–coronene composites. (b) Photographs of the aqueous solutions of CS, EG–CS, and HG–CS and (c) corresponding images under UV/vis illumination. (d) Schematic illustration of the exfoliation of few-layer graphene with CS to yield monolayer graphene–CS composites. Reprinted with permission from ref 291. Copyright 2010 Wiley.

Chen et al.²⁹² presented a noncovalent functionalization of graphene at low temperature in aqueous solution with thionine, which results in the formation of a stable aqueous solution of single- and double-layer graphene nanoplatelets. Optical spectroscopy clearly verified the presence of π – π interactions between the graphene and thionine. The conductivity of the functionalized hybrid material was around 7 orders of magnitude larger than that observed for GO.

Graphene modified with poly(*N*-isopropylacrylamide) [PNI-PAAm] via π – π stacking interactions was successfully prepared by Liu et al.,²⁹³ with aqueous suspensions of this nanocomposite being very stable below 24 °C. This π – π stacking attachment methodology can be used with any polymer and should allow retention of the electrical properties of graphene.

By taking advantage of the solubility in water of the poly(2,5-bis(3-sulfonatopropoxy)-1,4-ethynyl-phenylene-*alt*-1,4-ethynyl-phenylene) sodium salt (PPE-SO₃[−]) and the π stacking interaction between PPE-SO₃[−] and graphene nanoplatelets, Yang et al.²⁹⁴ reported a facile method of processing graphene through noncovalent functionalization to obtain highly conductive graphene-based materials that are stable for long periods of time. The successful attachment of PPE-SO₃[−] onto graphene not only stabilizes the graphene dispersion in water but also endows the resulting graphene with negative charges, which makes further functionalization of graphene feasible. Moreover, PPE-SO₃[−] molecules exhibit interesting optoelectronic properties, and the resulting graphene nanoplatelets functionalized with PPE-SO₃[−] should realize a variety of optoelectronic device applications utilizing graphene.

Li et al.⁵⁹ developed a simple chemical method to produce graphene nanoribbons by graphite exfoliation. The exfoliated graphite was dispersed in a 1,2-dichloroethane (DCE) solution of poly(*m*-phenylenevinylene-*co*-2,5-dioctoxy-*p*-phenylenevinylene) (PmPV) by sonication for 30 min to give a homogeneous suspension. Centrifugation removed large pieces of materials

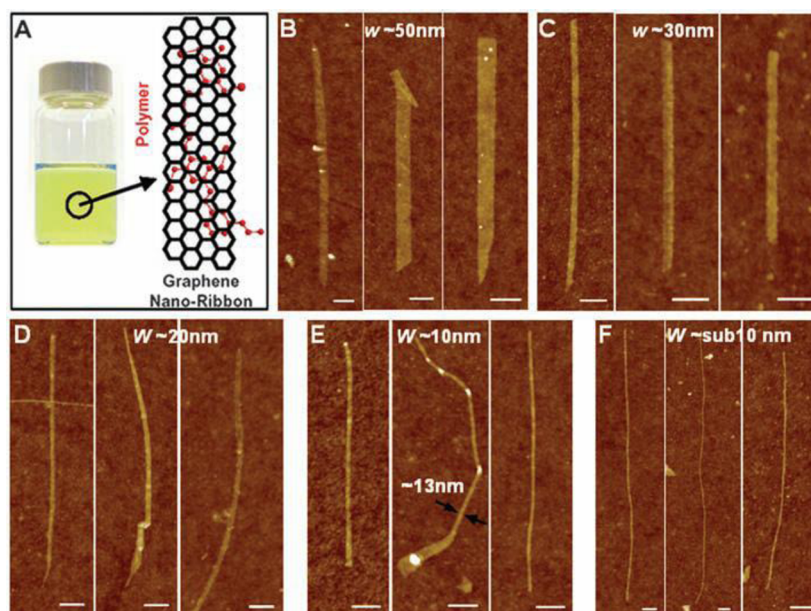


Figure 48. (A) (left) Photograph of a polymer PmPV/DCE solution with GNRs stably suspended in the solution and (right) schematic drawing of a graphene nanoribbon with two units of a PmPV polymer chain adsorbed on top of the graphene via π stacking. (B–F) Chemically derived graphene nanoribbons down to sub-10-nm width. Reprinted with permission from ref 59. Copyright 2008 American Association for the Advancement of Science.

from the supernatant (Figure 48). The obtained graphene nanoribbons (GNR) have widths below 10 nm, as well as single ribbons with varying widths along their lengths. The GNRs exhibited ultrasmooth edges with well-defined zigzag or armchair edge structures. Electrical transport experiments showed that, unlike single-walled carbon nanotubes, all of the sub-10-nm GNRs produced were semiconductors, affording graphene field effect transistors with on–off ratios of about 10^7 at room temperature.

A simple wet-chemical strategy for synthesizing hemin–graphene hybrid nanoplatelets (H-GNs) through π – π interactions has been reported by Guo et al.²⁹⁵ This new nanomaterial exhibits high solubility and stability in water. Using this composite, the authors were able to differentiate between ss- and double-stranded (ds-) DNA in optimum ion concentrations due to the different affinities of ss- and ds-DNA toward graphene. With this information, a novel assay for single-nucleotide polymorphism (SNP) detection was developed. This assay is simple, rapid, and cost-efficient, and there is no need to label the DNA substrate. The most important characteristic of the assay is a sensitive probe for direct visualization of SNPs by the naked eye at room temperature. This makes it more convenient than other methods that rely on complex instrumentation.

Wang and co-workers²⁹⁶ reported a green and facile strategy for the fabrication of soluble RGO. The method is based on the reduction of exfoliated GO in green tea solution by making use of the reducing capability and the aromatic rings of tea polyphenols (TP). Measurements of the resultant graphene (TPG) confirm the efficient removal of the oxygen-containing groups in GO. The strong interactions between the RGO and the aromatic TPs guarantee a good dispersion of the RGO in both aqueous solution and a variety of organic solvents. These features endow this green approach with great potential in constructing various graphene-based materials, especially for high-performance biorelated materials as demonstrated with the chitosan/TPG composites.

A stable, biocompatible, free-standing “paperlike” material composed of polyoxyethylene sorbitan laurate (TWEEN) and RGO platelets has been presented.²⁹⁷ The TWEEN paper is highly stable in water (no leakage of TWEEN) and sufficiently robust to be handled by hand without breaking. Furthermore, the material is noncytotoxic to three mammalian cell lines and inhibits nonspecific binding of Gram-positive bacteria.

Graphene flakes with controlled thicknesses have been isolated in solution using density gradient ultracentrifugation.²⁹⁸ These stable graphene dispersions are produced using the bile salt sodium cholate, which promotes graphite exfoliation and results in graphene–surfactant complexes having buoyant densities that vary with graphene thickness. The sorted graphene flakes were characterized using atomic force microscopy and Raman spectroscopy.

The dual role of Pluronic copolymer in dispersing graphene and in forming supramolecular hydrogels has been reported.²⁹⁹ The required amount of Pluronic copolymer was dispersed in aqueous GO solution, and subsequent reduction was performed with hydrazine hydrate. The aqueous graphene solutions were stable for three months, and the viscosity behavior of the hydrogels as a function of shear rate diminished.³⁰⁰ Liu et al.³⁰¹ successfully prepared an aqueous dispersion of graphene nanoplatelets (GNs) via chemical reduction of GO using hydrazine hydrate in the presence of poly[(2-ethyl-dimethylammonioethyl methacrylate ethyl sulfate)-*co*-(1-vinylpyrrolidone)] (PQ11), a cationic polyelectrolyte. The noncovalent functionalization of graphene nanoplatelets by PQ11 leads to a stable dispersion for several months. PQ11 is a positively charged polymer that exhibits the ability to reduce silver salts to Ag nanoparticles. They found that such Ag/graphene nanocomposites exhibit good catalytic activity toward the reduction of hydrogen peroxide (H_2O_2), leading to an enzymeless sensor with a fast amperometric response time of less than 2 s.

Noncovalent functionalization leading to solubilization of graphene and single-walled carbon nanotubes (SWNTs) has been explored in nonpolar organic solvents using various

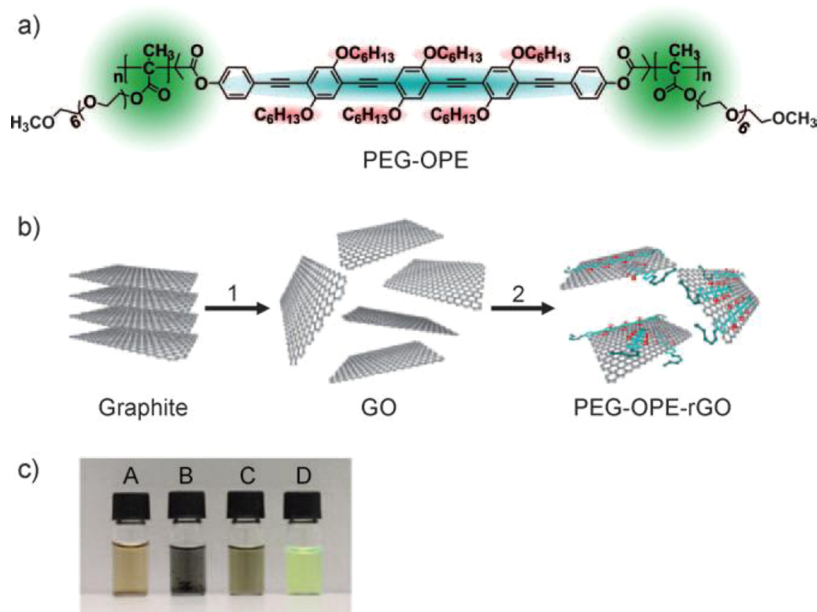


Figure 49. (a) Chemical structure of PEG-OPE. (b) The synthesis of PEG-OPE–RGO in H₂O. Step 1, oxidation of graphite yields single-layer GO nanoplatelets. Step 2, Chemical reduction of GO with hydrazine in the presence of PEG-OPE produces a stable aqueous suspension of PEG-OPE–RGO. (c) Photograph of (A) GO and (B) RGO in water and (C) PEG-OPE–RGO and (D) PEG-OPE in methanol. Reprinted with permission from ref 305. Copyright 2010 Wiley.

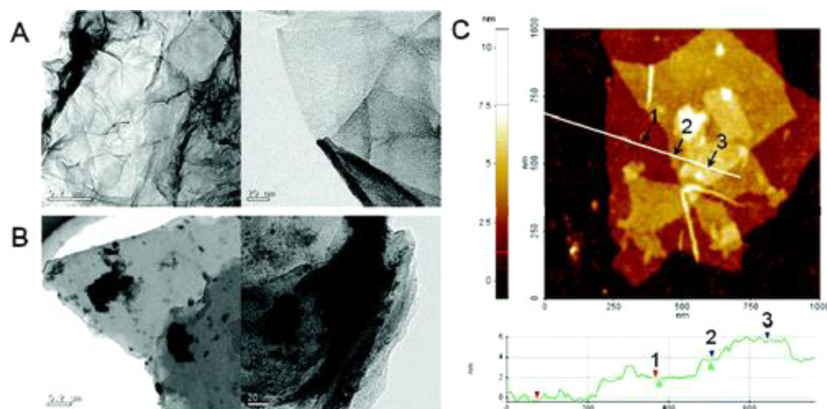


Figure 50. TEM images of chemically converted graphene nanoplatelets (a) in the presence of and (b) in the absence of ILP and (c) tapping mode AFM image of the ILP-G processed from organic suspension and height profiles across the ILP-G sheets indicating a thickness of ~ 1.9 nm. Reprinted with permission from ref 306. Copyright 2010 American Chemical Society.

electron donor and acceptor molecules.³⁰² The large aromatic surfaces of electron donor and acceptor molecules direct themselves onto the surface of the graphene/SWNTs through π – π stacking interactions whereas the alkyl chains or glycol chains on the aromatic molecules promote solubility and thus produce stable dispersions of SWNT/graphene composites in nonpolar solvents. Composites of graphene and SWNTs with electron donors and acceptors show significant change in their electronic and Raman spectra, and these changes were found to be characteristic of charge-transfer interactions.

Choi et al.³⁰³ reported a novel method for dispersing graphene in various organic solvents via noncovalent functionalization with amine-terminated polymers. The carboxylate groups remaining after chemical reduction of GO successfully provided noncovalent functionalization sites for the protonated amine terminal group of end-functional polymers. The noncovalent functionalization facilitated the phase transfer of graphene nanoplatelets from a water phase to an organic phase via simple

sonication. The noncovalent grafting via ionic interaction was confirmed by attenuated total reflection Fourier transform infrared and Raman spectroscopy. The dispersibility of RGO in 16 different organic solvents was tested, and photographs were taken after one month. UV–vis absorption spectroscopy was employed to confirm the dispersibility of the RGO. The absorption peaks of the graphene were observed at 270 nm for 1-propanol, EtOH, and EG, confirming the stable dispersibility of RGO in these solvents.³⁰⁴

An effective method to prepare amphiphilic RGO nanoplatelets by using a coil–rod–coil conjugated triblock copolymer (PEG-OPE) as the π – π binding stabilizer has been shown by Qi et al.³⁰⁵ (Figure 49). PEG-OPE is composed of one lipophilic π -conjugated oligomer and two hydrophilic PEG coils and is synthesized by atom-transfer radical polymerization (ATRP). Due to the amphiphilicity and π -conjugation of PEG-OPE, PEG-OPE functionalized RGO form a sandwich structure, making the composite soluble in a variety of solvents including toluene and

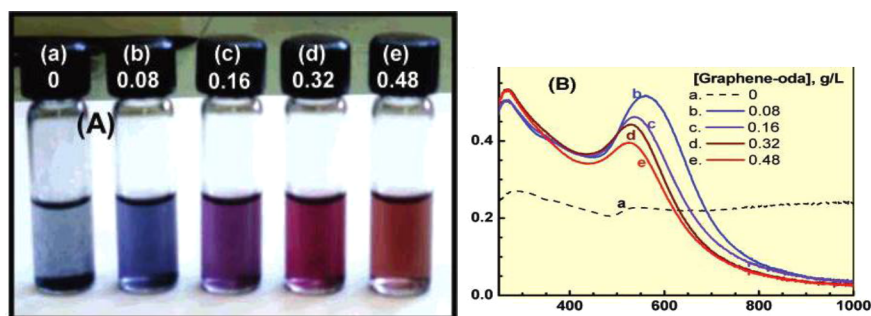


Figure 51. (Left) Photograph of several dispersions of gold nanoparticles (1 mM) in THF with different concentrations of GO–ODA (octadecylamine) and (right) the characteristic UV–vis absorption spectra of the dispersions. Reprinted with permission from ref 318. Copyright 2008 American Chemical Society.

water. The presence of PEG moieties in graphene allows for its use in the exploration of biological systems, as well as its potential application in the attachment and delivery of aromatic water-insoluble drugs into cells.

Kim et al.³⁰⁶ demonstrated an effective method for the preparation of solution-processable graphene nanoplatelets (Figure 50) using ionic liquid polymers (ILP). These graphene nanoplatelets were readily transferred between the aqueous and organic phases using ILP as the transferring vehicle. Chemically converted graphene nanoplatelets decorated with ILP were found to be stable against chemical reduction and were well dispersed in an aqueous phase without any agglomeration. The reversible hydrophilic-to-hydrophobic switching of graphene nanoplatelets was possible by simply exchanging the anions associated with ILP.

Zhang et al.³⁰⁷ theoretically investigated the binding of organic donor, acceptor, and metal atoms on graphene sheets. These calculations revealed the effect of the different noncovalent functionalizations on the electronic structure and transport properties of graphene. The adsorption of 2,3-dichloro-5,6-dicyano-1,4-benzoquinone (DDQ) and tetrathiafulvalene (TTF) induce hybridization between the molecular levels and the graphene valence bands. This transforms the zero-gap semiconducting graphene into metallic graphene. However, the current versus voltage (I – V) simulation indicates that non-covalent modification by organic molecules is not sufficient to significantly alter the transport properties of graphene for sensing applications.

4. FUNCTIONALIZATION WITH NANOPARTICLES

Composite materials derived from fine dispersions of metallic nanoparticles or oxides on carbon nanotubes have been extensively studied and applied in catalytic or optoelectronic applications, supercapacitors, fuel cells, batteries, etc.^{308,309} Due to the increased interest in graphene arising from its exceptional electrical and mechanical properties, the immobilization of metallic and other nanoparticles on graphene sheets has become the focus of many researchers.

A typical pristine graphene sheet can be characterized as an ideal substrate for the dispersion of nanoparticles due to its large active surface area per mass unit, in comparison with carbon nanotubes, amorphous carbon, or graphite, which have a lower active surface area because only the external surface is active. Additionally pristine graphene has high conductivity and mechanical strength, and it is free of metallic or carbon impurities since the preparative methods are not catalytic, such as in carbon nanotubes, and the graphite starting material is of the

highest purity.³¹⁰ Excluding conductivity, the other forms of graphene (GO and partially RGO) also exhibit these advantages for the deposition of nanoparticles.

4.1. Deposition of Precious Metal Nanoparticles

Noble metals such as Pt, Au, Ag, Rh, Pd, and related alloys are often used in the form of nanostructures in a variety of applications ranging from catalytic systems to fuel cells, sensors, supercapacitors, and storage batteries.^{311–316} Considering its reducibility, GO could be used to prepare graphene–metal particle nanocomposites. As such dispersions of metal nanoparticles on graphene sheets potentially provide a new way to develop catalytic, magnetic, and optoelectronic materials. Efforts are being made to utilize graphene sheets as supports to disperse semiconductor and Pt particles and use them in solar cells and fuel cells.

Usually, the precursors for NPs are metal salts, which are reduced in a solvent that contains dispersed GO, RGO, or pristine graphene nanoplatelets. The last two are preferred when the conductivity of the substrate is of high importance. In some cases, the reducing agents or procedures are strong enough to reduce GO simultaneously. The formed NPs are spread onto the relatively huge surface area of graphitic nanoplatelets.

Graphene-stabilized gold nanoparticles (3–30 nm in diameter) have been synthesized using chemically modified graphene nanoplatelets, which support the gold nanoparticles. In this method, gold atoms were deposited onto few-layer graphene. These gold atoms are then condensed upon annealing to form nanoparticles.³¹⁶ Recently, affinity of gold nanoparticles to graphene has been compared with that of palladium and silver nanoparticles with the conclusion that palladium has the highest affinity to graphene. The theoretical calculations (at MP2 and vdW-DF levels) suggested that the high affinity of palladium to graphene is caused by the partial covalent nature of binding between Pd and graphene.³¹⁷

The deposition of gold nanoparticles on GO nanoplatelets has also been achieved by the direct reduction of AuCl_4 by NaBH_4 in a GO THF suspension.³¹⁸ The GO nanoplatelets used in the synthesis were first functionalized with octadecyl amine (GO–ODA) in order to be dispersible in the organic solvent. The formation of the Au nanoparticles (NP) was confirmed using UV–vis absorption where the evolution of the characteristic absorption band around 550 nm was observed (Figure 51). The size and the dispersibility of the as formed Au NPs were determined by the concentration of GO–ODA in the solution. As presented in Figure 52, in the absence of GO–ODA, the Au NPs formed large aggregates, and this caused precipitation. As the concentration of GO–ODA was increased, the Au NPs were

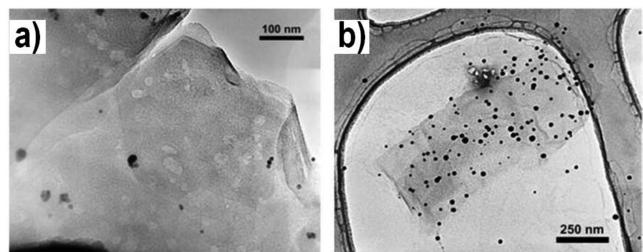


Figure 52. TEM images of the RGO–Au composite on a holey carbon grid: (a) sequential reduction sample; (b) simultaneous reduction sample. Reprinted with permission from ref 319. Copyright 2010 American Chemical Society.

evenly dispersed onto the carbon surface resulting in enhanced liquid phase stability, as well as a size decrease as revealed by the red shift of the analogous absorption bands.

The application of high-frequency ultrasound to a GO dispersion in a 2% poly(ethylene glycol) (PEG) aqueous solution leads to the reduction of GO. The presence in the solution of tetrachloroauric acid (HAuCl_4) leads to the simultaneous formation of Au NPs by the reduction of Au cations, with the majority of the Au NPs immobilized on the RGO surfaces. A sequential reduction of the components had less success in terms of the amount of Au NPs deposited on the RGO nanoplatelets (Figure 52).³¹⁹

Au NPs have been deposited on GO nanoplatelets in the fabrication of ambipolar memory devices.³²⁰ In this case, GO is assembled onto a Si/SiO₂ substrate covered by a positively charged molecular layer of aminopropyl-triethoxysilane (APTES) and then reduced to obtain high conductivity. After the formation of an insulating film of Al₂O₃ over the RGO layer, Au NPs were deposited and finally a top gate was fabricated completing the device. The device can be operated as a conventional conductivity switching memory or a new type-switching memory by adjusting the charge density on the NPs (Figure 53).

Pt or Pt/Ru NPs dispersed onto a conductive surface are used as catalytic systems in proton exchange membrane fuel cell devices (PEM fuel cells). These devices are designed to produce electricity from the oxidation of hydrogen over a catalytic system. Alternatively, methanol can be used as fuel in the so-called direct methanol fuel cells (DMFC).

The conductivity of the surface is important for the collection of the produced electrons and their transport to the collecting electrode. Carbon black, carbon nanotubes, and graphitic nanofibers are often utilized as supports for the dispersion of Pt NPs in these devices. Some of the advantages of carbon materials as catalyst supports are high surface area, conductivity, and low cost. The large surface area provides improved mass transport of the reactants to the catalytic centers. Graphene sheets exhibit remarkable electrical conductivity and the highest specific surface area among carbon materials; as such they could prove to be ideal as a support material to improve the electrocatalytic activity of Pt or Pt/Ru NPs in PEM fuel cells or DMFC.^{321–324}

The formation of Pt NPs was achieved by the borohydride reduction of H_2PtCl_6 in a RGO suspension. The final product, which contained RGO nanoplatelets decorated with Pt NPs, was deposited as a film onto a glassy carbon electrode for use as an electrocatalyst in a PEM fuel cell.³²¹ The use of RGO in this device showed a limited improvement in electrical power output, RGO/Pt NPs delivered a maximum power output of 161 mW/cm² compared with 96 mW/cm² for Pt NPs without a support.

RGO/Pt NPs have also been examined as an effective system for the electrocatalytic oxidation of methanol in DMFC's. The deposition of a fine dispersion of Pt NPs or PtRu alloys on RGO can be realized by the reduction of the Pt or Pt/Ru salts mixed with GO via reductive annealing under a H₂/Ar atmosphere,³²³ reduction using ethylene glycol,^{324–326} reduction utilizing oleylamine and sodium borohydride (NaBH_4),³²⁷ or electrochemical reduction (Figure 54).³²⁸

The use of RGO as support in DMFC electrodes resulted in a slight improvement in the electrocatalytic activity.³²³ In another report a much higher methanol electrooxidation catalytic activity

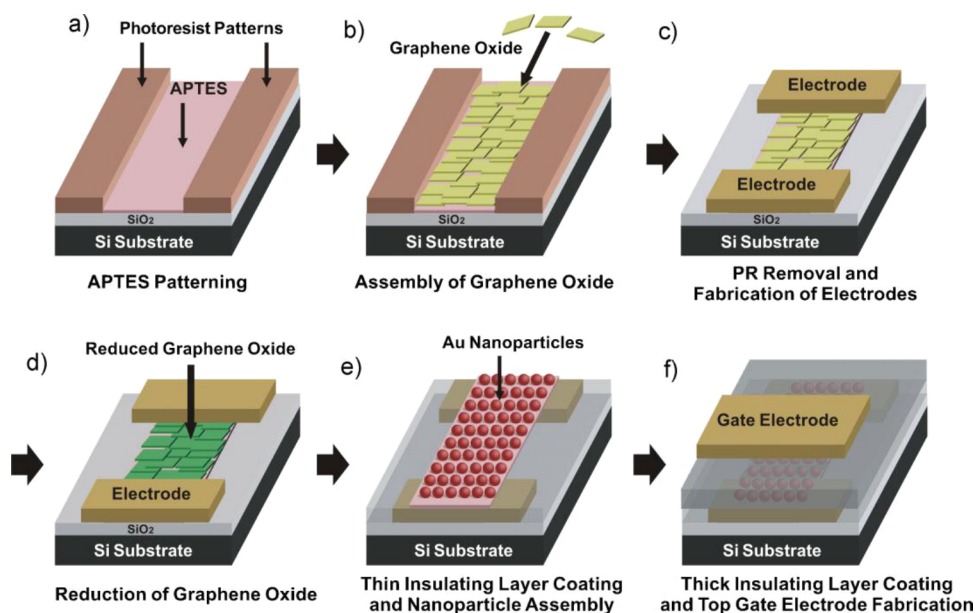


Figure 53. Schematic representation of the fabrication process of RGO-based memory devices using Au NPs. Reprinted with permission from ref 320. Copyright 2010 Wiley.

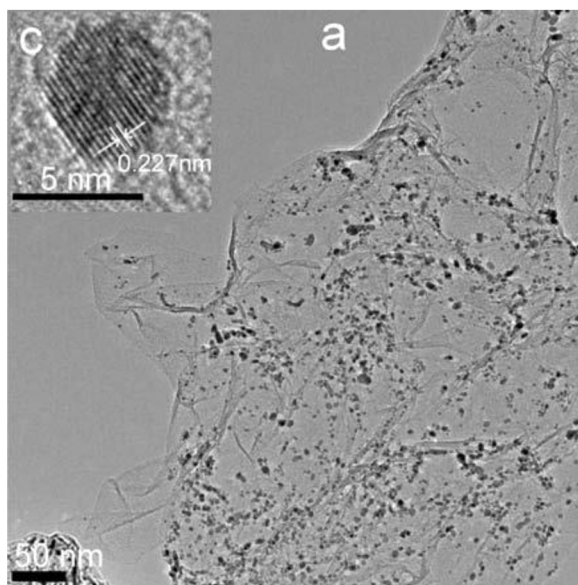
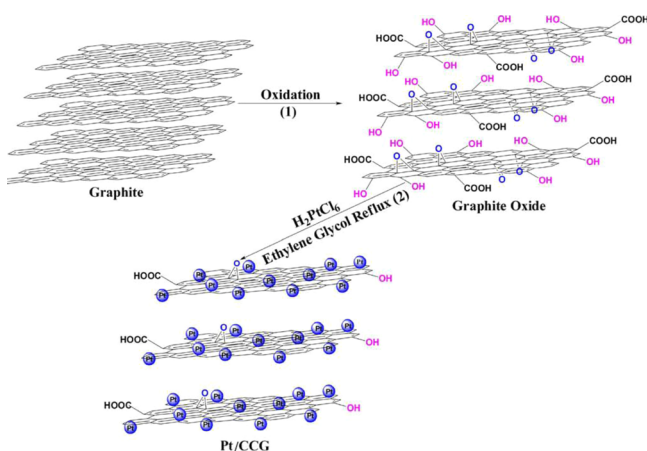


Figure 54. (Top) Schematic of formation of RGO/Pt and (bottom) TEM images of dispersion of Pt nanoparticles on graphenes. Reprinted with permission from ref 328. Copyright 2010 Royal Society of Chemistry.

was measured when a RGO support was used compared with a carbon black support.³²⁸

A general method for the reduction of GO with simultaneous deposition of metal NPs or nanoalloys has been developed by Hassan and co-workers.³²⁹ In this method, microwaves are utilized to reduce aqueous dispersions of GO in the presence of various reducing agents like hydrazine hydrate, ethylenediamine, or ammonium hydroxide. Thermogravimetric analysis of GO and the as prepared RGO showed that this method was effective in removing oxygen functionalities, with the RGO showing no significant weight loss up to 750 °C (Figure 55).

In the case that a metal salt such as palladium nitrate, copper nitrate, or a mixture is present in the aquatic phase together with GO, the analogous metal NPs were formed and deposited on the RGO nanoplatelets (Figure 56).

An oleylamine and oleic acid mixture is a powerful reducing agent for the formation of Ag, Au, and Cu NPs in the presence of GO. This method is superior to others because it exhibits a narrow size distribution as well as fine dispersion of the produced NPs on the GO surface. Ag, Au, and Cu NPs display a characteristic absorption band in the UV–vis region due to surface plasmon resonance (Figure 57). The ethylene glycol/

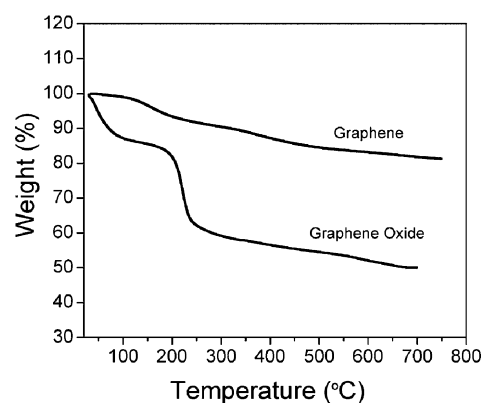


Figure 55. Thermal gravimetric analysis (TGA) plots of GO and chemically converted graphene nanoplatelets obtained using microwave irradiation. Reprinted with permission from ref 329. Copyright 2009 Royal Society of Chemistry.

water system has also been used for the reduction of Au, Pt, and Pd cations in the presence of GO. The as formed NPs are then capable of catalytically reducing the GO surface in the presence of ethylene glycol.³²⁶

4.2. Deposition of Metal Oxide Nanoparticles

Metal oxide nanostructures have been used in catalytic systems, gas sensors, energy storage, transparent conducting electrodes, flexible electronics, photonics, photovoltaic systems, etc.^{330–338} As an example, tin oxide (SnO₂), manganese oxide (Mn₃O₄), cobalt oxide (Co₃O₄), and titanium oxide (TiO₂) nanocrystals supported on carbon substrates have been used successfully as anodes in Li-ion batteries. A high degree of nanocrystal dispersion and conductivity of the substrate are the most important factors for high charge capacity and cycling performance. Graphene nanostructures are ideally suited as a carbon substrate for use as anodes in Li-ion batteries.

SnO₂ should be a good material as an anode for Li-ion batteries with a theoretical Li storage capacity of 782 mA·h·g⁻¹ compared with graphite, which has a storage capacity of 372 mA·h·g⁻¹. The disadvantage of SnO₂ is that during the charge/discharge cycle its volume increases 3 times, causing breaks and cracks in the anode and thus shortening its life. This obstacle could be avoided or minimized by inserting RGO nanoplatelets between SnO₂ NPs. This was achieved by mixing homogeneously with RGO nanoplatelets. The pores and void spaces that formed in this case protect the anode from cracking, minimizing the expansion of SnO₂ (Figure 58). In an alternate synthesis, SnO₂ NPs were deposited on RGO nanoplatelets via an alkaline hydrolysis of SnCl₄ in the presence of RGO. It was shown that the initial reversible capacity (810 mA·h·g⁻¹) of the RGO/SnO₂ composite is only moderately reduced after 30 cycles (570 mA·h·g⁻¹), showing remarkable improvement compared with that of pure SnO₂ NPs.³³⁰

Zhang et al.³³⁹ have presented a method to increase remarkably the loaded amount of metal oxide on graphene substrate without affecting the quality of the dispersion. The higher loading of metal oxide NPs could increase the charge capacity of the composite. Starting from graphene oxide, the oxygen groups here were used as anchors attracting Sn⁴⁺ cations through electrostatic forces when GO and SnCl₂ are dispersed in water. After drying by heating, SnO₂ nanocrystals are formed and immobilized on the GO surface. TEM images showed the dense decoration of SnO₂ NPs on the GO nanoplatelets (Figure 59), while AFM images showed that SnO₂ NPs are possibly deposited

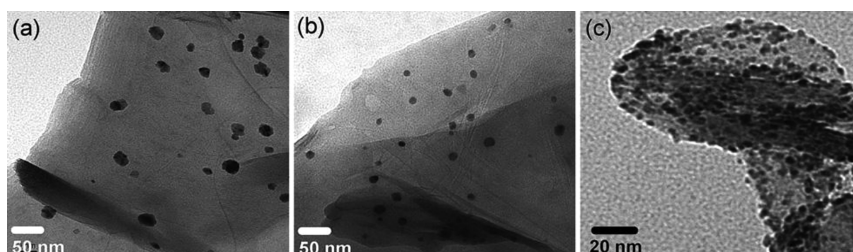


Figure 56. TEM images of RGO nanoplatelets decorated with (a) Pd, (b) Cu, and (c) CuPd NPs. Reprinted with permission from ref 329. Copyright 2009 Royal Society of Chemistry.

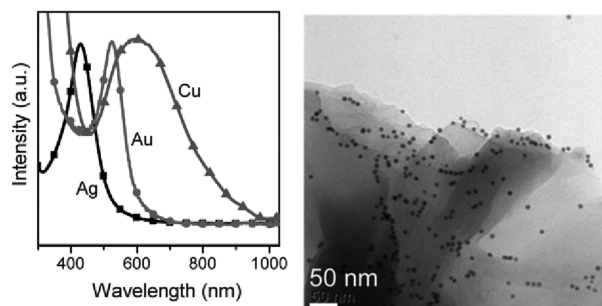


Figure 57. (Left) UV-vis absorption spectra of Ag, Au and Cu NPs deposited on RGO and (right) TEM image of the RGO nanoplatelet with Au NPs deposited on the surface. Reprinted with permission from ref 329. Copyright 2009 Royal Society of Chemistry.

on both sides of graphene oxide nanoplatelets explaining the observed high loading in this case.

Since high conductivity is essential for the use of graphene/SnO₂ composites in Li-ion batteries, thermal reduction of the GO/SnO₂ composite at 300 °C is needed to afford the RGO–SnO₂ composite. The content of the SnO₂ in the final composite was about 60%, compared with other carbon supports where the SnO₂ content is usually less than 25%. The RGO/SnO₂ showed an initial reversible charge capacity of 786 mA·h·g⁻¹, which after 50 cycles drops to a capacity of 560 mA·h·g⁻¹, is comparable to results reported by other groups.³³⁹

Although Mn₃O₄ exhibits very low conductivity, it could be considered an attractive oxide for use as an anode material for Li-

ion batteries, mainly due to its high abundance and low cost. Graphene nanostructures, as highly conductive materials, acting as substrates for the deposition of Mn₃O₄ could help overcome the low conductivity of this metal oxide. In a characteristic example a RGO/Mn₃O₄ composite afforded a high capacity of 810 mA·h·g⁻¹ with good rate capability and cycling stability.³⁴⁰ The decoration of RGO by well crystallized Mn₃O₄ NPs was achieved by the hydrolysis of a Mn salt in a suspension of GO in DMF/H₂O followed by hydrothermal reduction of the GO (Figure 60).

Improved anode performance in Li-ion batteries has also been noted using composites of graphene or RGO and metal oxides such as MnO₂,³⁴¹ CuO,³⁴² Co₃O₄,^{343–345} CoO,³⁴⁶ Fe₃O₄,³⁴⁷ TiO₂,³⁴⁸ and Li₄Ti₅O₁₂.³⁴⁹ For example, the RGO/Co₃O₄ composite is formed by deposition of cobalt on RGO nanoplatelets in the form of Co(OH)₂ followed by calcination at 450 °C (Figure 61).

The graphene/TiO₂ composite has been widely examined and its synthesis and physical properties have been reported by several researchers.^{18,348,350–353} An illustrative example of the use of the nanostructured RGO/TiO₂ hybrid is presented by Wang et al.³⁴⁸ where they demonstrated the enhanced Li-ion insertion/extraction kinetics in TiO₂. This makes the material a candidate for use in Li-ion batteries or other energy storage materials. For the preparation of the composite, RGO nanoplatelets were dispersed in water by stabilizing them with sodium dodecyl sulfate. To this solution, a TiCl₃ solution was added, which resulted in deposition of TiO₂ NPs upon hydrolysis (Figure 62).

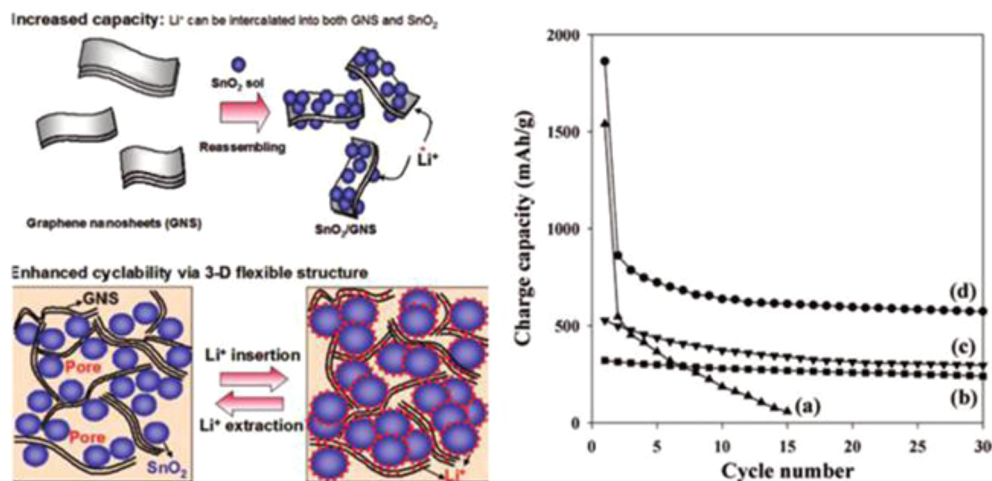


Figure 58. (left) Schematic representation of the formation of RGO/SnO₂ and its use in Li ion batteries and (right) cyclic performances for (a) SnO₂ nanoparticles, (b) graphite, (c) RGO nanoplatelets, and (d) RGO/SnO₂. Reprinted with permission from ref 330. Copyright 2008 American Chemical Society.

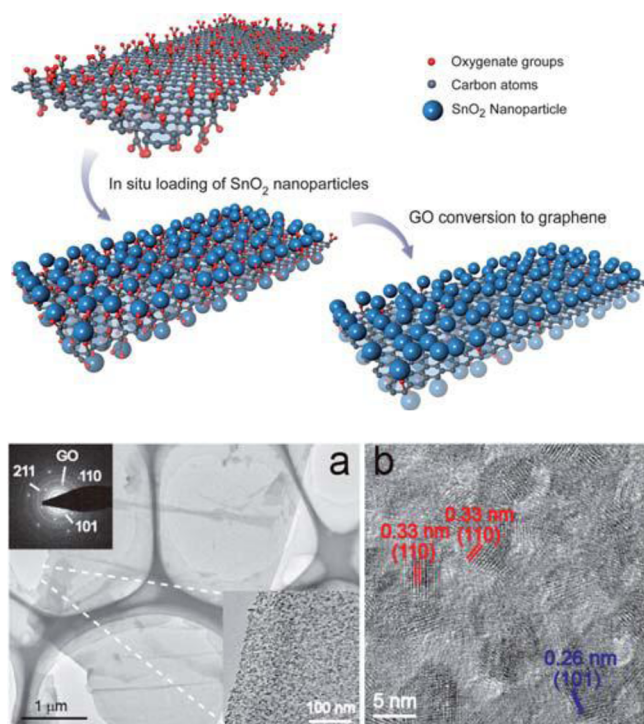


Figure 59. (top) Schematic representation of the formation of the GO/SnO₂ composite. (bottom) (a) TEM image of SnO₂ NPs loaded on GO with corresponding SAED pattern and (b) HRTEM image of the SnO₂-GO composite. Reprinted with permission from ref 339. Copyright 2010 Royal Society of Chemistry.

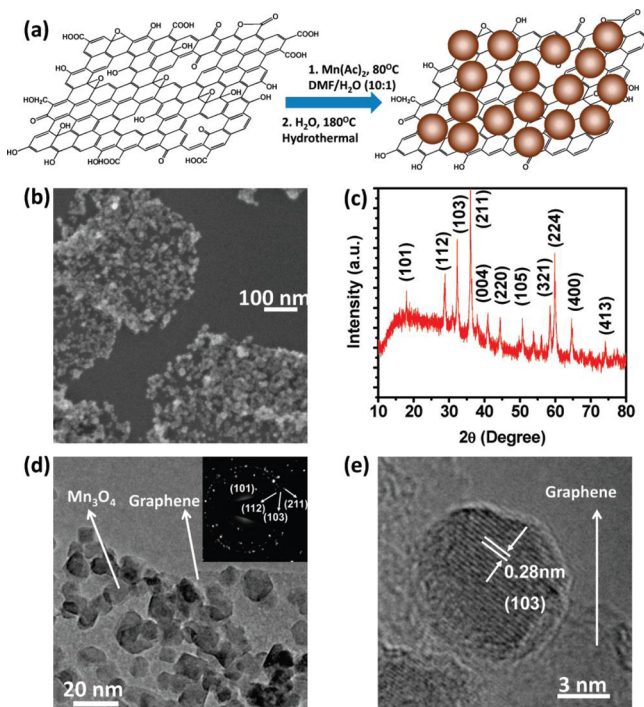


Figure 60. Mn₃O₄ NPs grown on GO: (a) schematic two-step synthesis of Mn₃O₄/RGO, (b) SEM image of the Mn₃O₄/RGO composite, (c) XRD spectrum of Mn₃O₄/RGO, (d) TEM image of Mn₃O₄/RGO with inset showing the electron diffraction pattern of the Mn₃O₄ NPs on RGO, and (e) high-resolution TEM image of an individual Mn₃O₄ NP on RGO. Reprinted with permission from ref 340. Copyright 2010 American Chemical Society.

TiO₂ nanocrystals have been considered one of the most promising materials for photocatalytic water splitting.³⁵¹ Under optimized conditions photoinduced electrons in TiO₂ can escape recombination with the photoinduced holes, thereby splitting water molecules to produce hydrogen. RGO has been used as support with TiO₂ in an effort to minimize the recombination of the photogenerated electron-hole pairs and thus to improve the water-splitting efficiency. Zhang and co-workers³⁵¹ showed that the RGO/TiO₂ composite could be synthesized by the hydrolysis of tetra-butyl titanate in a dispersion of RGO nanoplatelets followed by thermal annealing at 450 °C (Figure 63). The efficiency of photocatalytic water splitting by the RGO/TiO₂ composite was determined by measuring the H₂ evolution during irradiation using simulated solar light.

It was shown that when the concentration of RGO in the composite is 5% the evolution of H₂ is almost two times higher than commercially available P25. This enhancement in the photosplitting of water is due to the high conductivity of the RGO substrate, which helps the photogenerated electrons of TiO₂ escape recombination with holes and thus increase the water splitting efficiency.

TiO₂ NPs also serve as charge carriers in the photocatalytic reduction of GO. UV irradiation of TiO₂ NPs mixed with GO in a water suspension led to the reduction of GO. As the mixture of TiO₂ and GO was irradiated, its light brown color turns to dark brown or black (Figure 64). The absorption spectrum of UV-irradiated TiO₂ decreases as the amount of added GO increases. By monitoring of this decrease in absorbance, the number of electrons that were transferred from TiO₂ to GO was estimated to be 0.01 mol/g. At a carbon to oxygen ratio of 2.25, the concentration of oxygen groups on GO was estimated to be 0.02 mol g⁻¹. Taking into account these estimations, the yield for the photocatalytic reduction of GO was approximately 50%.¹⁸

Continuing this attractive subject, Lightcap et al.³⁵⁴ showed how the RGO nanoplatelets can act as a conductive pathway for the reduction Ag⁺ to Ag⁰ by TiO₂ NPs. This process then leads to the formation of Ag NPs.³⁵⁴ It is believed that photoinduced electrons from the photoexcited TiO₂ move through the RGO nanoplatelets before reaching Ag cations and reducing them; a scheme of this process is presented in Figure 65.

TiO₂NPs/GO composites have also been used in the photodegradation of methylene blue. This shows that the composite may have application as a photocatalyst for the degradation of organic compounds. The composite was synthesized via a hydrothermal method whereby commercially available P25 was deposited on GO, with the subsequent reduction of the GO nanoplatelets by heating the P25/GO suspension in an autoclave. The P25/GO composite showed improved photodegradation catalytic activity of methylene blue compared with pure P25 or P25 supported on carbon nanotubes (Figure 66). The presence of GO improved the photocatalytic activity in three ways: (a) due to its high conductivity, RGO facilitates the charge separation in TiO₂ NPs and thus reduces charge recombination that lowers the yield of photocatalysis, (b) the absorption of the organic dye is maximized due to the interaction of the organic dye with the extended aromatic system of RGO, and (c) the Ti-O-C bond causes a red shift in the absorption spectra. This increases the utilization of natural sunlight.³⁵²

Additionally composite materials of graphene or GO and metal oxide NPs such as Bi₂WO₆ (ref 355) or ZnO (ref 356) have been successfully applied as photocatalysts.

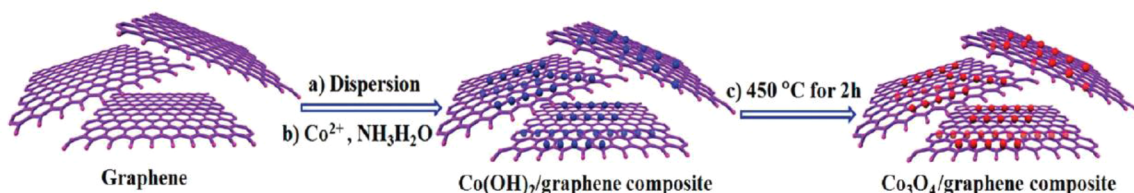


Figure 61. Schematic representation of the formation of the RGO/Co₃O₄ composite: (a) dispersion of RGO in isopropyl alcohol/water solution, (b) formation of RGO/Co(OH)₂ composite, and (c) formation of RGO/Co₃O₄ composite by calcination. Reprinted with permission from ref 343. Copyright 2010 American Chemical Society.

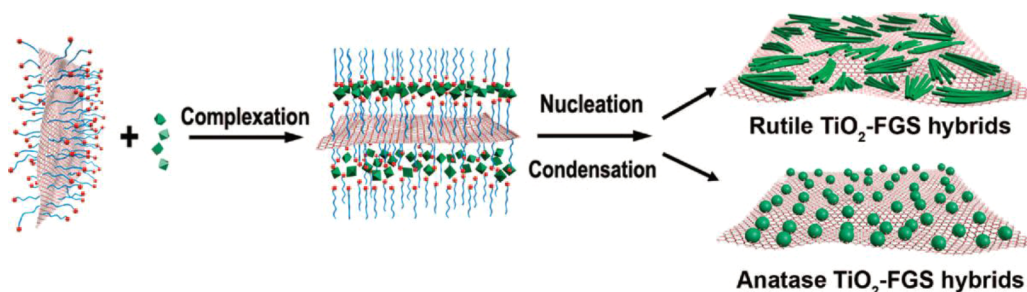


Figure 62. The growth of TiO₂ on surfactant-stabilized GO nanoplatelets. Reprinted with permission from ref 348. Copyright 2009 American Chemical Society.

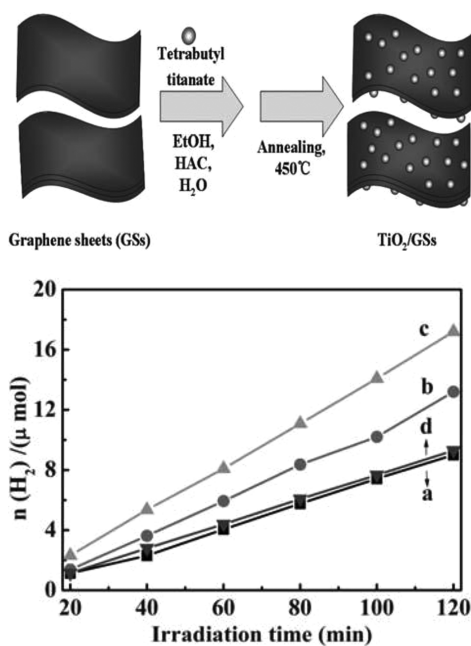


Figure 63. (top) Synthetic procedure for the preparation of RGO/TiO₂ composites. (bottom) Reaction time profiles of H₂ evolution under UV-vis irradiation over the photocatalysts: (a) TiO₂ P25 and (b) 1%, (c) 5%, and (d) 10% GO-TiO₂. Reprinted with permission from ref 351. Copyright 2010 Royal Society of Chemistry.

ZnO is a semiconductor with a band gap of 3.37 eV, which can act as photocatalyst in the form of NPs suspended in a conductive carbon substrate such as GO under UV irradiation. UV irradiation of GO/ZnO composite results in the partial reduction of GO. Electrons from the excited ZnO NPs are transferred to GO and react with the epoxy and other oxygen groups, resulting in the reduction of GO. The deposition of ZnO NPs on GO was achieved by simply mixing GO nanoplatelets and ZnO NPs in ethanol. After irradiation, the light brown ethanol suspension becomes dark brown due to the formation of RGO (Figure 67).

Proof for the above reaction mechanism is obtained from analysis of fluorescence emission spectra of ZnO in the presence of several concentrations of GO, as shown in Figure 68. The fluorescence weakens as the concentration of GO increases; this is indicative of a quenching pathway for the excited ZnO NPs by the GO.³⁵⁶ ZnO nanorods and nanowires have also been deposited on the surface of GO; this results in interesting optoelectronic properties.^{357,358} The GO/ZnO nanorod composite showed increased efficiency as a visible-blind UV sensor. The function of the device is based on the ability of ZnO nanorods to absorb photons and the high conductivity of GO, which facilitates the charge transfer. The ZnO nanorods were grown after the immersion of a GO/ZnO NPs precursor in a zinc nitrate solution, which uses the ZnO NPs as nucleation centers. The photoresponse of the as prepared device reached 22.7 A·W⁻¹ at 20 V.³⁵⁷

Magnetically modified graphene and GO nanoplatelets formed by the deposition of magnetite (Fe₃O₄) on GO can be used for the removal of heavy metals from aqueous media,^{30,359} drug carriers,³⁶⁰ and magnetic resonance imaging (MRI).³⁶¹

The formation of the GO/magnetite NP composite can be obtained by the coprecipitation of Fe³⁺/Fe²⁺ ions by the addition of an ammonia solution to an aqueous dispersion of FeCl₃, FeCl₂, and GO. Chandra et al.³⁰ deposited magnetic Fe₃O₄ NPs with a size of about 10 nm onto the GO. Because of their small size, the NPs in graphene show superparamagnetism. This composite material is then reduced using hydrazine. The magnetic RGO showed remarkable efficiency in the removal of arsenic (99.9%) from water, which could then be separated by application of an external magnetic force (Figure 69).³⁰

Magnetite microspheres on RGO surfaces have been prepared using a solvothermal method. In this method, a dispersion of GO and FeCl₃ was reduced in the presence of NaAc and poly(ethylene glycol) in an autoclave at 200 °C (Figure 70).³⁶² The composite reveals a significant saturation magnetization of about 45.5 emu/g, which is lower than that of pure magnetite NPs, due to the presence of the nonmagnetic GO. From TEM measurements, it can be seen that the magnetite microspheres

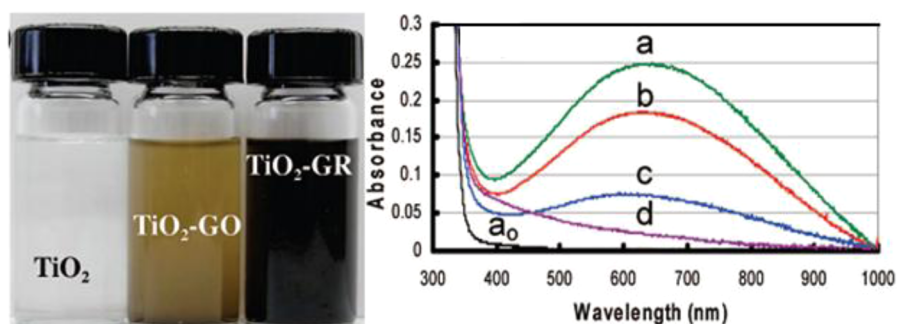


Figure 64. (left) The change in color of a suspension of GO/TiO₂ before and after UV irradiation. A suspension of TiO₂ NPs is also shown for comparison. (right) Absorption spectra of UV-irradiated TiO₂ suspension (a) before and (b–d) after the addition of GO suspensions: (b) 50, (c) 150, and (d) 300 μg of GO (*a*₀ corresponds to the TiO₂ suspension prior to UV irradiation). Reprinted with permission from ref 18. Copyright 2008 American Chemical Society.

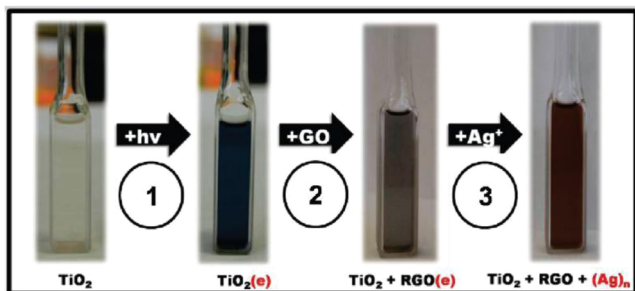
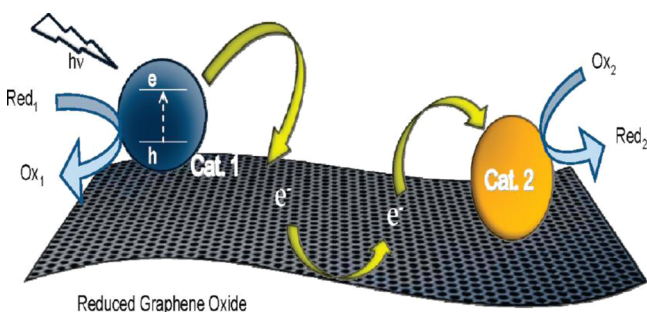


Figure 65. (top) RGO as a conducting pathway. (bottom) Photographs showing the color changes observed during stepwise transfer of electrons: (1) storage of electrons in TiO₂ by irradiation of the suspension with UV light; (2) addition of GO; the resulting gray color is due to the formation of RGO; (3) upon the addition of AgNO₃, reduction of Ag⁺ to Ag NPs (red color) by stored electrons in the RGO occurs. Reprinted with permission from ref 354. Copyright 2010 American Chemical Society.

have an average diameter of 15 nm. This aggregation is attributed to the magnetic forces that develop between the magnetite NPs.

A different method for the preparation of GO/Fe₃O₄ hybrids is schematically illustrated in Figure 71. In this case, preformed magnetite NPs were modified with tetraethyl orthosilicate (TEOS) and (3-aminopropyl)triethoxysilane (APTES), in order to introduce amino groups onto their surface. These amino-modified magnetite NPs were then attached to the carboxylic groups of GO by use of the cross-linking agents 1-ethyl-3-(3-dimethylaminopropyl)-carbodiimide (EDS) and *N*-hydroxysuccinimide (NHS).³⁶³

4.3. Deposition of Quantum Dots

Quantum dots (QDs) are nanostructures composed of groups III–V or II–VI elements that exhibit interesting optical and electronic properties that make them very attractive in

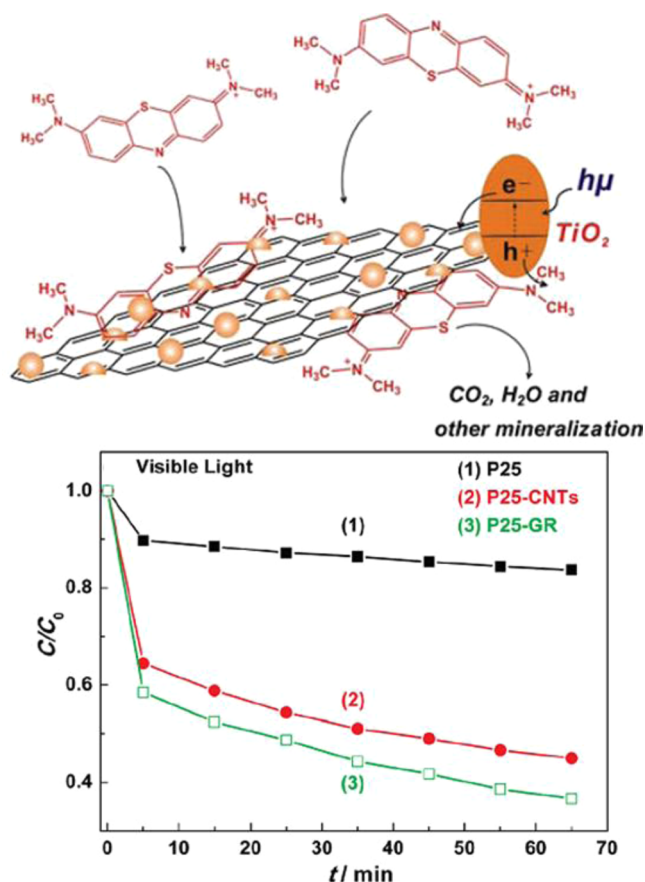


Figure 66. (top) Schematic representation of the photodegradation of methylene blue on the P25/GO composite and (bottom) photo-degradation of methylene blue under visible light using (1) P25, (2) P25-carbon nanotubes, and (3) P25-RGO photocatalysts. Reprinted with permission from ref 352. Copyright 2010 American Chemical Society.

applications such as biological labeling, solar cells, and light-emitting devices.^{364–367} However, several obstacles need to be overcome for their use. As an example, the use of QDs in solar cells suffers from difficulty in transferring the charge carriers away from the QD in the device.³⁶⁸ GO nanoplatelets decorated with QDs could act as nanowires that promote direct charge transport and efficient charge transfer to QDs, thus increasing their efficiency in solar cells.

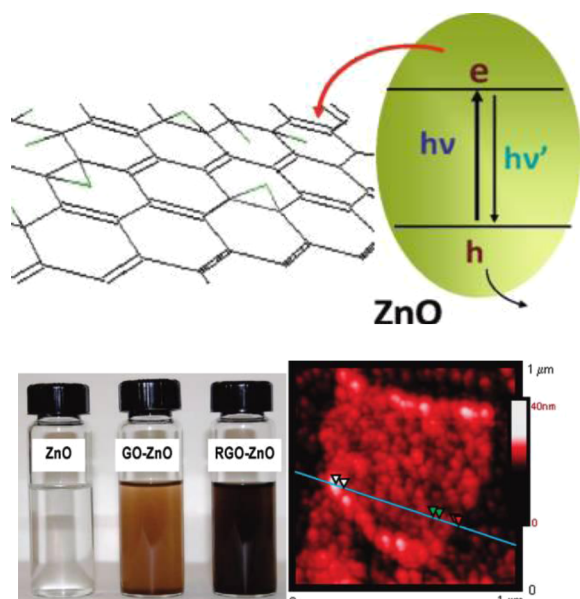


Figure 67. (left) Suspensions of ZnO, ZnO–GO, and ZnO–RGO resulting from irradiation and (right) AFM analysis of ZnO NPs deposited onto GO nanoplatelets. Reprinted with permission from ref 356. Copyright 2009 American Chemical Society.

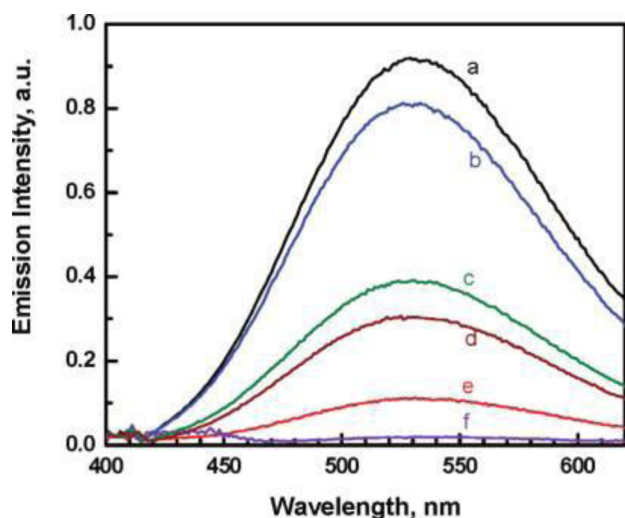


Figure 68. Emission spectra of a 1 mM ZnO suspension at different GO concentrations: (a) 0, (b) 0.035, (c) 0.09, (d) 0.14, (e) 0.20, and (f) 0.24 mg/mL. Reprinted with permission from ref 356. Copyright 2009 American Chemical Society.

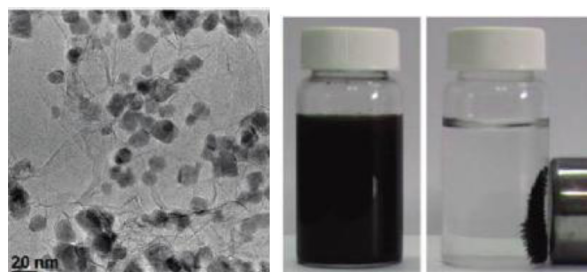


Figure 69. (left) Magnetite NPs immobilized on GO nanoplatelets and (right) RGO/Fe₃O₄ removal from the water using an external magnetic force. Reprinted with permission from ref 30. Copyright 2010 American Chemical Society.

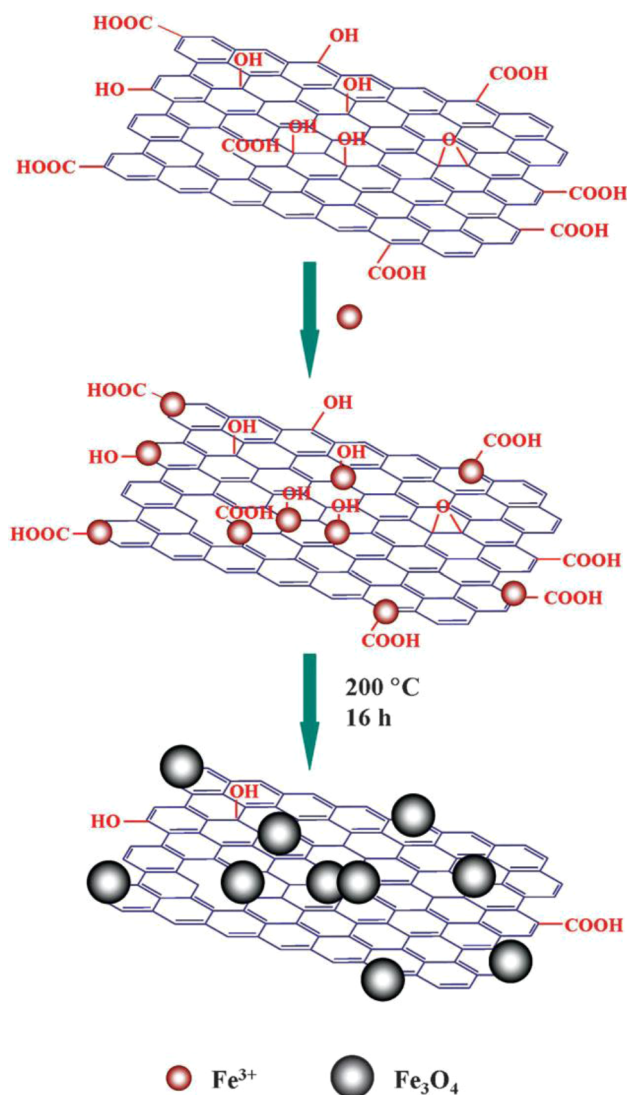


Figure 70. Deposition of magnetite nanoparticles on RGO nanoplatelets. Reprinted with permission from ref 362. Copyright 2010 Royal Society of Chemistry.

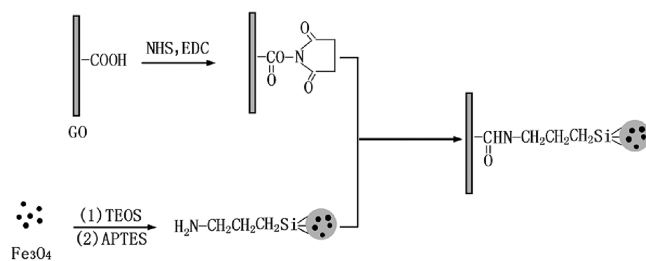


Figure 71. Schematic representation of the GO/Fe₃O₄ NPs. Reprinted with permission from ref 363. Copyright 2010 Elsevier.

In a recent article, Chen et al.³⁶⁹ showed that upon irradiation of CdSe/ZnS nanocrystals deposited on graphene, an efficient energy transfer occurs from the individual NPs to the graphene surface. This energy transfer is indicated by a fluorescence intensity quenching of the CdSe/ZnS nanocrystals by a factor of 70.

The CdSe/ZnS nanocrystals were deposited by spin casting onto the graphene sample deposited on quartz substrates at a low density. Under illumination, fluorescence from individual

nanocrystals located on the graphene layer or on the quartz substrate could be observed, with strong fluorescence quenching observed for particles deposited on the graphene sheets (Figure 72). A similar fluorescence quenching was observed when CdS and CdSe NPs were dispersed on GO nanoplatelets.^{370,371}

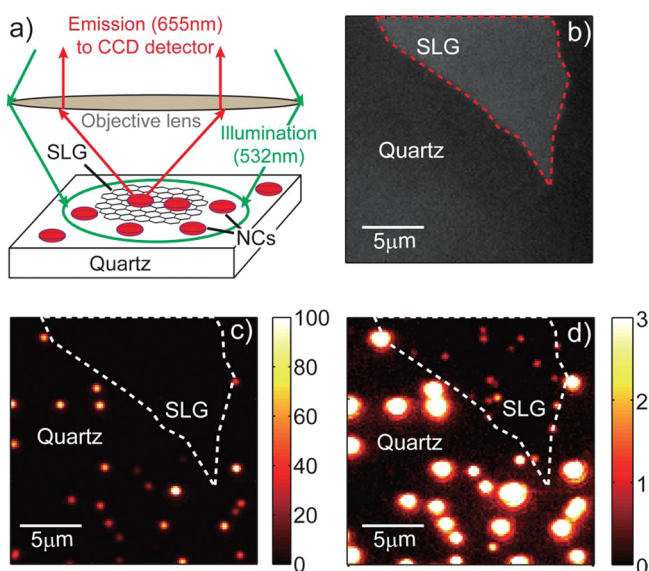


Figure 72. (a) Schematic representation of the experiment. (b) Optical reflectivity image in the emission range of the nanocrystals. (c, d) Wide-field fluorescence images of individual CdSe/ZnS nanocrystals in the region shown in panel b. Reprinted with permission from ref 369. Copyright 2010 American Chemical Society.

The fluorescence quenching of QDs from GO can be avoided by blocking the direct attachment of these species by an “insulating layer”. As an example GO can be covered during its reduction step by a monolayer of the reductive agent such as the positively charged *p*-phenylene diamine, while CdSe NPs during their formation were covered by the negatively charged hexadecanoic chains as described by Wang et al.³⁷² The composite is formed due to the electrostatic forces between the two components (Figure 73). The presence of the organic aliphatic molecules provides the composite with high solubility in organic solvents, such as toluene. Due to this insulating layer the composite showed a characteristic fluorescence spectrum after photoexcitation of QDs, and furthermore this fluorescence band can be tuned by controlling the size of the formed QDs through the reaction time of its preparation route. Thus using several sized QDs on RGO, a variety of colors that cover the visible light

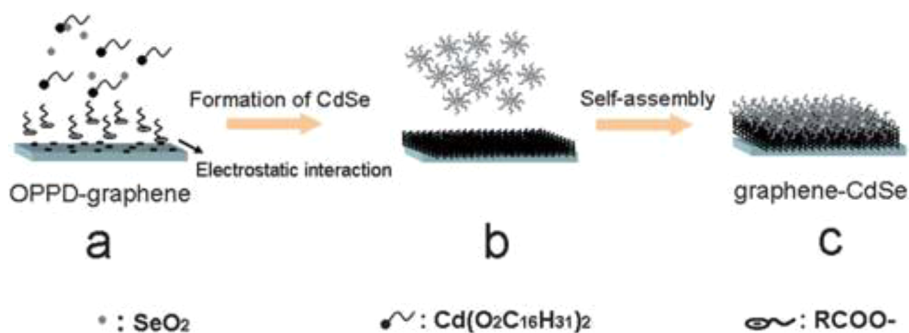


Figure 73. Schematic representation of the formation of RGO/CdSe NP composite. Reprinted with permission from ref 372. Copyright 2011 Royal Society of Chemistry.

region from blue to red can be produced by the fluorescence of the composite solutions (Figure 74).

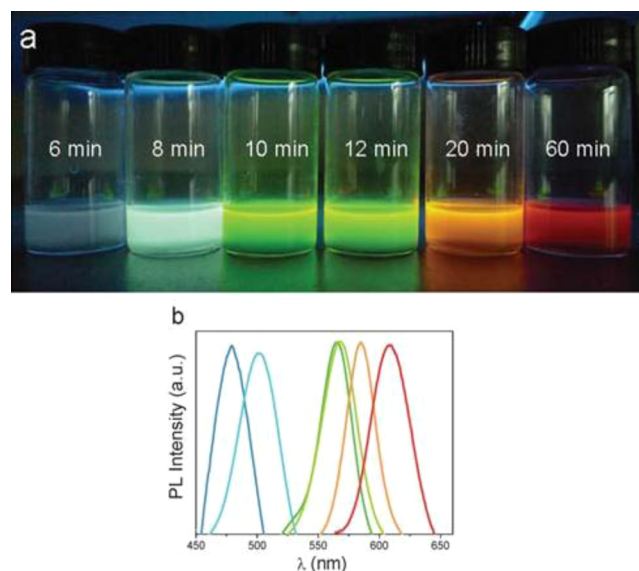


Figure 74. (a) Photographs of a series of RGO–CdSe NPs composite dispersions prepared with different reaction times under UV light irradiation of 365 nm and (b) fluorescence spectra of a series of RGO–CdSe NPs composites prepared after different reaction times. Reprinted with permission from ref 372. Copyright 2011 Royal Society of Chemistry.

4.4. Deposition of Other Nanoparticles

Apart from the metal oxide/GO composites, alternative Li-ion anode materials have been synthesized by dispersing other nanoparticles such as Si or Sn on GO surfaces.^{373,374} Si is an attractive material for energy storage because it is known to have the highest theoretical energy density among the common elements, as well as being cheap and abundant.

A dispersion of Si NPs with size less than 30 nm in diameter on RGO nanoplatelets results in the formation of a composite material with high Li ion storage capacities and cycling stability. After preparation of an electrode from this material, a storage capacity of 2200 mA·h·g⁻¹ was measured after 50 cycles, while a capacity of 1500 mA·h·g⁻¹ was observed after 200 cycles.³⁷³

A thin film of the composite was prepared by addition of an aqueous GO dispersion to a Si NP dispersion, followed by filtration and air drying before thermal annealing in a H₂/Ar atmosphere at 700 °C (Figure 75).

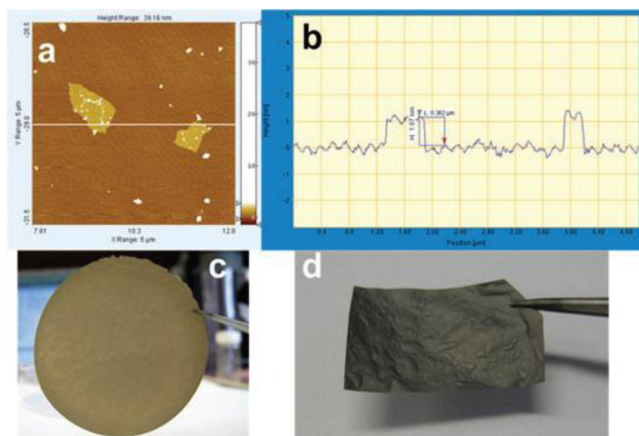


Figure 75. (a) AFM image of GO and (b) related height profile, (c) Si/GO composite paper, and (d) Si/RGO composite paper obtained by reduction of Si/GO. Reprinted with permission from ref 373. Copyright 2010 Royal Society of Chemistry.

Cobalt hydroxide ($\text{Co}(\text{OH})_2$) materials usually display a layered structure with a high interlayer spacing and a well-defined electrochemical redox activity. The combination of cobalt hydroxide NPs with GO nanoplatelets are promising candidates for use in alkaline batteries, fuel cells, and supercapacitors. Chen et al.³⁷⁵ showed that the abundance of hydroxyl anions produced by the hydrolysis of disodium sulfide (Na_2S) in an aqueous solution of GO and $\text{CoCl}_2 \cdot 6\text{H}_2\text{O}$ is sufficient to reduce GO, as well as facilitate the formation of $\text{Co}(\text{OH})_2$ NPs (Figure 76).

The GO/ $\text{Co}(\text{OH})_2$ composite was applied as a supercapacitor electrode, which displayed enhanced electrochemical performance. This performance was examined using cyclic voltammetry, electrical impedance spectroscopy, and galvanostatic charge-discharge measurements.³⁷⁵

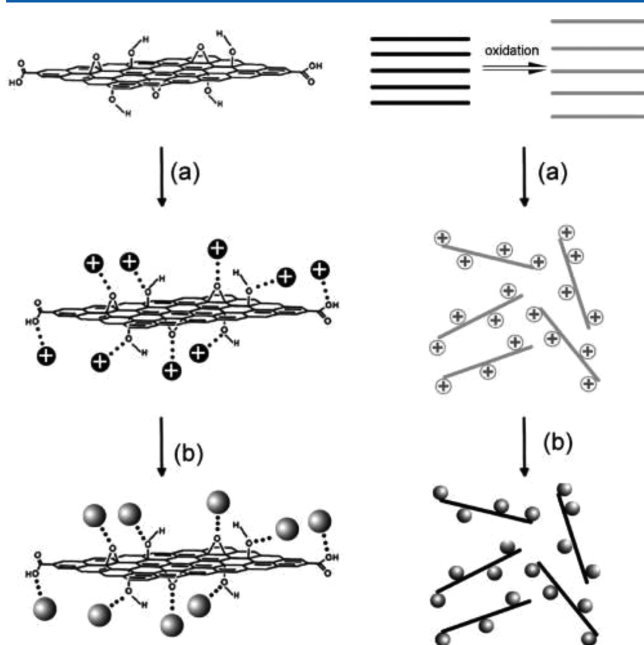


Figure 76. The formation process of RGO/ $\text{Co}(\text{OH})_2$ nanocomposites: (a) interactions between GO and Co^{2+} and (b) the simultaneous deposition of Co^{2+} and reduction of GO. Reprinted with permission from ref 375. Copyright 2010 American Chemical Society.

5. SUBSTITUTIONAL DOPING

A particularly distinctive position in this chapter should be given to the substitutional doping of graphenes, where carbon atoms from the hexagonal honeycomb lattice of graphene can be substituted by nitrogen or boron atoms. Depending on the electrophilic character of the atoms that substitute the carbon atoms, the doped graphene sheets show n- or p-type behavior. In addition, by controlling the degree of this doping modification, the electrical properties of graphene could be potentially tailored, thereby expanding remarkably the application of graphene in nanoelectronics.

The incorporation of nitrogen atoms is made using their three sp^3 orbitals; this leads to their lone pair electrons being conjugated with the graphitic π -system. The N-doped graphene sheets are electron-rich so that n-type semiconducting behavior is expected. In general, N-doped graphene sheets are formed by the substitution of O or C atoms with N during reduction or annealing^{43,376–378} or in situ during graphene growth using CVD,³⁷⁹ arc discharge,³⁸⁰ or solvothermal methods.³⁸¹ Oxygen or sp^3 carbon atoms that are situated at the defect sites of GO can be substituted by nitrogen during the reduction step using a nitrogen-rich reductive source like ammonia or hydrazine, at high temperature.

Starting from graphene nanoribbons (GNRs), Wang et al.⁴³ demonstrated N-doping using high-power electrical joule heating in ammonia gas. The chemically derived GNRs were dispersed on a SiO_2/Si chip and immobilized between a palladium metal source/drain (S–D) forming a FET-like device (Figure 77). The GNR was electrically annealed under an NH_3/Ar atmosphere. The existence of C–N bonds in the derived GNR was identified by X-ray photoelectron spectroscopy (XPS) and nanometer-scale secondary ion mass spectroscopy. In this case, the C–N bonds are formed mostly at the edges of graphene sheets where the chemical reactivity is higher.

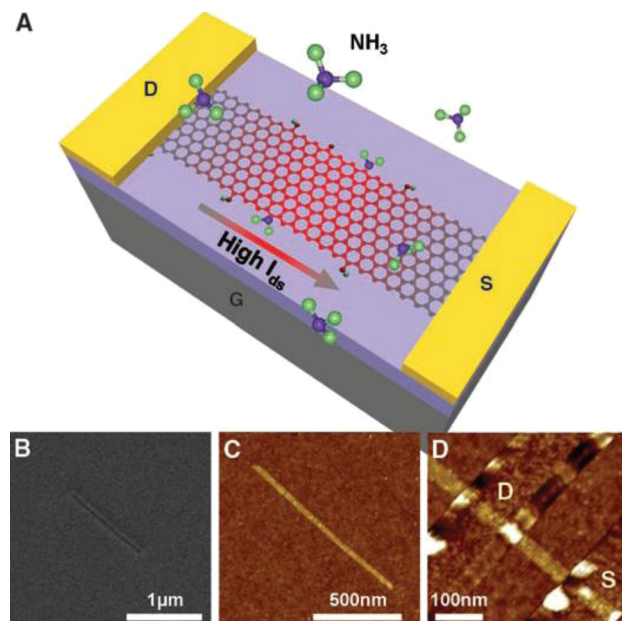


Figure 77. Electrothermal reaction of an individual GNR in NH_3 : (a) schematic representation of the device electrically annealed under NH_3 (where D is the drain, S the source, and G the gate); (b) SEM and (c) AFM images of a ~ 30 nm wide GNR and (d) AFM image of the device fabricated on the GNR. Reprinted with permission from ref 43. Copyright 2009 American Association for the Advancement of Science.

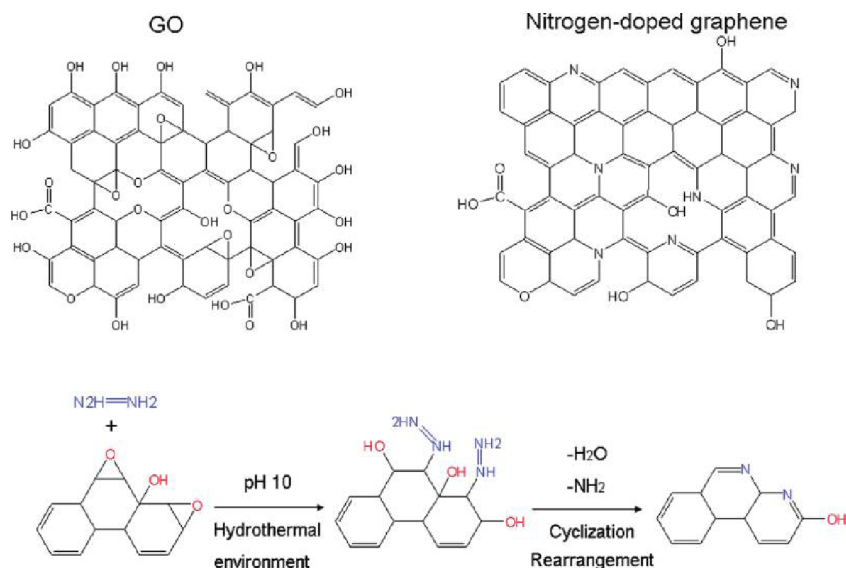


Figure 78. Schematic structure of GO and N-doped GO produced by hydrothermal reduction. Reprinted with permission from ref 377. Copyright 2010 American Chemical Society.

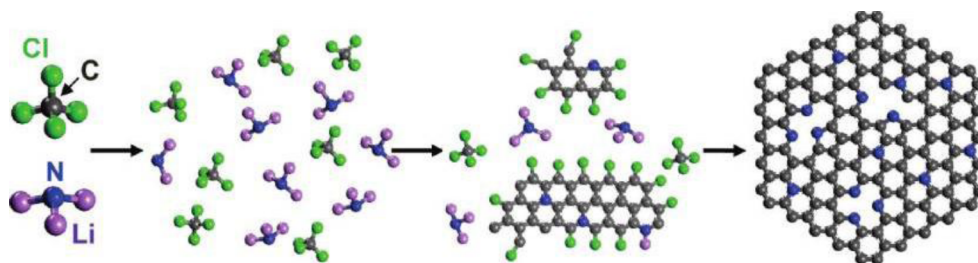


Figure 79. A possible mechanism for the solvothermal synthesis of N-doped graphene. Reprinted with permission from ref 381. Copyright 2011 American Chemical Society.

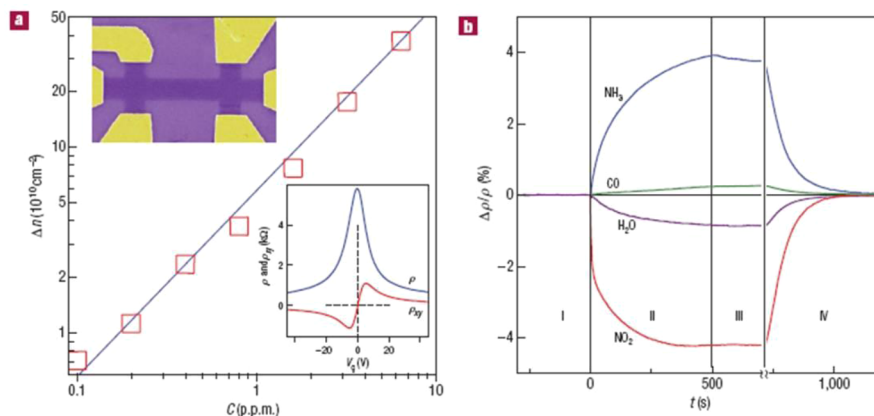


Figure 80. (a) Concentration of chemically induced charge carriers in SLG exposed to different concentrations of NO_2 and (b) changes in resistivity at zero \mathbf{B} field caused by graphene's exposure to various gases diluted to 1 ppm. Reprinted with permission from ref 384a. Copyright 2008 American Chemical Society.

In another approach, the same group has studied the nitrogen doping and simultaneous reduction of GO during annealing in NH_3 .³⁷⁶ GO was heated in a 2 Torr NH_3/Ar (10%) atmosphere. N-doping started at 300 °C and reached a maximum level of 5% doping by heating at 500 °C. Several grams of N-doped GO could be produced by the described method. It was further observed that NH_3 reduced GO more effectively than H_2 under the same conditions. The N-doping as well as the reduction was characterized by XPS and electrical transport measurements.

Here the efficiency of the N-doping tends to be dependent on the amount of oxygen groups at the defect and edge sites of GO.

In a similar manner, partially nitrogen-doped reduced GO nanoplatelets were produced by hydrothermal treatment of GO in a colloidal dispersion in the presence of hydrazine and ammonia (Figure 78).³⁷⁷ The structure and surface chemistry of the resulting GO nanoplatelets is strongly dependent on the temperature of hydrothermal treatments.

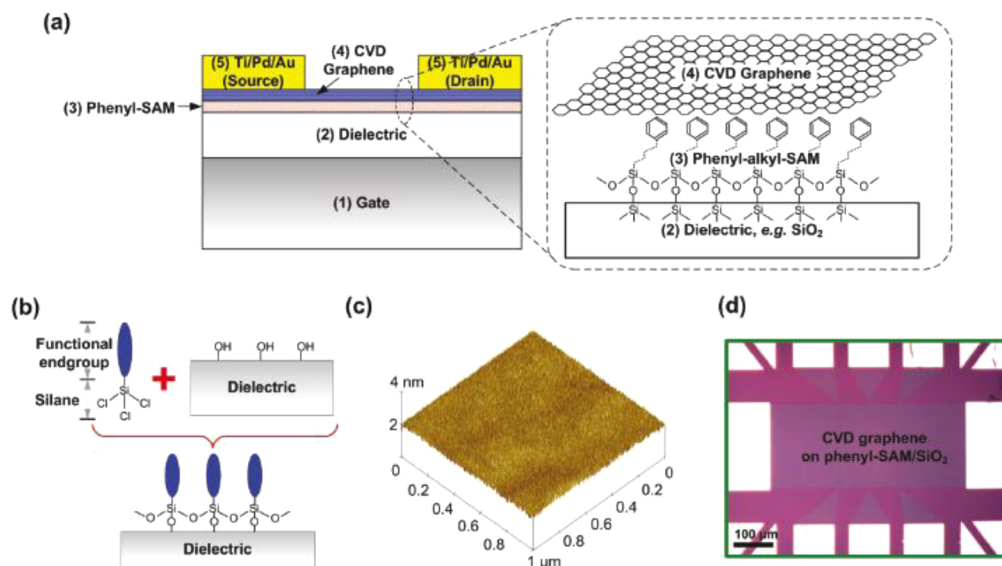


Figure 81. (a) A general bottom-gated graphene FET structure with phenyl-SAM interface engineering. (b) Illustration of chemical bonding of the organosilane SAM to the hydroxyl group-enriched dielectric surface. (c) AFM image of a spin-coated ultrasmooth phenyl-SAM with surface roughness of 0.1–0.2 nm in rms. (d) Microscopy image of a large-area, uniform CVD graphene as patterned to various shapes on a phenyl-SAM engineered silicon oxide wafer. Reprinted with permission from ref 390. Copyright 2011 American Chemical Society.

N-doped graphene has been directly synthesized using a CVD method, as demonstrated by Wei et al.³⁷⁹ The product was deposited on a Cu film catalyst when a mixture of CH_4/NH_3 was heated at 800 °C. Here the incorporation of nitrogen in the graphitic lattice occurred simultaneously with the formation of graphene layers. The N-doping of the product was confirmed by XPS and EDS spectra to be about 8.9%, so that the N-doped graphene behaves as an n-type semiconductor.

Nitrogen- or boron-doped graphene has also been produced using an arc discharge technique. As described by Panchokarla et al.,³⁸⁰ N-doped graphene sheets are produced by carrying out the arc discharge between carbon electrodes in the presence of hydrogen and pyridine or ammonia. To produce boron-doped graphene, it was necessary to use boron-stuffed graphite electrodes or a mixture of hydrogen and diborane vapor; the B-doped graphene showed a p-type semiconductor behavior. Large scale sheets consisting of co-doped N and B graphene sheets have been synthesized using a CVD approach, where the B and N form randomly distributed domains within the graphene plane.³⁸² The presence of these randomly distributed domains creates a typical semiconductor behavior in the graphene lattice.

In a different approach, N-doped graphene has been synthesized by a one-step solvothermal method through the reaction of tetrachloromethane and lithium nitride (Figure 79).³⁸¹ Gram scale production is easily obtained in the laboratory, showing that this method allows for scalable synthesis. Characterization results suggest that nitrogen species have been incorporated into the graphene structure with content in the range of 4.5–16.4%. The detailed atomic structures of such N-doping induced defects were investigated using STM.³⁸³ This revealed a perturbed electronic structure due to N doping.³⁸³

6. APPLICATION OF FUNCTIONALIZED GRAPHENE

6.1. Devices of Doped Graphene

There has been much interest in doping graphene because tunable electrical properties of graphene are attainable by instantaneous doping. Graphene can be doped by both electric

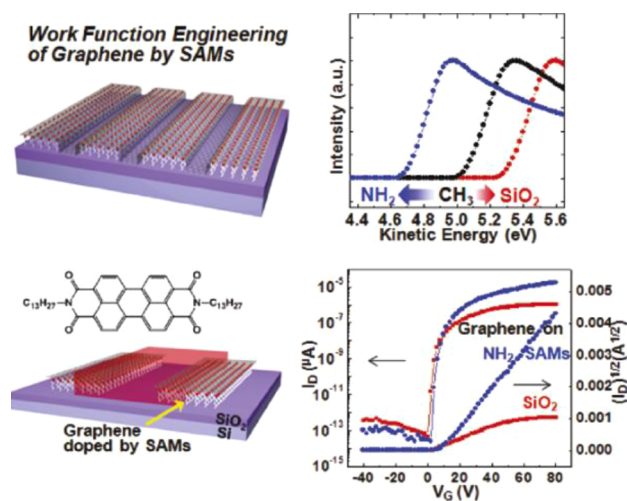


Figure 82. Transferred monolayer graphene on patterned self-assembled monolayer (SAM)-modified SiO_2 substrate (top left). UV photoemission spectra of the graphene films on different SAM-modified substrates show work function changes (top right). Chemical structure of N,N' -ditridenyl-3,4,9,10-perylene-tetracarboxylic diimide (PTCDI-C13) and schematic FET structure using PTCDI-C13 as an active layer and graphene as source/drain electrodes (bottom left). Transfer characteristics of PTCDI-C13 FETs with graphene electrodes on different SAM-modified SiO_2 's (bottom right). Reprinted with permission from ref 46. Copyright 2011 American Chemical Society.

field^{1,20,22} and chemical species.^{23,384} Depositing dopant atoms or simple molecules on graphene surface induces interstitial doping by charge transfer processes between graphene and dopant atoms, which results in a change in the work function of graphene. For example, to create p-type semiconductors, one can use water, NO_2 , and O_2 as dopants, while in the creation of n-type semiconductors NH_3 can be used (Figure 80).^{23,384–387} Simple charge transfer as well as carrier doping by electric field is limited to doping levels smaller than 10^{14} cm^{-2} , whereas higher doping

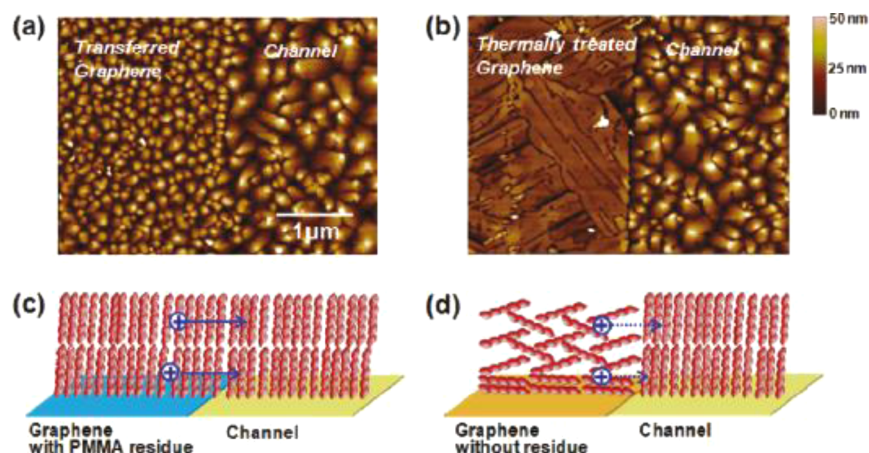


Figure 83. AFM images of pentacene films (50 nm) near the interface between SiO₂: (a) untreated graphene electrodes and (b) thermally treated graphene electrodes. Schematic representations of the possible molecular packing orientations near the interface between SiO₂ and (c) untreated graphene electrodes or (d) thermally treated graphene electrodes. Reprinted with permission from ref 391b. Copyright 2011 Wiley.

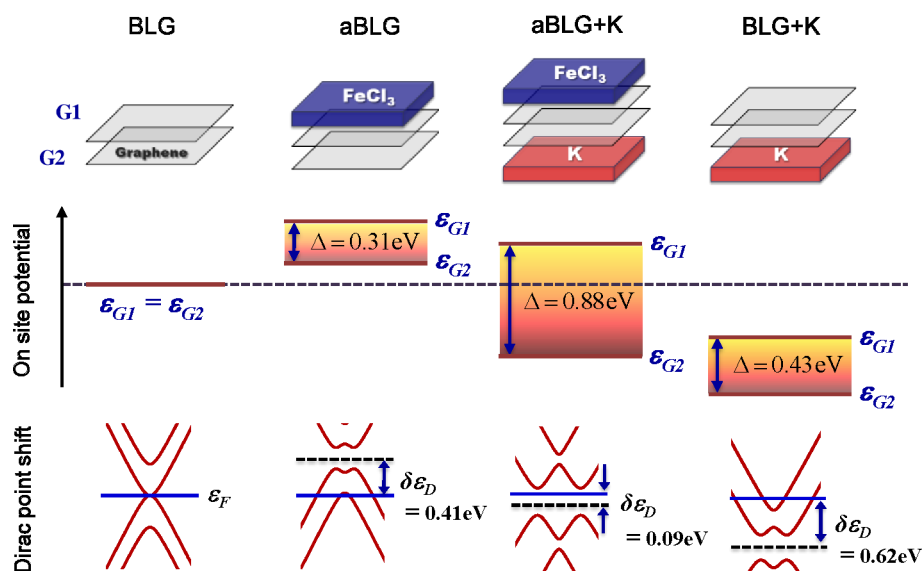


Figure 84. Schematic models of the bilayer graphene (BLG), the BLG doped with FeCl₃ (aBLG) composite system, the BLG dual-doped with FeCl₃ and K (aBLG+K), and the BLG doped with K (BLG+K) (top), tight binding parameters for the onsite potential difference (Δ) obtained by DFT calculation (center), and band structures calculated by tight binding method and the Dirac point shifts ($\delta\epsilon_D$) obtained by DFT calculation (bottom). Reprinted with permission from ref 394. Copyright 2011 American Chemical Society.

levels can be achieved using ionic polymer electrolytes or alkali atoms.^{388,389}

Most simple molecular doping in the atmosphere makes it difficult to control the position and magnitude of doping. For this reason, interstitial doping investigated so far is usually done under vacuum conditions to avoid unwanted adsorption of dopant molecules. Thus, stable doping methods, using organic molecules or polymeric molecules such as tetrafluoro-tetracyanoquinodimethane (F4-TCNQ), tetracyanoethylene (TCNE), aniline, anisole, benzene, chlorobenzene, or nitrobenzene, are required for use in applications.^{385–387} Aromatic molecules,³⁸⁵ including 1,5-naphthalenediamine (Na-NH₂), 9,10-dimethylanthracene (An-CH₃), 9,10-dibromoanthracene (An-Br), and tetrasodium 1,3,6,8-pyrenetetrasulfonic acid (TPA), can stably bind to single-layer graphene (SLG) through strong π - π interactions between their aromatic rings and the graphene. Electrical measurements of SLG/aromatic molecule composites suggest that the aromatic molecules impose carriers on the SLG.

Another method toward doped graphene is to deposit nanoparticles instead of unstable metallic atoms on the graphene surface, as described in section 4.

Self-assembled monolayers (SAMs) are ultrathin molecular films spontaneously formed at oxide surfaces or interfaces due to chemical or physical interactions of molecules with a substrate, frequently without necessity of high-vacuum or high-temperature processing.^{46,390–393} The robust ultrathin layer in a defined area is constructed by spontaneous chemical reaction at the interface, which makes SAMs technologically attractive for surface and interface engineering (Figure 81). In addition, surface energy, dipole moments, and chemical reactivity of the surface can be easily tuned by attaching functional groups to the SAMs. SAMs have received considerable attention due to their use in organic electronics as active materials or insulators. SAM-graphene systems are found to be very stable in high vacuum and ambient environments. The robustness and the large electronic effect suggest that the integration of a SAM with graphene

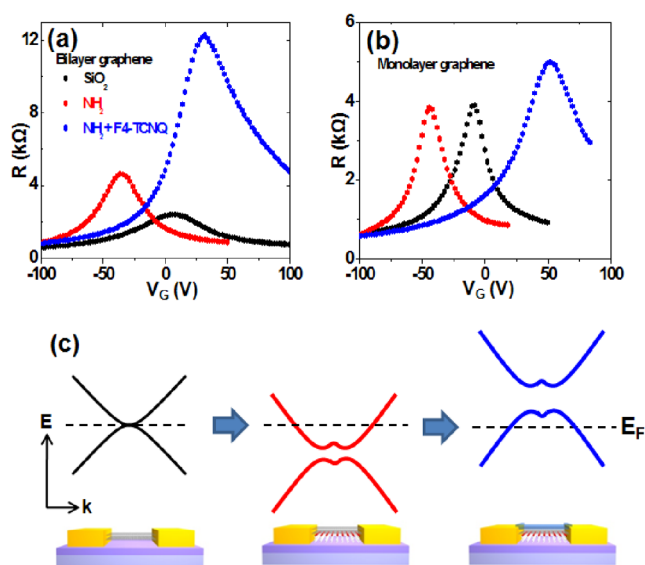


Figure 85. Current–voltage transfer characteristics of (a) bilayer graphene FETs and (b) monolayer graphene FETs with molecular doping agents: SiO₂, untreated SiO₂/Si (no doping); NH₂, NH₂-SAM modified SiO₂/Si (N-doping); F4-TCNQ, 2,3,5,6-tetrafluoro-7,7,8,8-tetracyanoquino-dimethane (thickness of 10 Å, p-doping). (c) The electronic band structures of bilayer graphene on untreated, NH₂-SAMs modified SiO₂/Si substrate, and F4-TCNQ deposited bilayer graphene on NH₂-SAM modified SiO₂/Si substrate (from left to right). Reprinted with permission from ref 47. Copyright 2012 Wiley.

provides a new and reliable method of carrier doping in graphene. The SAM doping approach offers the potential for

chemical modification of graphene electronic properties using methods of molecular engineering and self-assembly.^{390–393}

Recently, Liu et al.³⁹⁰ have investigated the physics associated with the dielectric–graphene interface for integrated back-gated FETs by controlling some of the detrimental scattering effects via application of a phenyl-SAM. Electrical characterization of the FET device with a phenyl-SAM interface exhibited a 150% improvement in extrinsic carrier mobility compared with the FET device with no SAM interface. Furthermore, the I – V characteristics exhibit no hysteresis during the process as the gate voltage is scanned from one polarity to the other, and it remains very stable and uniform for devices fabricated over a relatively large area. The authors further analyzed the I – V characteristics for devices with and without the phenyl-SAM, applying models previously developed to predict the Dirac point shift during the voltage sweep. From this analysis, the authors attributed the enhanced carrier mobility to reduced interfacial impurity and surface polar phonon scattering as well as the ultrasoft SAM surface. Additionally it was shown that the hysteresis present in devices at room temperature without the interface treatment was dominated by charge injection from the graphene to the graphene–dielectric interface. This finding was further supported by the Dirac point shift model results.³⁹⁰

In Figure 82, SAMs have been used as a buffer layer to induce instantaneous doping of graphene and tune the work function of graphene electrodes for high-performance organic field-effect transistors (OFETs).^{46,391} The doping type and position are determined by patterning SAMs with different functional groups. A microscopic study of the work function can be investigated by utilizing scanning Kelvin probe microscopy (SKPM).³⁹³

The fabrication of a pentacene organic transistor that utilizes graphene electrodes has been presented by Lee and co-

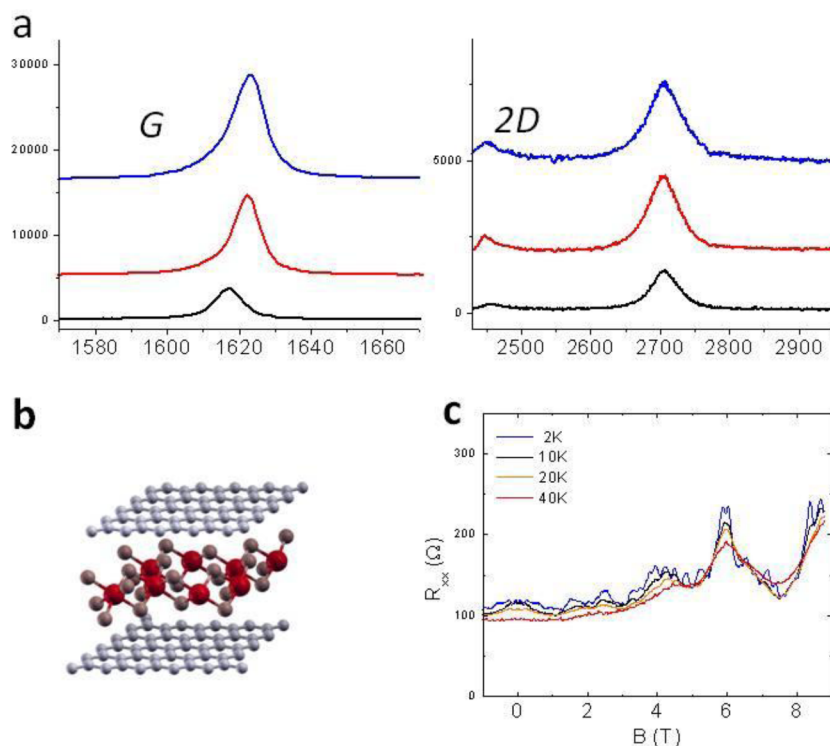


Figure 86. (a) Raman spectra of intercalated FLGs. (b) Atomic structural model; carbon atoms are shown as gray spheres, iron atoms as red, and chlorine atoms as brown. (c) Transport measurements of an intercalated bilayer device; Shubnikov-de Haas (SdH) oscillations seen in $R_{xx}(B)$ are recorded at temperatures 2, 10, 20, and 40 K. Reprinted with permission from ref 396. Copyright 2011 American Chemical Society.

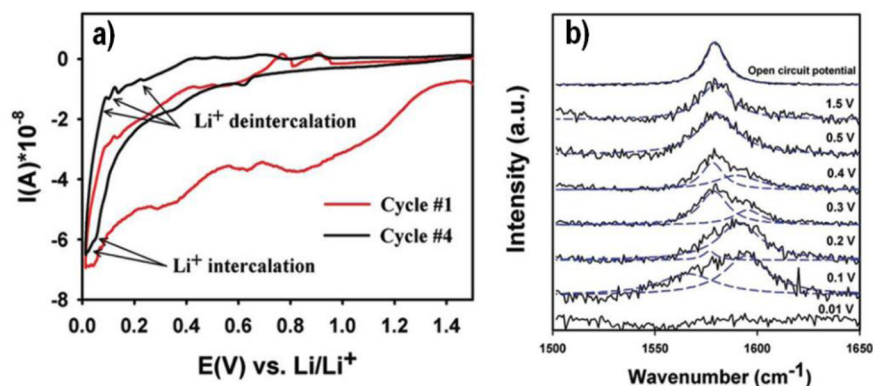


Figure 87. (a) First and fourth cyclic voltammograms of the Ni/FLG electrode in polymer electrolyte and (b) in situ Raman spectra of the Ni/FLG electrode at selected potentials during electrochemical lithiation. Reprinted with permission from ref 398a. Copyright 2010 American Chemical Society.

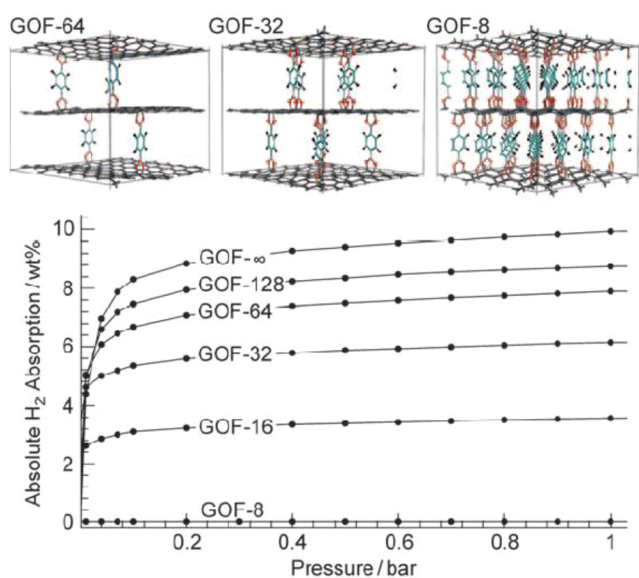


Figure 88. Grand canonical Monte Carlo simulations for ideal GOF- n structures with n graphene carbons per linker. The structures of three examples with $n = 64, 32,$ and 8 are also shown. GOF materials are formed of layers of GO connected by benzenediboric acid pillars. Reprinted with permission from ref 399. Copyright 2010 Wiley.

workers.³⁹¹ The polymer residues remaining on the graphene surface were shown to alter the performance of the transistor, with a stand-up orientation of pentacene formed on the polymer residue surface, which results in a molecular assembly that is optimal for charge transport (Figure 83). In contrast, epitaxial growth of pentacene on a polymer-free graphene surface results in a lying-down structure of the pentacene; this molecular assembly facilitated by π - π interactions between pentacene and graphene adversely affects lateral charge transport at the interface between electrode and channel.

These results ultimately improve the potential applications of graphene transistors toward VLSI circuits³⁹⁰ and graphene electrodes for high-performance organic field-effect transistors (OFETs).^{46,391} Chemical doping can decrease sheet resistance of graphene while maintaining its high transparency. Lee et al.³⁹² developed a new method to simultaneously transfer and dope chemical vapor deposition grown graphene onto a target substrate using a fluoropolymer as both the supporting and doping layer. This method was used to fabricate a flexible and transparent graphene electrode on a plastic substrate.

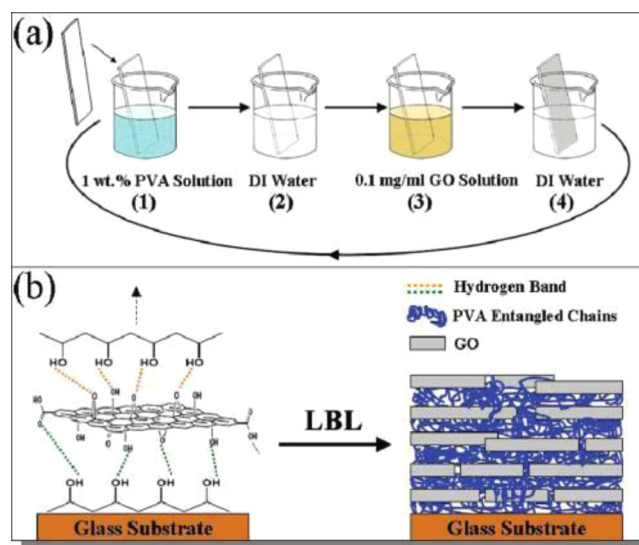


Figure 89. (a) Schematic representation of the layer by layer deposition procedure and (b) the assembly process of PVA/GO: (left) the interaction of a GO layer and PVA chains and (right) the internal architecture of PVA/GO. Reprinted with permission from ref 405. Copyright 2010 American Chemical Society.

The band gap opening of graphene is the most desired property in the device industry because it is vital to the application of graphene as field effect transistor (FET). Chemical doping of graphene can open the band gap of graphene. However, it accompanies significant Dirac point shifts, which give a low on/off current ratio and a poor switching property. Recently, both theoretical and experimental studies show how to make a wide band gap and reasonable Dirac point shift in graphene system by using dual doping of bilayer graphene. Yang et al.³⁹⁴ have investigated bilayer graphene (BLG) dual-doped with FeCl_3 acceptor and K donor by employing the first principles method taking into account van der Waals interaction. Due to high electronegativity of the FeCl_3 molecular layer, FeCl_3 adsorbed BLG is hole-doped. Also the asymmetric composite of BLG with the FeCl_3 layer adsorption is shown to exhibit an energy gap opening (Figure 84). By utilizing this asymmetric behavior, which increases the band gap, the bilayer graphene with dual FeCl_3 acceptor and K donor doping makes a significant energy gap opening (0.3 eV) with a proper Dirac point shift (-0.09 eV) toward practical FET device applications.

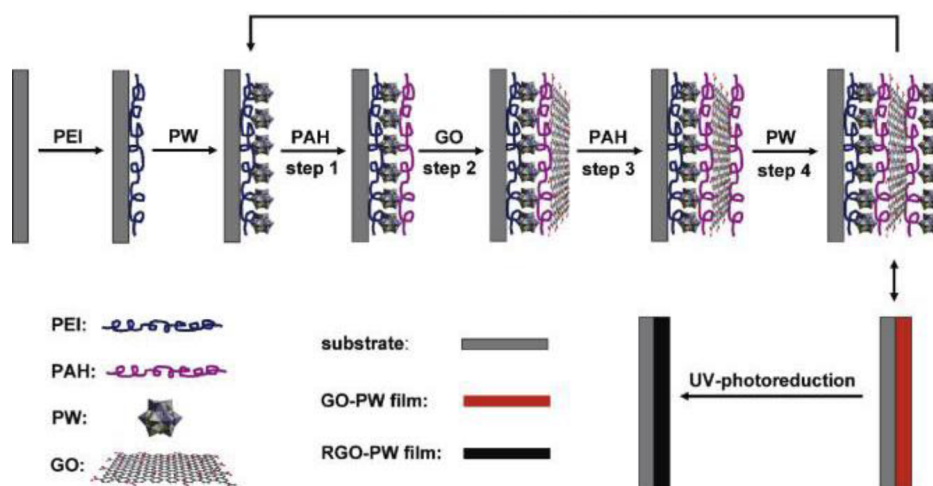


Figure 90. Schematic illustration of the LbL deposition of GO and PW clusters and the photoreduction of GO. Cationic polyelectrolytes polyethyleneimine (PEI) and PAH are used as electrostatic linkers. Reprinted with permission from ref 402. Copyright 2011 American Chemical Society.

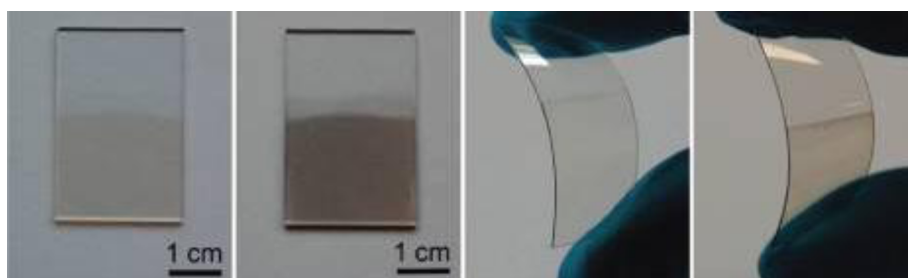


Figure 91. Optical images of a GO/PW multilayer film on a quartz substrate before (A) and after (B) 6 h of UV photoreduction and on a flexible PET substrate before (C) and after (D) 6 h of UV photoreduction. Both substrates were coated using a PET/PW precursor film. Reprinted with permission from ref 402. Copyright 2011 American Chemical Society.

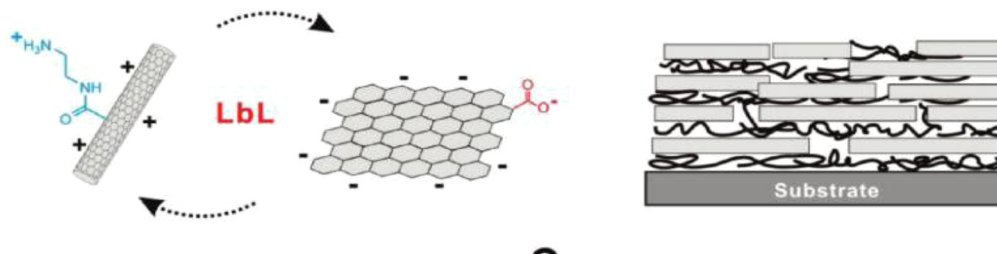


Figure 92. Schematic representation of a hybrid multilayer composite of functionalized MWNTs and RGO. Reprinted with permission from ref 401. Copyright 2010 American Chemical Society.

Park et al.^{46,47} developed a new method for band gap opening of bilayer graphene by dual molecular doping. The 2,3,5,6-tetrafluoro-7,7,8,8-tetracyanoquinodimethane (F4-TCNQ) molecules deposited onto bilayer graphene induce p-doping from the top, while NH_2 -functionalized self-assembled monolayers (SAMs) constructed on SiO_2/Si substrate induce n-doping from the bottom side. These dual doping-driven perpendicular electric fields with opposite directions remarkably increase the on/off current ratio of bilayer graphene field-effect transistors (FETs), which unambiguously proves that it is possible to open a band gap with two molecular dopants (namely, F4-TCNQ and NH_2 -functionalized SAMs) (Figure 85). Both theoretical and experimental results indicate that band gap opening of bilayer graphene can be accomplished by dual molecular doping, which does not require a complicated fabrication step for preparing a device with a dual-gate structure.

6.2. Multilayered Graphene Intercalates and Composites

Few layer graphene (FLG) can be chemically modified interstitially by intercalating molecules into the structure. Intercalation between layered crystalline materials and graphene occurs through van der Waals interactions, providing new chemical and physical functionality such as superconductivity and quasi-low-dimensional magnetism.³⁹⁵ An FeCl_3 bilayer graphene (BLG) intercalate has been synthesized and electrically characterized as a minimal graphite intercalation compound (GIC, Figure 86).³⁹⁶ Interestingly, the resistance behavior of this intercalation product is related to a magnetic transition. This work demonstrates the first step toward the synthesis of various different functional bilayer intercalates including sandwich-like structures.³⁹⁷

Besides the fundamental study of 2DESs (two-dimensional electron systems), FLG intercalation materials can be considered

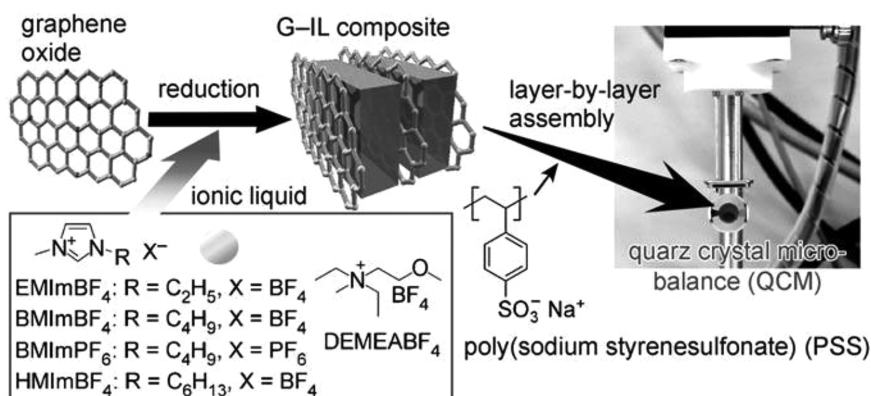


Figure 93. Schematic illustration of the preparation of a GO/ionic liquid multilayered composite and their LbL assembly on a quartz crystal microbalance (QCM). Reprinted with permission from ref 403. Copyright 2010 Wiley.

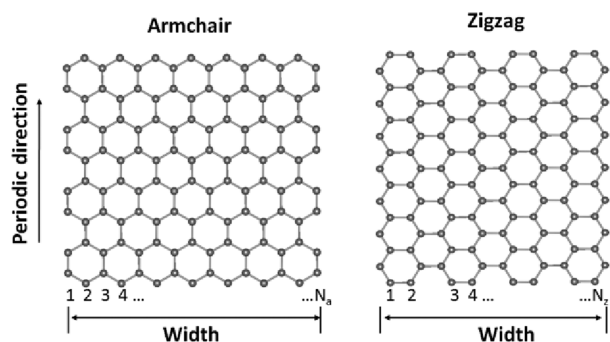


Figure 94. Structure of armchair and zigzag nanoribbons.

for storage applications based on their exotic material properties. For example, the intercalation of ionic Li⁺ in FLGs³⁹⁸ occurs during the electrochemical lithiation of FLGs (Figure 87). This is

explored due to its reversible Li⁺ intercalation/deintercalation capability in layered FLGs, which could potentially lead to a higher Li-ion storage capacity. Besides ion batteries, it would be possible to consider FLG intercalates for hydrogen storage applications.³⁹⁹

Instead of using multilayer graphenes, hydrogen can be stored between layers of GO, which are separated without filling the space between them. GO layers can be linked together to form a new layered structure, that is, GO framework (GOF, Figure 88).³⁹⁹ Such GOF structures have tunable pore widths, volumes, and binding sites depending on the linkers chosen and could exhibit interesting gas sorption properties. Ideal GOF structures can adsorb hydrogen up to 6 wt % at 77 K and 1 bar, a value higher than any other porous material known. The synthesized GOF materials exhibit 9 and 32 kJ/mol isosteric heat adsorption for H₂ and CO₂, significantly larger than those found in similar nanoporous materials. However, the current experimental

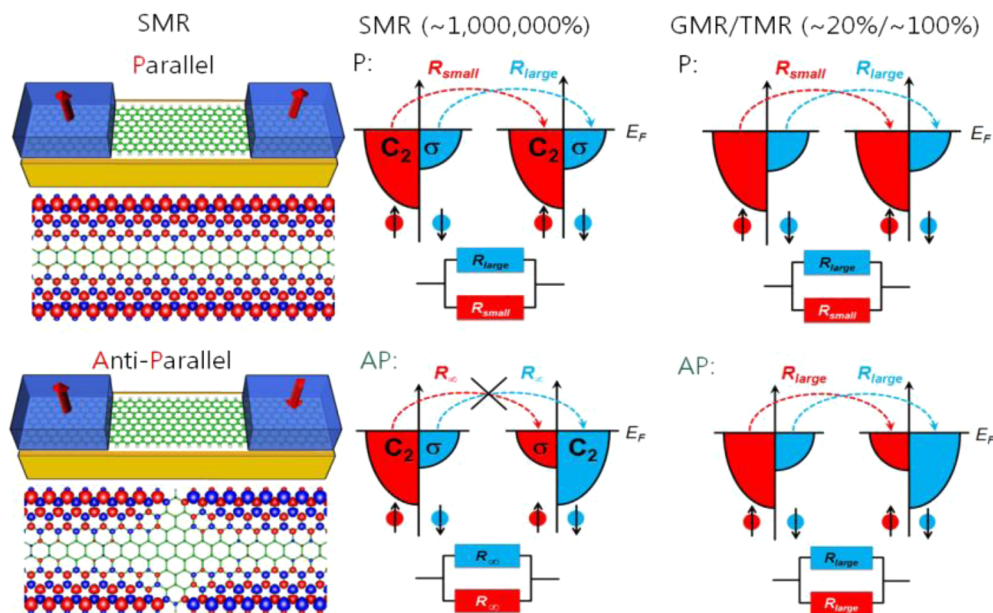


Figure 95. Schematic ZGNR-based spin-valve device (left) with parallel and antiparallel spin configurations and the corresponding spin-magnetization density isosurfaces. The blue boxes represent ferromagnetic electrodes to control spin polarization of the ZGNR device and the red arrows indicate the directions of spin configurations. In the isosurfaces, red/blue color denotes up/down spin, and a ZGNR skeleton is drawn in green color. Spin-transfer paths (right) from the left to right density of states of the ferromagnetic leads for parallel (P) and antiparallel (AP) spin configurations in a ZGNR spin-valve device are compared with those in a conventional spin-valve device. Reprinted with permission from refs 29 and 409. Copyright 2008 Nature Publishing group and Copyright 2010 American Chemical Society, respectively.

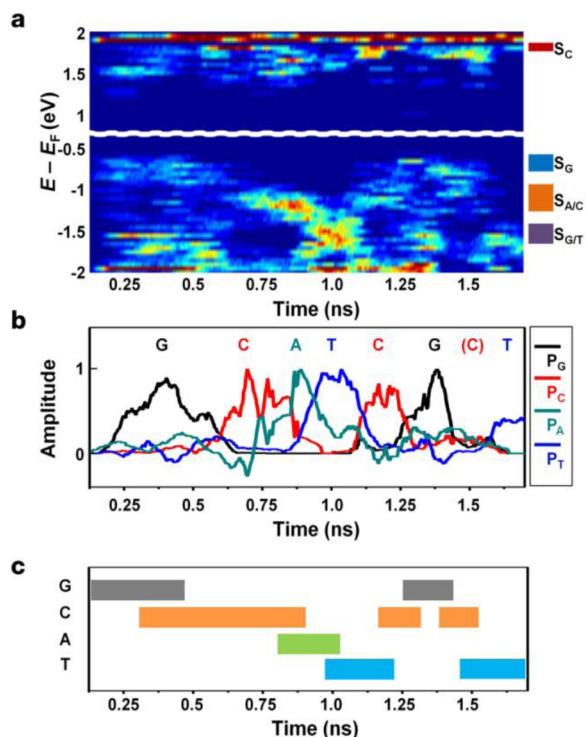


Figure 96. Simulation results of the transport property for 5'-GCATCGCT-3'. (a) Time-dependent histogram of the transmission peak positions (red (blue) denoting maximal (minimal) values). The histogram shows features of Cyt (S_C), Gua (S_G), Ade/Cyt ($S_{A/C}$), and Gua/Thy ($S_{G/T}$) corresponding to the band centered around $E - E_F = E_s = 1.8, -0.65, -1.2,$ and -1.65 eV, respectively. The height of each right box represents the energy range of integration for S_{base} . (b) Plots of $S_{base}(t)$ with respect to time as a ssDNA passes. The sequence GCATCGCT can be partly resolved. (c) Final base sequence obtained from the analysis of panel b and 2D TACF, $C(t, t_0; \tau)$ analysis. Reprinted with permission from ref 37. Copyright 2011 Nature Publishing Group.

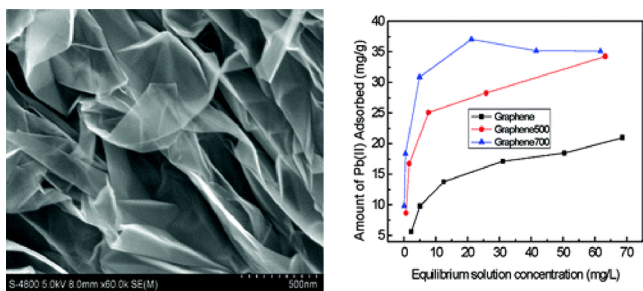


Figure 97. SEM image of a low-temperature exfoliated GNS (left) and effect of the pH on the adsorption capacity (right). Reprinted with permission from ref 417. Copyright 2011 American Chemical Society.

capacity observed is 1 wt % H_2 uptake at 1 bar for GOF; this value needs to be improved for future application.

The 2-D layer morphology of graphene offers the opportunity to form multilayered composite nanostructures by applying well-known techniques and procedures. The important properties of graphene such as transparency, conductivity, and mechanical strength can be combined with the properties of other components such as carbon nanotubes,^{400,401} polymers,^{402–406} etc., with fascinating results.

A graphene/polymer multilayered composite can be prepared in solution through a layer-by-layer (LbL) assembly technique (Figure 89). Shen et al.⁴⁰⁴ have covered RGO sheets with

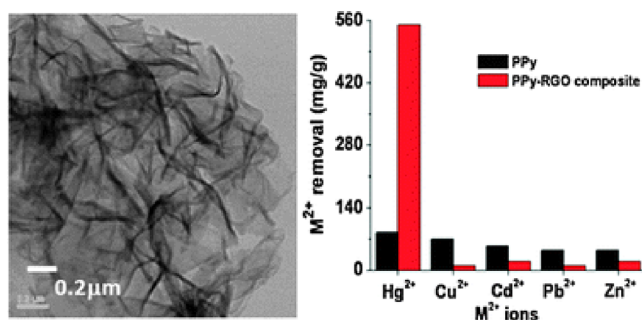


Figure 98. TEM image of graphene functionalized with polypyrrole (left) and selective adsorption of mercury from water (right). Reprinted with permission from ref 422. Copyright 2011 Royal Society of Chemistry.

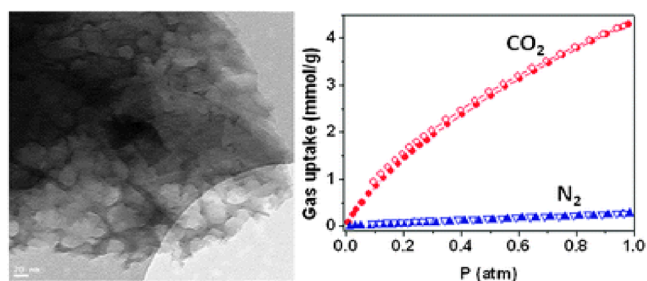


Figure 99. (left) TEM image of the polypyrrole graphene hybrid activated at 600 °C and (right) absorption selectivity of CO_2 gas over N_2 gas at 298 K. Reprinted with permission from ref 427. Copyright 2012 Royal Society of Chemistry.

poly(acrylic acid) (PAA) and polyacrylamide (PAM) through covalent attachment forming two charged composites: the negatively charged PAA/GO and the positively charged PAM/GO. The two polymeric GO composites were dispersible in water and the multilayered film was formed by a sequential adsorption of the two charged composites through electrostatic interactions. The same technique has been used for the preparation of a GO/poly(vinyl alcohol) multilayer composite material.⁴⁰⁵ A glass substrate was immersed in a dispersion of GO and a solution of poly(vinyl alcohol) PVA sequentially.

For example, a GO/polyoxometalate composite film has been prepared as follows.⁴⁰² GO and a Keggin-type polyoxometalate cluster $H_3PW_{12}O_{40}$ (PW) are alternatively deposited on a substrate via electrostatic adsorption (Figure 90). The PW cluster acts as a photocatalyst and reduces GO, yielding a product with good conductivity. The multilayered RGO/PW composite film can be produced on several substrates such as quartz glass, silicon wafers, and flexible polymers (Figure 91).

Positively charged ammonium-modified CNTs were employed between the RGO multilayers by the LbL deposition technique through electrostatic interactions (Figure 92). The CNT acts as a conducting bridge between GO sheets enhancing the conductivity and mechanical flexibility of the graphene film.⁴⁰¹

Through a LbL assembly, Ji et al.⁴⁰³ inserted ionic liquids between partially RGO layers and poly(sodium styrenesulfonate) (PSS) as shown in Figure 93. The multilayered composite has a higher affinity for toxic aromatic hydrocarbons than for their aliphatic analogues. Such multilayered composite materials can be used for a functionalized device like a gas sensor, with enhanced electrical/mechanical functionalities.

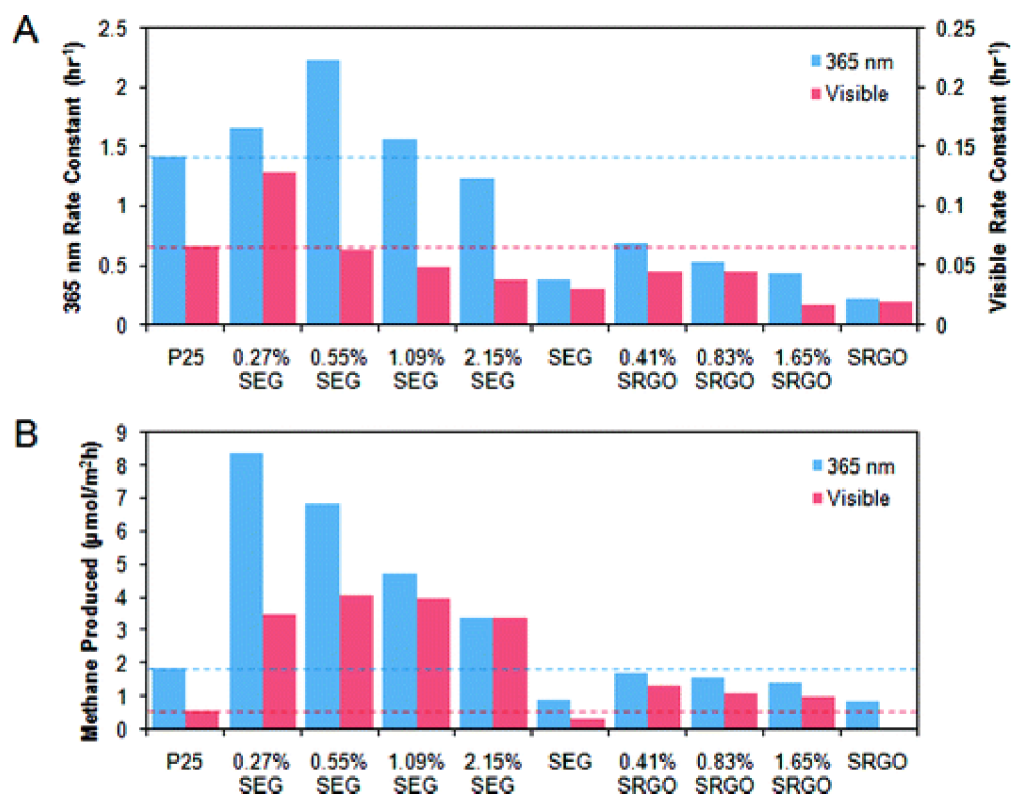


Figure 100. Photocatalytic activity of SEG–P25 and SRGO–P25 nanocomposites. (A) Pseudofirst-order CH₃CHO photo-oxidation rate constants for SEG–P25 and SRGO–P25 nanocomposites under ultraviolet (365 nm) and visible illumination. (B) CO₂ photoreduction for SEG–P25 and SRGO–P25 nanocomposites under ultraviolet (365 nm) and visible illumination. Reprinted with permission from ref 429. Copyright 2011 American Chemical Society.

6.3. Electronic/Spintronic Devices Including Ultrafast DNA Sequencing

Structural and electronic/magnetic properties of graphene nanoribbons (GNRs) have been intensively studied both experimentally and theoretically. Depending on their various edge structures, GNRs present different electronic properties ranging from normal semiconductors to spin-polarized half-metals (Figure 94). Unlike graphene sheets as a zero gap semiconductor, armchair GNRs open an energy band gap, as semiconductors with energy gaps, which enables the basic electric logic states. The electronic structures of GNRs as electric devices have been investigated based on theoretical calculations.⁴⁰⁷ Energy gaps decrease as a function of increasing ribbon widths arising from the quantum confinement effect, which can be characterized by $E_g \approx 1/W$. Thus, enhancing such I_{on}/I_{off} ratios by introducing an appreciable band gap has been a major issue in graphene-based logic devices. No magnetism has been found in armchair GNRs. In contrast, metallic zigzag GNRs (ZGNRs) are considered as an element for spintronic application.⁴⁰⁸

Since ZGNRs favor a ferromagnetic state, the ZGNR can be a potential spintronic device by controlling the spin state. Based on calculations of the quantum transport property for the ferromagnetic state with both the parallel spin configuration (ferromagnetic parallel; FMP) and the antiparallel spin configuration (ferromagnetic antiparallel; FMA), ZGNR exhibits an extreme enhancement of magnetoresistance (MR).²⁹ This abnormality arises not only from the spin symmetry, which is the major origin of the giant magnetoresistance (GMR) and the tunneling magnetoresistance (TMR), but also from the unique orbital symmetry of the ZGNR (Figure 95).^{29,409} For the ZGNR,

the occupied bands below the Fermi energy (E_F) have “ C_2 ” symmetry, while the unoccupied bands have “ σ ” symmetry. Since both occupied and unoccupied bands have orbital symmetries orthogonal to each other, spin-transfer to FMA is not allowed due to mismatching between the orbital symmetries at both sides, which lead to an ideal spin-valve with infinite MR value.

Although theoretical works have proposed and predicted many interesting properties of GNRs, the experimental realizations of GNRs are still not easy. Sub-50 nm nanoribbons were first fabricated by e-beam patterning and oxygen plasma etching from mechanically exfoliated graphene.⁴¹⁰ Although the process yielded I_{on}/I_{off} ratios of up to 10^4 , devices showed high variability due to the lack of control over edge termination. On the other hand, the challenge of synthesizing reproducible GNRs is an interesting one. Isolation of GNRs directly from bulk graphite involved sonication of expanded graphite in the presence of a polymer.^{59,411} The polymer acted to noncovalently functionalize and consequently stabilize nanoribbons formed by mechanical fracture. In the presence of the polymer, the ribbons can be suspended in organic solvents and then deposited by spin-coating. For such sub-10-nm GNRs, the band gap was inversely proportional to their width, with an energy gap of ~ 0.4 eV. This led to on–off ratios of up to 10^6 for the thinnest strips.⁴¹¹ In addition, recently, high-resolution temperature distribution was measured for a self-heated GNR.⁴¹²

Even though it is difficult to synthesize the ideal GNR with clear edge structures experimentally, theoretical results suggest that GNRs can be candidates for a sensitive molecular sensor as well as future electronic FET devices and spintronic devices. Recently, Cai et al.⁴¹³ have reported atomically precise bottom-up fabrication of GNRs. They used surface-assisted coupling of

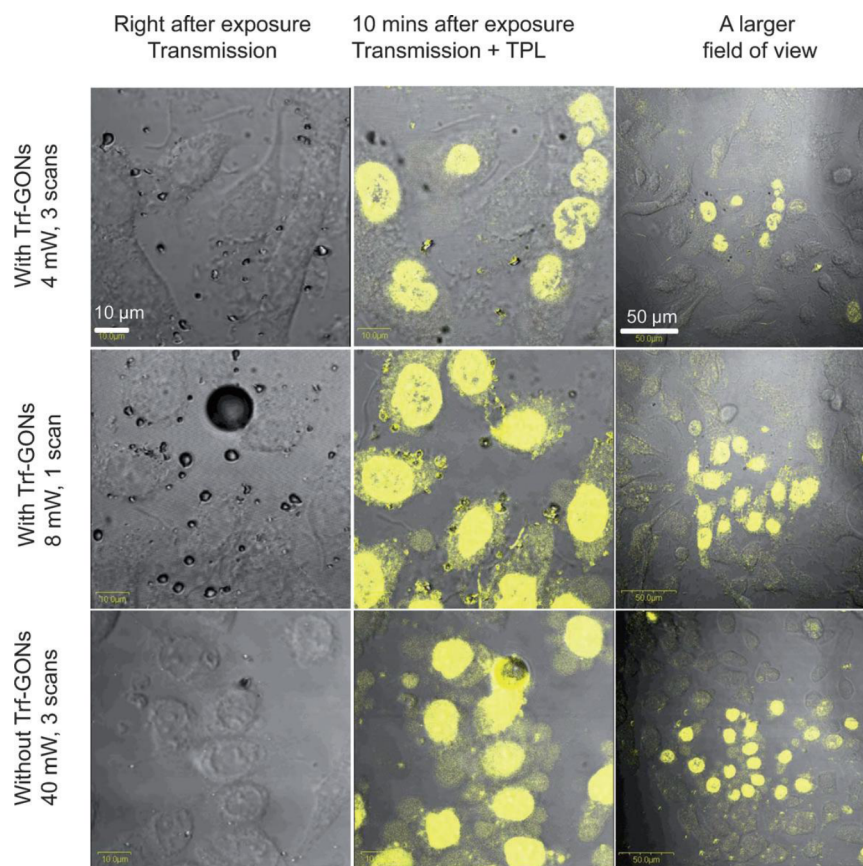


Figure 101. GON-induced cancer cell therapy. Reprinted with permission from ref 443. Copyright 2012 Wiley.

molecular precursors into linear polyphenylenes and their subsequent cyclodehydrogenation. Since edge structures, width, and length of GNRs are difficult to control, finding an effective way to overcome these problems becomes more and more important, both for academic research and for industry applications.

As an interesting application, a new method for ultrafast DNA sequencing using a GNR-based nanochannel device has been suggested.³⁷ While a single-strand DNA passes beneath a GNR, each nucleobase interacts with the GNR via π - π stacking interactions. Because the conducting properties of a GNR differ when they interact with different nucleobases due to the Fano resonance phenomena, real-time DNA sequencing is possible by analyzing the real-time conductance of the GNR. Since the stable π - π stacking interaction reduces stochastic motion of a nucleobase during the conductance measurement, the overlap between the signals from each nucleobase can be minimized. Thus, more reliable DNA sequencing can be realized after several statistical analyses including a data-mining approach and a two-dimensional transient autocorrelation function (Figure 96).

Modification of the electronic structure of nanoribbons by chemical functionalization is an effective way to make them efficient for their applications. This can be achieved through edge modification or adsorption of functional groups.^{43,414,415} A simple chemical modification of nanoribbons is to saturate the edges by atomic functional groups, such as -H, -O, -F, -OH, and -NH₂, which change electronic/magnetic states of GNRs. Working on obtaining desirable properties by modifying nanoribbons with appropriate functional groups will help us find the suitable form of graphene nanoribbons for each application. Modification with various types of elements and

functional groups can give us a variety of properties, for example semiconductivity with a wide range of band gaps, that is, metallic, ferromagnetic, antiferromagnetic, half-metallic, or half-semiconducting.

6.4. Green Chemistry

Graphene-based materials display green chemistry applications such as water remediation, CO₂ capture, and renewable energy production.^{30,416–432}

For water remediation, graphene needs to be functionalized to be dispersible in solution. Indeed, graphene has been shown to be effective at absorbing organic pollutants from aqueous solutions via π - π and other electrostatic interactions. In several cases, small organic molecules or surfactants have been used to disperse graphene in organic media or water. These molecules/surfactants stack permanently on the graphene sheets, thereby preventing aggregation. This kind of dispersion could be characterized as a noncovalent type of chemical functionalization, because these molecules are immobilized on the graphene surface via π - π stacking, H bonds, electrostatic forces, etc.

Xu et al.⁴¹⁶ showed that bisphenol A could be removed from an aqueous solution with a higher capacity than that with other known carbonaceous adsorbents. The high capacity of adsorption is believed to be due to hydrogen bonding as well as π - π interactions. Huang et al.⁴¹⁷ have shown that graphene can be used to absorb Pb(II) cations from aqueous solution. The authors noted that the adsorption capacity was strongly dependent on solution pH (Figure 97). In a similar way, Vasudevan and Lakshmi⁴¹⁸ have demonstrated that phosphate anions can be removed from aqueous solutions by graphene at an optimal pH value of ~ 7 . The adsorption kinetics followed a

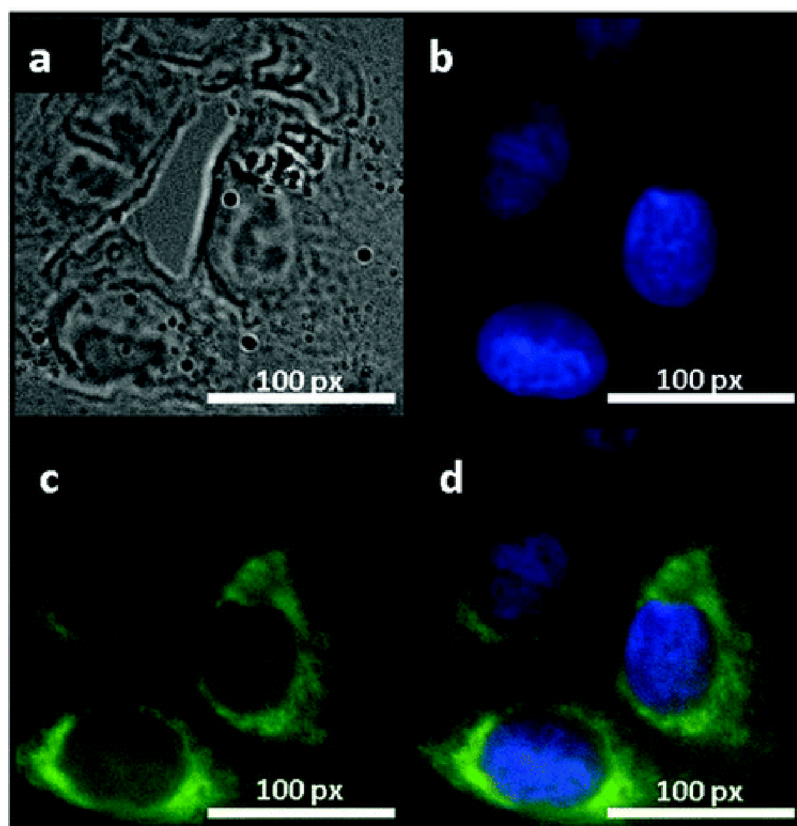


Figure 102. Fluorescent images of human breast cancer cell T47D after incubation with green QDs for 4 h: (a) phase contrast picture of T47D cells; (b) individual nucleus stained blue with DAPI; (c) agglomerated green QDs surrounding each nucleus; (d) the overlay high contrast image of nucleolus stained with blue DAPI and QDs (green) staining. Reprinted with permission from ref 445. Copyright 2012 American Chemical Society.

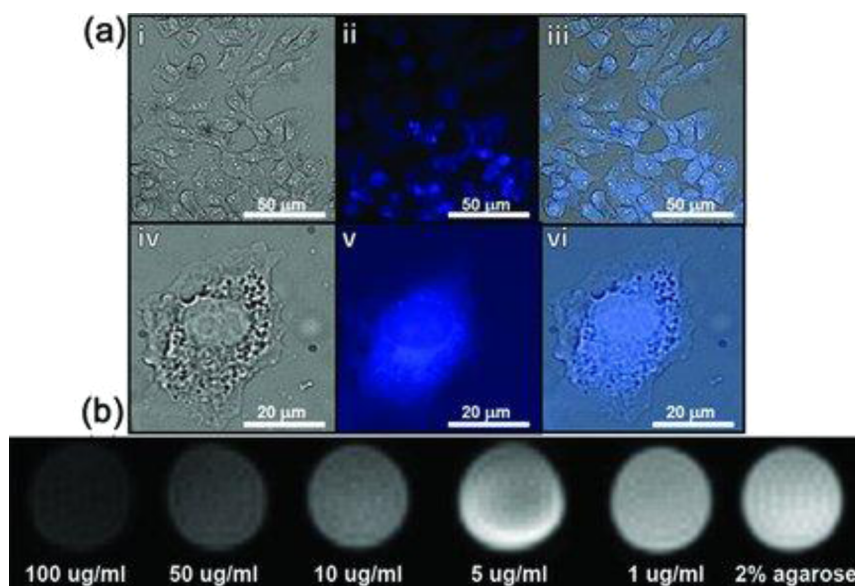


Figure 103. (a) In vitro fluorescence microscopy images of T47D cells treated with GO-F ($50 \mu\text{g mL}^{-1}$) for 24 h. (i–iii) Low magnification images of T47D cells: (i) phase contrast picture, (ii) fluorescence images of GO-F, and (iii) overlay of images i and ii. (iv–vi) High magnification images of an individual T47D cell: (iv) phase contrast picture of an individual T47D cell, (v) fluorescence image of GO-F, and (vi) overlay of images iv and v. (b) T2-weighted MR image showing strong T2 contrast in agarose phantoms. It shows alginate phantoms doped with different concentrations (as shown) of GO-F. The T2-weighted image was acquired in a 7 T scanner with multislice multiecho sequence. The T2 relaxivity was $297.06 \text{ mM}^{-1} \text{ s}^{-1}$. Reprinted with permission from ref 447. Copyright 2012 Wiley.

second-order kinetic model, suggesting that the absorption was chemically controlled.⁴¹⁸ GO has been shown by Zhao et al.⁴¹⁹ to be an effective absorbent of both Cd(II) and Co(II) from large

volumes of water. Yang and co-workers⁴²⁰ further showed that methylene blue can be effectively removed from aqueous solutions using GO; the authors recorded removal efficiency

higher than 99%. Sulfonated graphene nanosheets prepared from GO were shown by Zhao and colleagues⁴²¹ to be highly effective at the removal of naphthalene and 1-naphthol, with very high absorption capacities. Chandra and Kim⁴²² functionalized graphene sheets with polypyrrole (PPy), with the resulting composite material showing high and selective absorption capacity for Hg(II) cations (Figure 98).⁴²² The presence of graphene in PPy enhances the charge density of the pyrrolic nitrogen, thus increasing the electrostatic interaction between adsorbate and adsorbent. Sui et al.⁴²³ have shown that carbon nanotube–graphene hybrid aerogels fabricated by supercritical CO₂ drying of their hydrogel precursors display extremely high desalination capacity, high binding capacities to some heavy metal ions and high adsorption capacities for dye stuffs. This hybrid material shows promise in water purification due to its high versatility, which can be attributed to its light weight, high conductivity, large BET surface area, and hierarchically porous structure.

Graphene sheets decorated with magnetite nanoparticles have been shown by Chandra et al.³⁰ to be extremely effective in As(III) and As(V) removal. The benefit of using this magnetic graphene material in water remediation is that it can be separated easily using an external magnetic field once absorption has taken place. In a similar manner, Geng et al.⁴²⁴ synthesized RGO/Fe₃O₄ composites for dye removal from aqueous solutions.⁴²⁴ They demonstrated that by simple annealing in moderate conditions, this hybrid adsorbent can be easily and efficiently regenerated for reuse with hardly any compromise of the adsorption capacity. Graphene decorated with photocatalytically active SnO₂ and TiO₂ has been employed in the degradation of dyes under visible light irradiation as illustrated by Zhang et al.⁴²⁵ The degradation activity of these materials were shown to be higher than that of the commercially available P25 benchmark catalyst. Zhang and co-workers⁴²⁶ have reported that a TiO₂/RGO hybrid material is capable of efficient Cr(VI) to Cr(III) reduction.

The greenhouse gas CO₂ can be captured using N-doped porous graphene with a large surface area as demonstrated by Chandra et al.⁴²⁷ The authors achieved a high selective absorption capacity of 4.3 mmol/g CO₂ at 298 K, thereby showing the composite materials potential for industrial application (Figure 99). In a similar manner Mishra and Ramaprabhu⁴²⁸ have shown that by using polyaniline decorated graphene sheets CO₂ could be reversibly captured. The increase in CO₂ absorption over RGO sheets is attributed to the chemical interaction of CO₂ molecules with the nitrogen containing functional groups of the polyaniline.

Beside “end-of-pipe” or remediation issues, renewable energy production is conceptualized as alternative processes for green fuels in the near future. The current trend of sustainable technology is the harvesting of solar energy, specifically photo-assisted water splitting and photovoltaic conversion. Liang and colleagues⁴²⁹ have reported that TiO₂ modified nanographene enhances the photocatalytic reduction of CO₂ 7 times compared with pure TiO₂. The importance in this work is the role of less-defective graphene in the hybrid photocatalyst. This work illustrates the use of the nanocomposite in solar cells as it facilitates the diffusion of photoexcited electrons to the reactive sites (Figure 100).

In water splitting, the performance of semiconductor nanomaterials can be significantly enhanced with the electronic support of graphene. In the system of BiVO₄/RGO composite connected to a collecting electrode, which was investigated by Ng

et al.,⁴³⁰ the water splitting reaction electrophotochemically occurred with a 10-fold enhancement of H₂ evolution in comparison with pure BiVO₄ under visible illumination. Xiang and co-workers⁴³¹ have shown that photocatalytic H₂ production can be achieved in the presence of a TiO₂/MoS₂/graphene nanocomposite. The positive synergetic effect between the MoS₂ and graphene sheets can efficiently suppress charge recombination, improve interfacial charge transfer, and provide a greater number of active adsorption sites and photocatalytic reaction centers for H₂ production. Graphene nanomaterials also have been used as effective replacements for Pt-based materials (Pt–C) in the oxygen reduction reaction (ORR) as has been reported by Liang and colleagues.⁴³² They showed that a Co₃O₄/N-doped graphene hybrid material exhibits comparable electrocatalytic performance with superior stability compared with Pt-based materials (Pt–C) in alkaline solutions for the ORR reaction, this result shows that this material can be applied to fuel cells. Graphene–CNT complexes have also been shown to be excellent ORR electrocatalysts. The bis-(trifluoromethanesulfonyl)amide doped graphene could enhance the power conversion efficiency of solar cell to 8.6% in producing electricity from solar energy.⁴³³

6.5. Bio-imaging

Graphene can be made luminescent (i.e., quantum dots) by inducing a band gap. This can be achieved by reducing the connectivity of the π -electron network using chemical or physical methods.^{434–436} This makes graphene a strong candidate for bioimaging applications because it is biocompatible and displays fluorescence in the infrared and near-infrared.^{435–440}

Sun et al.⁴⁴¹ reported that pegylated (poly(ethylene glycol)) nanographene oxide (NGO) displays photoluminescence in the visible and infrared regions. They showed that the anticancer drug doxorubicin could be physisorbed onto the pegylated NGO surface that had been functionalized with antibodies. These antibodies allowed for selective killing of cancer cells in vitro, which could be monitored using fluorescence. In a similar manner, Peng and co-workers⁴⁴² demonstrated that fluorescein-functionalized pegylated graphene oxide (GO) could be used in intracellular imaging. The poly(ethylene glycol) spacer was introduced to prevent GO-induced quenching of the conjugated fluorescein. Moreover, the composite material exhibited excellent pH tunable properties. Li and colleagues⁴⁴³ have shown that pegylated NGO functionalized with transferrin can be used for two-photon luminescence cell imaging and phototherapy. It was observed that irradiation by a laser source creates microbubbling in the presence of NGO, which causes instant cell damage at an order of magnitude lower irradiation power (Figure 101). It was noted that the damage caused by the irradiation was extremely site specific, only causing cell death at the point of irradiation, thereby offering localized therapy.

Graphene quantum dots (GQDs) have been used for cellular imaging due to their low toxicity and high photoluminescence yield as has been illustrated by Zhu et al.⁴⁴⁴ The authors showed that the GQDs synthesized by a one-step solvothermal method display biocompatibility as well as low cytotoxicity, making them excellent bioimaging agents. Peng and co-workers⁴⁴⁵ reported that GQDs can be synthesized from readily available pitch carbon fibers via chemical exfoliation. It was shown by the authors that the photoluminescence of the GQDs can be tailored by changing the reaction temperature. The QDs were shown to display minimal toxicity and were employed as imaging agents in two human breast cancer cell lines (Figure 102).

Hu et al.⁴⁴⁶ have demonstrated that GO functionalized with CdSe/ZnS quantum dots can be used for visible-light imaging and near-infrared phototherapy of cancer cells. The authors showed that as the QDs are irradiated in the near-infrared region they display a reduction in fluorescence, thereby making this composite material suitable for in situ monitoring of the treatment. Narayanan and co-workers⁴⁴⁷ have shown that NGO functionalized with Fe₃O₄ can be used as a dual imaging material, utilizing photoluminescence as well as magnetic resonance imaging (Figure 103).

Kim et al.⁴⁴⁸ reported that GO modified with low-molecular weight branched polyethylenimine (BPEI-GO) is able to act as a cationic gene carrier. It was shown that the composite had a high delivery efficiency and biocompatibility when used in transfection studies. The use of the composite for bioimaging was shown when a labeled DNA strand was attached and the movement of the composite into the cells was monitored using confocal microscopy. Mao and colleagues⁴⁴⁹ have reported that *p*-sulfonated calyx[6]arene modified graphene can be used as a “turn on” fluorescent probe for L-carnitine both in vitro and in living cells. The as formed composite displays good stability in biological systems as well as a low toxicity, making this composite material potentially useful in imaging as well as drug delivery.

7. SUMMARY AND OUTLOOK

In 2004, the initial measurements of the electrical conductivity of graphene by Geim and Novoselov sent ripples of excitement through the scientific community. In the past years, the initial interest in the so-called “wonder” material has not faded, with a number of potential applications already proposed ranging from water remediation to supercapacitors, DNA-sequencing, photocatalysts, and oxygen reduction reaction catalysts. This says that there is clearly much work to still be done to understand the properties of graphene and functionalized graphene, thereby opening new avenues of research. One just has to consider the structure of GO to realize that there are multiple manipulations that can be chemically achieved, if only we understood the structure fully.⁴⁵⁰ This review provides insight into the various ways to functionalize graphene and graphene derivatives, thereby expanding the number of potential applications for graphene-based materials. The functionalization modes can be classified according to the method and materials used and as such have been categorized as covalent functionalization, noncovalent functionalization, substitutional doping of graphene, and hybridization with nanoparticles, nanowires, and other materials. These various methods of functionalization offer various ways to expand on the current uses of graphene, that is, bioimaging or band gap opening, which can be used in electronics.

Graphene as a 2-D material still suffers from controlled synthetic growth conditions, especially when graphene derivatives are considered. It is imperative that these synthetic issues are addressed so that graphene and its derivatives can attain the highly promised application potential. With improved synthetic procedures graphene should be able to be employed far more easily in electronics as well as other applications that require fast electron transfer like photocatalytic applications toward renewable energy. The 3-D manipulation of the 2-D graphene material is another very important issue to be addressed as the manipulation of graphene into higher order nanostructures is already showing promise in supercapacitors,⁴⁵¹ fuel cells,⁴⁵² water remediation,⁴²² and drug delivery⁴⁵³ among others. However, as has been noted in the main text, the main

applications of graphene and graphene composite materials will more than likely be in devices.⁴⁵⁴

The use of graphene nanoparticle materials is another important issue that needs to find solutions with respect to repeatable and controllable synthetic procedures if their true potential is to be attained. The performance of these graphene nanocomposite materials are highly dependent on the architecture of the nanoscale building blocks, which can often result in nonrepeatable experiments, which makes this another important point that needs to be addressed. It is only with an advance in these synthetic areas that the promised uses of graphene nanocomposite material in green chemistry will finally be achieved. It may be that for photocatalytic water splitting the separation of holes and electrons can be successfully achieved using a graphene nanoparticle composite material.

Whatever the future holds for graphene research, one can be assured that there will continuously be interesting topics because the material has already found interesting applications in fields as far apart as stem cell differentiation,⁴⁵⁵ highly selective separation,⁴⁵⁶ graphene–nanowire hybrid structure based photoconductive devices,⁴⁵⁷ graphene charge-doping based π plasmon control,⁴⁵⁸ and high-resolution spectroscopy.⁴⁵⁹ Looking toward the future use of graphene, it may be that in expanding on the already studied synthetic procedures lies a key to unlocking a new realm of opportunities for this material.

AUTHOR INFORMATION

Corresponding Author

*R.Z.: e-mail address radek.zboril@upol.cz; telephone +420-58-563-4947; fax +420-58-563-4958. K.S.K.: e-mail address kim@postech.ac.kr; telephone +82-54-279-2110; fax +82-54-279-8137.

Notes

The authors declare no competing financial interest.

Biographies



Vasilios Georgakilas received his B.Sc. and Ph.D. degrees in Chemistry and Organic Chemistry from the University of Ioannina (Greece) in 1989 and 1998, respectively. He then worked in the Institute of Material Science of N.CSR “Demokritos” and at the University of Trieste as a Postdoctoral Fellow and Research Associate. In 2010, he was elected Assistant Professor in the Material Science Department of the University of Patras. His research interest lies in the functionalization of carbon nanostructured materials and their application.



Michal Otyepka received his Ph.D. degree in Physical Chemistry at the Palacky University, Olomouc (2004). Currently, he is a head of the Department of Physical Chemistry at the Palacky University, Olomouc, and senior researcher at Regional Centre of Advanced Technologies and Materials, Palacky University, Olomouc. His research is focused on modeling of biomacromolecules, complex molecular systems, and hybrid materials.



Athanasios B. Bourlinos holds B.Sc. (1991–1995), M.Sc. (1997–1999), and Ph.D. (1999–2002) degrees in Chemistry from Athens University, Greece. He spent 2 years (2002–2004) as a postdoctoral fellow at the Materials Science & Engineering Department, Cornell University (Ithaca NY, USA), 6 years (2005–2011) as a research associate at the Institute of Materials Science, NCSR “Demokritos” (Athens, Greece), and 1 year (2011–2012) as a research associate at the Physics Department, University of Ioannina (Ioannina, Greece). He currently holds a position as Assistant Professor at the Physics Department, University of Ioannina. His research area focuses on the synthesis or surface modification, characterization, and properties of nanoscale materials with emphasis on carbon nanostructures.



Vimlesh Chandra studied Natural Sciences at Lucknow University and received his Ph.D. degree from Indian Institute of Technology, Kanpur (2009). He has been a postdoctoral research fellow in the Department of Chemistry at Center for Superfunctional Materials at Pohang University of Science and Technology since January 2009. He is developing graphene functionalized materials for environmental application.



Namdong Kim received his Ph.D. degree in experimental condensed matter physics at Pohang University of Science and Technology (POSTECH), Korea (2005). He was a postdoctoral research scientist at the Physics department, Columbia University (through 2009). Currently, he is a research assistant professor at the Chemistry department of POSTECH and focuses on graphene-related phenomena.



K. Christian Kemp received his M.Sc. in Chemistry from the University of the Free State, South Africa. He is currently pursuing a Ph.D. at the Department of Chemistry, Pohang University of Science and Technology, under the guidance of Prof. Kwang S. Kim.



Pavel Hobza received his Ph.D. (with R. Zahradnik) degree in Prague. After postdoctoral study with Camille Sandorfy at the Université de Montreal, he spent several periods as a visiting professor and a visiting scientist at Montreal, Erlangen, and Muenchen. In 2001, he moved from Heyrovsky Institute of Physical Chemistry, Academy of Sciences of the Czech Republic, to the Institute of Organic Chemistry and Biochemistry where he is currently Head of Department of Molecular Modeling. He is a professor of Physical Chemistry at the Charles University in Prague. His research interests focus on molecular interactions and their role in physical chemistry and biodisciplines.



Radek Zboril received his Ph.D. degree at the Palacky University, Olomouc. After the Ph.D. study, he underwent several foreign stays at the universities in Tokyo, Delaware, and Johannesburg. Currently, he is a professor at the Department of Physical Chemistry and a general director of the Regional Centre of Advanced Technologies and Materials at the Palacky University, Olomouc. His research interests focus on nanomaterial research including iron and iron oxide based nanoparticles, silver nanoparticles, carbon nanostructures, and magnetic nanoparticles and their syntheses, physicochemical characterization, and applications in the field of catalysis, water treatment, antimicrobial treatment, medicine, and biotechnologies.



Kwang S. Kim received his Ph.D. degree from University of California, Berkeley. He was a postdoctoral fellow at IBM and a visiting professor or scientist at Rutgers University, MIT, and Columbia University. Currently, he is a professor in the Department of Chemistry and the director of the Center for Superfunctional Materials at Pohang University of Science and Technology. His research interests include design and development of novel nanomaterials and molecular devices.

ACKNOWLEDGMENTS

This work was supported by Korea NRF (National Honor Scientist Program Grant 2010-0020414, WCU Grant R32-2008-000-10180-0), KISTI (Grant KSC-2011-G3-02), Grant Agency

of the Czech Republic (Grant P208/12/G016), Grant Agency of the Academy of Sciences of the Czech Republic (Grant KAN115600801), Operational Program Research and Development for Innovations – European Regional Development Fund (Grant CZ.1.05/2.1.00/03.0058), and Operational Program Education for Competitiveness – European Social Fund (Grant CZ.1.07/2.3.00/20.0017). This work was also a part of the research project RVO:61388963 of the Institute of Organic Chemistry and Biochemistry, Academy of Sciences of the Czech Republic. The authors deeply thank Dr. J. Tucek (Palacky University, Olomouc, Czech Republic) for the manuscript editing.

REFERENCES

- (1) Novoselov, K. S.; Geim, A. K.; Morozov, S. V.; Jiang, D.; Zhang, Y.; Dubonos, S. V.; Grigorieva, I. V.; Firsov, A. A. *Science* **2004**, *306*, 666.
- (2) Berger, C.; Song, Z. M.; Li, X. B.; Wu, X. S.; Brown, N.; Naud, C.; Mayou, D.; Li, T. B.; Hass, J.; Marchenkov, A. N.; Conrad, E. H.; First, P. N.; de Heer, W. A. *Science* **2006**, *312*, 1191.
- (3) Stankovich, S.; Dikin, D. A.; Dommett, G. H. B.; Kohlhaas, K. M.; Zimney, E. J.; Stach, E. A.; Piner, R. D.; Nguyen, S. T.; Ruoff, R. S. *Nature* **2006**, *442*, 282.
- (4) Li, D.; Muller, M. B.; Gilje, S.; Kaner, R. B.; Wallace, G. G. *Nat. Nanotechnol.* **2008**, *3*, 101.
- (5) Hernandez, Y.; Nicolosi, V.; Lotya, M.; Blighe, F. M.; Sun, Z. Y.; De, S.; McGovern, I. T.; Holland, B.; Byrne, M.; Gun'ko, Y. K.; Boland, J. J.; Niraj, P.; Duesberg, G.; Krishnamurthy, S.; Goodhue, R.; Hutchison, J.; Scardaci, V.; Ferrari, A. C.; Coleman, J. N. *Nat. Nanotechnol.* **2008**, *3*, 563.
- (6) Kim, K. S.; Zhao, Y.; Jang, H.; Lee, S. Y.; Kim, J. M.; Kim, K. S.; Ahn, J.-H.; Kim, P.; Choi, J.-Y.; Hong, B. H. *Nature* **2009**, *457*, 706.
- (7) Li, X.; Cai, W.; An, J.; Kim, S.; Nah, J.; Yang, D.; Piner, R.; Velamakanni, A.; Jung, I.; Tutuc, E.; Banerjee, S. K.; Colombo, L.; Ruoff, R. S. *Science* **2009**, *324*, 5932.
- (8) Bae, S.; Kim, H.; Lee, Y.; Xu, X.; Park, J.-S.; Zheng, Y.; Balakrishnan, J.; Lei, T.; Kim, H. R.; Song, Y. I.; Kim, Y. J.; Kim, K. S.; Ozyilmaz, B.; Ahn, J.-H.; Hong, B. H.; Iijima, S. *Nat. Nanotechnol.* **2010**, *5*, 574.
- (9) Reina, A.; Jia, X.; Ho, J.; Nezich, D.; Son, H.; Bulovic, V.; Dresselhaus, M. S.; Kong, J. *Nano Lett.* **2009**, *9*, 30.
- (10) Sun, Z.; Yan, Z.; Yao, J.; Beitler, E.; Zhu, Y.; Tour, J. M. *Nature* **2010**, *468*, 549.
- (11) Sutter, P. W.; Flege, J. I.; Sutter, E. A. *Nat. Mater.* **2008**, *7*, 406.
- (12) Obratsov, A. N. *Nat. Nanotechnol.* **2009**, *4*, 212.
- (13) Lotya, M.; Hernandez, Y.; King, P. J.; Smith, R. J.; Nicolosi, V.; Karlsson, L. S.; Blighe, F. M.; De, S.; Wang, Z. M.; McGovern, I. T.; Duesberg, G. S.; Coleman, J. N. *J. Am. Chem. Soc.* **2009**, *131*, 3611.
- (14) Guo, S.; Dong, S. *Chem. Soc. Rev.* **2010**, *6*, 2885.
- (15) Park, S.; Ruoff, R. S. *Nat. Nanotechnol.* **2009**, *4*, 217.
- (16) Shao, Y. Y.; Wang, J.; Engelhard, M.; Wang, C. M.; Lin, Y. H. *J. Mater. Chem.* **2010**, *20*, 743.
- (17) Zhu, Y. W.; Stoller, M. D.; Cai, W. W.; Velamakanni, A.; Piner, R. D.; Chen, D.; Ruoff, R. S. *ACS Nano* **2010**, *4*, 1227.
- (18) Williams, G.; Seger, B.; Kamat, P. V. *ACS Nano* **2008**, *2*, 1487.
- (19) Novoselov, K. S.; McCann, E.; Morozov, S. V.; Fal'ko, V. I.; Katsnelson, M. I.; Zeitler, U.; Jiang, D.; Schedin, F.; Geim, A. K. *Nat. Phys.* **2006**, *2*, 177.
- (20) Zhang, Y. B.; Tan, Y. W.; Stormer, H. L.; Kim, P. *Nature* **2005**, *438*, 201.
- (21) Novoselov, K. S.; Jiang, Z.; Zhang, Y.; Morozov, S. V.; Stormer, H. L.; Zeitler, U.; Maan, J. C.; Boebinger, G. S.; Kim, P.; Geim, A. K. *Science* **2007**, *315*, 1379.
- (22) Novoselov, K. S.; Geim, A. K.; Morozov, S. V.; Jiang, D.; Katsnelson, M. I.; Grigorieva, I. V.; Dubonos, S. V.; Firsov, A. A. *Nature* **2005**, *438*, 197.
- (23) Schedin, F.; Geim, A. K.; Morozov, S. V.; Hill, E. W.; Blake, P.; Katsnelson, M. I.; Novoselov, K. S. *Nat. Mater.* **2007**, *6*, 652.
- (24) Lee, C.; Wei, X. D.; Kysar, J. W.; Hone, J. *Science* **2008**, *321*, 385.

- (25) Stoller, M. D.; Park, S. J.; Zhu, Y. W.; An, J. H.; Ruoff, R. S. *Nano Lett.* **2008**, *8*, 3498.
- (26) Nair, R. R.; Blake, P.; Grigorenko, A. N.; Novoselov, K. S.; Booth, T. J.; Stauber, T.; Peres, N. M. R.; Geim, A. K. *Science* **2008**, *320*, 1308.
- (27) Balandin, A. A.; Ghosh, S.; Bao, W.; Calizo, I.; Teweldebrhan, D.; Miao, F.; Lau, C. N. *Nano Lett.* **2008**, *8*, 902.
- (28) van Noorden, R. *Nature* **2011**, *469*, 14.
- (29) Kim, W. Y.; Kim, K. S. *Nat. Nanotechnol.* **2008**, *3*, 162.
- (30) Chandra, V.; Park, J.; Chun, Y.; Woo Lee, J.; Hwang, I. C.; Kim, K. S. *ACS Nano* **2010**, *4*, 3979.
- (31) Lee, W. H.; Park, J.; Kim, Y.; Kim, K. S.; Hong, B. H.; Cho, K. *Adv. Mater.* **2011**, *23*, 3460.
- (32) Huh, S.; Park, J.; Kim, K. S.; Hong, B. H.; Kim, S. B. *ACS Nano* **2011**, *5*, 3639.
- (33) (a) Wang, Y.; Li, Z.; Wang, J.; Li, J.; Lin, Y. *Trends Biotechnol.* **2011**, *29*, 205. (b) Park, S. Y.; Park, J.; Sim, S. H.; Sung, M. G.; Kim, K. S.; Hong, B. H.; Hong, S. H. *Adv. Mater.* **2011**, *23*, H263. (c) Myung, S.; Solanki, A.; Kim, C.; Park, J.; Kim, K. S.; Lee, K. B. *Adv. Mater.* **2011**, *23*, 2221.
- (34) Chen, D.; Tang, L. H.; Li, J. H. *Chem. Soc. Rev.* **2010**, *39*, 3157.
- (35) Yi, J. W.; Park, J.; Kim, K. S.; Kim, B. H. *Org. Biomol. Chem.* **2011**, *9*, 7434.
- (36) Yi, J. W.; Park, J.; Singh, N. J.; Lee, I. J.; Kim, K. S.; Kim, B. H. *Bioorg. Med. Chem. Lett.* **2011**, *21*, 704.
- (37) Min, S. K.; Kim, W. Y.; Cho, Y.; Kim, K. S. *Nat. Nanotechnol.* **2011**, *6*, 162.
- (38) Wang, Q. H.; Hersam, M. C. *Nat. Chem.* **2009**, *1*, 206.
- (39) Si, Y.; Samulski, E. T. *Nano Lett.* **2008**, *8*, 1679.
- (40) Bostwick, A.; Ohta, T.; Seyller, T.; Horn, K.; Rotenberg, E. *Nat. Phys.* **2007**, *3*, 36.
- (41) Ohta, T.; Bostwick, A.; Seyller, T.; Horn, K.; Rotenberg, E. *Science* **2006**, *313*, 951.
- (42) Elias, D. C.; Nair, R. R.; Mohiuddin, T. M. G.; Morozov, S. V.; Blake, P.; Halsall, M. P.; Ferrari, A. C.; Boukhvalov, D. W.; Katsnelson, M. I.; Geim, A. K.; Novoselov, K. S. *Science* **2009**, *323*, 610.
- (43) Wang, X. R.; Li, X. L.; Zhang, L.; Yoon, Y.; Weber, P. K.; Wang, H. L.; Guo, J.; Dai, H. J. *Science* **2009**, *324*, 768.
- (44) Kosynkin, D. V.; Higginbotham, A. L.; Sinitskii, A.; Lomeda, J. R.; Dimiev, A.; Price, B. K.; Tour, J. M. *Nature* **2009**, *458*, 872.
- (45) Loh, K. P.; Bao, Q.; Ang, P. K.; Yang, J. J. *Mater. Chem.* **2010**, *20*, 2277.
- (46) Park, J.; Lee, W. H.; Huh, S.; Sim, S. H.; Kim, S. B.; Cho, K.; Hong, B. H.; Kim, K. S. *J. Phys. Chem. Lett.* **2011**, *2*, 841.
- (47) Park, J.; Jo, S. B.; Yu, Y. J.; Kim, Y.; Yang, J. W.; Lee, W. H.; Kim, H. H.; Hong, B. H.; Kim, P.; Cho, K.; Kim, K. S. *Adv. Mater.* **2012**, *24*, 407.
- (48) Huang, X.; Qi, X. Y.; Boey, F.; Zhang, H. *Chem. Soc. Rev.* **2012**, *41*, 666.
- (49) Liu, Y. X.; Dong, X. C.; Chen, P. *Chem. Soc. Rev.* **2012**, *41*, 2283.
- (50) Xiang, Q. J.; Yu, J. G.; Jaroniec, M. *Chem. Soc. Rev.* **2012**, *41*, 782.
- (51) Luo, B.; Liu, S.; Zhi, L. *Small* **2012**, *8*, 630.
- (52) (a) Stankovich, S.; Dikin, D. A.; Piner, R. D.; Kohlhaas, K. A.; Kleinhammes, A.; Jia, Y.; Wu, Y.; Nguyen, S. T.; Ruoff, R. S. *Carbon* **2007**, *4*, 1558. (b) Dreyer, D. R.; Park, S.; Bielawski, C. W.; Ruoff, R. S. *Chem. Soc. Rev.* **2010**, *39*, 228.
- (53) Stankovich, S.; Piner, R. D.; Chen, X. Q.; Wu, N. Q.; Nguyen, S. T.; Ruoff, R. S. *J. Mater. Chem.* **2006**, *16*, 155.
- (54) Bourlinos, A. B.; Gournis, D.; Petridis, D.; Szabo, T.; Szeri, A.; Dekany, I. *Langmuir* **2003**, *19*, 6050.
- (55) McAllister, M. J.; Li, J. L.; Adamson, D. H.; Schniepp, H. C.; Abdala, A. A.; Liu, J.; Herrera-Alonso, M.; Milius, D. L.; Car, R.; Prud'homme, R. K.; Aksay, I. A. *Chem. Mater.* **2007**, *19*, 4396.
- (56) Schniepp, H. C.; Li, J. L.; McAllister, M. J.; Sai, H.; Herrera-Alonso, M.; Adamson, D. H.; Prud'homme, R. K.; Car, R.; Saville, D. A.; Aksay, I. A. *J. Phys. Chem. B* **2006**, *110*, 8535.
- (57) (a) Hummers, W. S.; Offeman, R. E. *J. Am. Chem. Soc.* **1958**, *80*, 1339. (b) Brodie, B. *Ann. Chim. Phys.* **1855**, *45*, 351.
- (58) Huh, S.; Park, J.; Kim, Y. S.; Kim, K. S.; Hong, B. H.; Nam, J. M. *ACS Nano* **2011**, *5*, 9799.
- (59) Li, X. L.; Wang, X. R.; Zhang, L.; Lee, S. W.; Dai, H. J. *Science* **2008**, *319*, 1229.
- (60) Li, X.; Zhang, G.; Bai, X.; Sun, X.; Wang, X.; Wang, E.; Dai, H. *Nat. Nanotechnol.* **2008**, *3*, 538.
- (61) Zhu, J. *Nat. Nanotechnol.* **2008**, *3*, 528.
- (62) Hamilton, C. E.; Lomeda, J. R.; Sun, Z.; Tour, J. M.; Barron, A. R. *Nano Lett.* **2009**, *9*, 3460.
- (63) Bourlinos, A. B.; Georgakilas, V.; Zboril, R.; Steriotis, T. A.; Stubos, A. K. *Small* **2009**, *5*, 1841.
- (64) Sinitskii, A.; Dimiev, A.; Corley, D. A.; Fursina, A. A.; Kosynkin, D. V.; Tour, J. M. *ACS Nano* **2010**, *4*, 1949.
- (65) Niyogi, S.; Bekyarova, E.; Itkis, M. E.; Zhang, H.; Shepperd, K.; Hicks, J.; Sprinkle, M.; Berger, C.; Ning Lau, C.; de Heer, W. A.; Conrad, E. H.; Haddon, R. C. *Nano Lett.* **2010**, *10*, 4061.
- (66) Jin, Z.; Lomeda, J. R.; Price, B. K.; Lu, W.; Zhu, Y.; Tour, J. M. *Chem. Mater.* **2009**, *21*, 3045.
- (67) Lomeda, J. R.; Doyle, C. D.; Kosynkin, D. V.; Hwang, W. F.; Tour, J. M. *J. Am. Chem. Soc.* **2008**, *130*, 16201.
- (68) Bekyarova, E.; Itkis, M. E.; Ramesh, P.; Berger, C.; Sprinkle, M.; de Heer, W. A.; Haddon, R. C. *J. Am. Chem. Soc.* **2009**, *131*, 1336.
- (69) Sharma, R.; Baik, J. H.; Perera, C. J.; Strano, M. S. *Nano Lett.* **2010**, *10*, 398.
- (70) Hossain, M. Z.; Walsh, M. A.; Hersam, M. C. *J. Am. Chem. Soc.* **2010**, *132*, 15399.
- (71) Fang, M.; Wang, K.; Lu, H.; Yang, Y.; Nutt, S. J. *Mater. Chem.* **2009**, *19*, 7098.
- (72) Liu, H.; Ryu, S.; Chen, Z.; Steigerwald, M. L.; Nuckolls, C.; Brus, L. E. *J. Am. Chem. Soc.* **2009**, *131*, 17099.
- (73) Georgakilas, V.; Bourlinos, A. B.; Gournis, D.; Tsoufis, T.; Trapalis, C.; Alonso, A. M.; Prato, M. *J. Am. Chem. Soc.* **2008**, *130*, 8733.
- (74) Georgakilas, V.; Guldi, D. M.; Signorini, R.; Bozio, R.; Prato, M. *J. Am. Chem. Soc.* **2003**, *125*, 14268.
- (75) Kordatos, K.; Da Ros, T.; Bosi, S.; Vazquez, E.; Bergamin, M.; Cusan, C.; Pellarini, F.; Tomberli, V.; Baiti, B.; Pantarotto, D.; Georgakilas, V.; Spalluto, G.; Prato, M. *J. Org. Chem.* **2001**, *66*, 4915.
- (76) Cioffi, C.; Campidelli, S.; Brunetti, F. G.; Meneghetti, M.; Prato, M. *Chem. Commun.* **2006**, 2129.
- (77) Singh, R.; Pantarotto, D.; Lacerda, L.; Pastorin, G.; Klumpp, C.; Prato, M.; Bianco, A.; Kostarelos, K. *Proc. Natl. Acad. Sci. U.S.A.* **2006**, *103*, 3357.
- (78) Kostarelos, K.; Lacerda, L.; Pastorin, G.; Wu, W.; Wieckowski, S.; Luangsivilay, L.; Godefroy, S.; Pantarotto, D.; Briand, J. P.; Muller, S.; Prato, M.; Bianco, A. *Nat. Nanotechnol.* **2007**, *2*, 108.
- (79) Georgakilas, V.; Bourlinos, A. B.; Zboril, R.; Steriotis, T. A.; Dallas, P.; Stubos, A. K.; Trapalis, C. *Chem. Commun.* **2010**, *46*, 1766.
- (80) Nemes-Incze, P.; Osváth, Z.; Kamarás, K.; Biro, L. P. *Carbon* **2008**, *46*, 1435.
- (81) Zhang, X.; Hou, L.; Cnossen, A.; Coleman, A. C.; Ivashenko, O.; Rudolf, P.; van Wees, B. J.; Browne, W. R.; Feringa, B. L. *Chem.—Eur. J.* **2011**, *17*, 8957.
- (82) Quintana, M.; Spyrou, K.; Grzelczak, M.; Browne, W. R.; Rudolf, P.; Prato, M. *ACS Nano* **2010**, *4*, 3527.
- (83) Liu, L. H.; Lerner, M. M.; Yan, M. *Nano Lett.* **2010**, *10*, 3754.
- (84) Strom, T. A.; Dillon, E. P.; Hamilton, C. E.; Barron, A. R. *Chem. Commun.* **2010**, *46*, 4097.
- (85) Vadukumpully, S.; Gupta, J.; Zhang, Y.; Xu, C. Q.; Valiyaveetil, S. *Nanoscale* **2011**, *3*, 303.
- (86) He, H.; Gao, C. *Chem. Mater.* **2010**, *22*, 5054.
- (87) Choi, J.; Kim, K.; Kim, B.; Lee, H.; Kim, S. *J. Phys. Chem. C* **2009**, *113*, 9433.
- (88) Zhong, X.; Jin, J.; Li, S.; Niu, Z.; Hu, W.; Li, R.; Ma, J. *Chem. Commun.* **2010**, *46*, 7340.
- (89) Niyogi, S.; Bekyarova, E.; Itkis, M. E.; McWilliams, J. L.; Hamon, M. A.; Haddon, R. C. *J. Am. Chem. Soc.* **2006**, *128*, 7720.
- (90) Liu, N.; Luo, F.; Wu, H.; Liu, Y.; Zhang, C.; Chen, J. *J. Adv. Funct. Mater.* **2008**, *18*, 1518.
- (91) Su, Q.; Pang, S. P.; Alijani, V.; Li, C.; Feng, X. L.; Mullen, K. *Adv. Mater.* **2009**, *21*, 3191.

- (92) Liang, Y. Y.; Wu, D. Q.; Feng, X. L.; Müllen, K. *Adv. Mater.* **2009**, *21*, 1679.
- (93) Watcharotone, S.; Dikin, D. A.; Stankovich, S.; Piner, R.; Jung, I.; Dommett, G. H. B.; Evmenenko, G.; Wu, S. E.; Chen, S. F.; Liu, C. P.; Nguyen, S. T.; Ruoff, R. S. *Nano Lett.* **2007**, *7*, 1888.
- (94) Chen, G.; Weng, W.; Wu, D.; Wu, C. *Eur. Polym. J.* **2003**, *39*, 2329.
- (95) Verdejo, R.; Barroso-Bujans, F.; Rodriguez-Perez, M. A.; Saja, J. A. D.; Lopez-Manchado, M. A. *J. Mater. Chem.* **2008**, *18*, 2221.
- (96) Patil, A. J.; Vickery, J. L.; Scott, T. B.; Mann, S. *Adv. Mater.* **2009**, *21*, 3159.
- (97) Salas, E. C.; Sun, Z.; Lüttge, A.; Tour, J. M. *ACS Nano* **2010**, *8*, 4852.
- (98) (a) Zhu, Y.; Murali, S.; Stoller, M. D.; Velamakanni, A.; Piner, R. D.; Ruoff, R. S. *Carbon* **2010**, *48*, 2106. (b) Moon, I. K.; Lee, J.; Ruoff, R. S.; Lee, H. *Nat. Commun.* **2010**, *1*, 73.
- (99) Wang, Z.; Zhou, X.; Zhang, J.; Boey, F.; Zhang, H. *J. Phys. Chem. C* **2009**, *113*, 14071.
- (100) Dubin, S.; Gilje, S.; Wang, K.; Tung, V. C.; Cha, K.; Hall, A. S.; Farrar, J.; Varshneya, R.; Yang, Y.; Kaner, R. B. *ACS Nano* **2010**, *4*, 3845.
- (101) Pasricha, R.; Gupta, S.; Srivastava, A. K. *Small* **2009**, *5*, 2253.
- (102) Zhang, T. Y.; Zhang, D. *Bull. Mater. Sci.* **2011**, *34*, 25.
- (103) Liu, Y.; Zhou, J.; Zhang, X.; Liu, Z.; Wan, X.; Tian, J.; Wang, T.; Chen, Y. *Carbon* **2009**, *47*, 3113.
- (104) Yu, D.; Yang, Y.; Durstock, M.; Baek, J. B.; Dai, L. *ACS Nano* **2010**, *4*, 5633.
- (105) Melucci, M.; Treossi, E.; Ortolani, L.; Giambastiani, G.; Morandi, V.; Klar, P.; Casiraghi, C.; Samori, P.; Palermo, V. *J. Mater. Chem.* **2010**, *20*, 9052.
- (106) Xu, Y.; Liu, Z.; Zhang, X.; Wang, Y.; Tian, J.; Huang, Y.; Ma, Y.; Zhang, X.; Chen, Y. *Adv. Mater.* **2009**, *21*, 1275.
- (107) Karousis, N.; Sandanayaka, A. S. D.; Hasobe, T.; Economopoulos, S. P.; Sarantopoulou, E.; Tagmatarchis, N. *J. Mater. Chem.* **2011**, *21*, 109.
- (108) Liu, Z. B.; Xu, Y. F.; Zhang, X. Y.; Zhang, X. L.; Chen, X. L.; Tian, J. *G. J. Phys. Chem. B* **2009**, *113*, 9681.
- (109) Zhang, X.; Feng, Y.; Huang, D.; Li, Y.; Feng, W. *Carbon* **2010**, *48*, 3236.
- (110) Liu, Z.; Robinson, J. T.; Sun, X.; Dai, H. *J. Am. Chem. Soc.* **2008**, *130*, 10876.
- (111) Yang, K.; Zhang, S.; Zhang, G.; Sun, X.; Lee, S. T.; Liu, Z. *Nano Lett.* **2010**, *10*, 3318.
- (112) Shan, C.; Yang, H.; Han, D.; Zhang, Q.; Ivaska, A.; Niu, L. *Langmuir* **2009**, *25*, 12030.
- (113) Park, S.; Dikin, D. A.; Nguyen, S. T.; Ruoff, R. S. *J. Phys. Chem. C* **2009**, *113*, 15801.
- (114) Salavagione, H. J.; Gomez, M. A.; Martinez, G. *Macromolecules* **2009**, *42*, 6331.
- (115) Veca, L. M.; Lu, F. S.; Meziani, M. J.; Cao, L.; Zhang, P. Y.; Qi, G.; Qu, L. W.; Shrestha, M.; Sun, Y. P. *Chem. Commun.* **2009**, 2565.
- (116) Lin, Y.; Zhou, B.; Fernando, K. A. S.; Liu, P.; Allard, L. F.; Sun, Y. P. *Macromolecules* **2003**, *36*, 7199.
- (117) Lin, Y.; Meziani, M. J.; Sun, Y. P. *J. Mater. Chem.* **2007**, *17*, 1.
- (118) Lin, Y. P.; Jin, J.; Song, M. *J. Mater. Chem.* **2011**, *21*, 3455.
- (119) Lee, S. H.; Dreyer, D. R.; An, J. H.; Velamakanni, A.; Piner, R. D.; Park, S.; Zhu, Y. W.; Kim, S. O.; Bielawski, C. W.; Ruoff, R. S. *Macromol. Rapid Commun.* **2010**, *31*, 281.
- (120) Kong, H.; Gao, C.; Yan, D. *J. Am. Chem. Soc.* **2004**, *126*, 412.
- (121) Gonçalves, G.; Marques, P. A. A. P.; Timmons, A. B.; Bdkin, I.; Singh, M. K.; Emami, N.; Grácio, J. *J. Mater. Chem.* **2010**, *20*, 9927.
- (122) Pramoda, K. P.; Hussain, H.; Koh, H. M.; Tan, H. R.; He, C. B. *J. Polym. Sci., Part A: Polym. Chem.* **2010**, *48*, 4262.
- (123) Ramanathan, T.; Abdala, A. A.; Stankovich, S.; Dikin, D. A.; Herrera-Alonso, M.; Piner, R. D.; Adamson, D. H.; Schniepp, H. C.; Chen, X.; Ruoff, R. S.; Nguyen, S. T.; Aksay, I. A.; Prud'Homme, R. K.; Brinson, L. C. *Nat. Nanotechnol.* **2008**, *3*, 327.
- (124) Das, B.; Eswar Prasad, K.; Ramamurty, U.; Rao, C. N. R. *Nanotechnology* **2009**, *20*, No. 125705.
- (125) Sun, S.; Cao, Y.; Feng, J.; Wu, P. *J. Mater. Chem.* **2010**, *20*, 5605.
- (126) Pham, T. A.; Kumar, N. A.; Jeong, Y. T. *Synth. Met.* **2010**, *160*, 2028.
- (127) Zhang, B.; Chen, Y.; Zhuang, X.; Liu, G.; Yu, B.; Kang, E. T.; Zhu, J.; Li, Y. *J. Polym. Sci., Part A: Polym. Chem.* **2010**, *48*, 2642.
- (128) (a) Raghu, A. V.; Lee, Y. R.; Jeong, H. M.; Shin, C. M. *Macromol. Chem. Phys.* **2008**, *209*, 2487. (b) Kim, H.; Miura, Y.; Macosko, C. W. *Chem. Mater.* **2010**, *22*, 3441.
- (129) Cao, Y.; Feng, J.; Wu, P. *Carbon* **2010**, *48*, 1670.
- (130) Chen, Y.; Zhang, X.; Yu, P.; Ma, Y. *Chem. Commun.* **2009**, 4527.
- (131) Liu, Y.; Yu, D.; Zeng, C.; Miao, Z.; Dai, L. *Langmuir* **2010**, *26*, 6158.
- (132) Zhang, X.; Huang, Y.; Wang, Y.; Ma, Y.; Liu, Z.; Chen, Y. *Carbon* **2008**, *47*, 313.
- (133) Nasibulin, A. G.; Pikhitsa, P. V.; Jiang, H.; Brown, D. P.; Krashennnikov, A. V.; Anisimov, A. S.; Queipo, P.; Moiala, A.; Gonzalez, D.; Lientschnig, G.; Hassani, A.; Shandakov, S. D.; Loll, G.; Resasco, D. E.; Choi, M.; Tomanek, D.; Kauppinen, E. I. *Nat. Nanotechnol.* **2007**, *2*, 156.
- (134) Delgado, J. L.; de la Cruz, P.; Urbina, A.; Lopez Navarrete, J. T.; Casado, J.; Langa, F. *Carbon* **2007**, *45*, 2250.
- (135) Yang, H.; Shan, C.; Li, F.; Han, D.; Zhang, Q.; Niu, L. *Chem. Commun.* **2009**, 3880.
- (136) Karousis, N.; Economopoulos, S. P.; Sarantopoulou, E.; Tagmatarchis, N. *Carbon* **2010**, *48*, 854.
- (137) Valentini, L.; Cardinali, M.; Bon, S. B.; Bagnis, D.; Verdejo, R.; Lopez-Manchado, M. A.; Kenny, J. M. *J. Mater. Chem.* **2010**, *20*, 995.
- (138) Bon, S. B.; Valentini, L.; Verdejo, R.; Fierro, J. L. G.; Peponi, L.; Lopez-Manchado, M. A.; Kenny, J. M. *Chem. Mater.* **2009**, *21*, 3433.
- (139) Homenick, C. M.; Lawson, G.; Adronov, A. *Polym. Rev.* **2007**, *47*, 265.
- (140) Coleman, J. N.; Khan, U.; Blau, W. J.; Gunko, Y. K. *Carbon* **2006**, *44*, 1624.
- (141) Liu, L.; Grunlan, J. C. *Adv. Funct. Mater.* **2007**, *17*, 2343.
- (142) Costache, M. C.; Heidecker, M. J.; Manias, E.; Camino, G.; Frache, A.; Beyer, G.; Gupta, R. K.; Wilkie, C. A. *Polymer* **2007**, *42*, 6532.
- (143) Yang, H.; Li, F.; Shan, C.; Han, D.; Zhang, Q.; Niu, L.; Ivaska, A. *J. Mater. Chem.* **2009**, *19*, 4632.
- (144) Liu, Z.; Liu, Q.; Huang, Y.; Ma, Y.; Yin, S.; Zhang, X.; Sun, W.; Chen, Y. *Adv. Mater.* **2008**, *20*, 3924.
- (145) Liu, Q.; Liu, Z.; Zhang, X.; Zhang, N.; Yang, L.; Yin, S.; Chen, Y. *Appl. Phys. Lett.* **2008**, *92*, No. 223303.
- (146) Liu, Q.; Liu, Z.; Zhang, X.; Yang, L.; Zhang, N.; Pan, G.; Yin, S.; Chen, Y.; Wei, J. *Adv. Funct. Mater.* **2009**, *19*, 894.
- (147) Avinash, M. B.; Subrahmanyam, K. S.; Sundarayya, Y.; Govindaraju, T. *Nanoscale* **2010**, *2*, 1762.
- (148) Gilje, S.; Dubin, S.; Badakhshan, A.; Farrar, J.; Danczyk, S. A.; Kaner, R. B. *Adv. Mater.* **2010**, *22*, 419.
- (149) Boukhalov, D. W.; Katsnelson, M. I. *J. Am. Chem. Soc.* **2008**, *130*, 10697.
- (150) Gao, X.; Jang, J.; Nagase, S. *J. Phys. Chem. C* **2010**, *114*, 832.
- (151) Ghaderi, N.; Peressi, M. *J. Phys. Chem. C* **2010**, *114*, 21625.
- (152) Hsiao, M. C.; Liao, S. H.; Yen, M. Y.; Liu, P. I.; Pu, N. W.; Wang, C. A.; Ma, C. C. M. *ACS Appl. Mater. Interfaces* **2010**, *2*, 3092.
- (153) Shen, J.; Hu, Y.; Li, C.; Qin, C.; Ye, M. *Small* **2009**, *5*, 82.
- (154) Sofo, J. O.; Chaudhari, A. S.; Barber, G. D. *Phys. Rev. B* **2007**, *75*, No. 153401.
- (155) Ryu, S.; Han, M. Y.; Maultzsch, J.; Heinz, T. F.; Kim, P.; Steigerwald, M. L.; Brus, L. E. *Nano Lett.* **2008**, *8*, 4597.
- (156) Chandrachud, P.; Pujari, B. S.; Haldar, S.; Sanyal, B.; Kanhere, D. G. *J. Phys.: Condens. Matter* **2010**, *22*, No. 465502.
- (157) Flores, M. Z. S.; Autreto, P. A. S.; Legolas, S. B.; Galvao, D. S. *Nanotechnology* **2009**, *20*, No. 465704.
- (158) (a) Zboril, R.; Karlicky, F.; Bourlinos, A. B.; Athanasios, B.; Steriotis, T. A.; Stubos, A. K.; Georgakilas, V.; Safarova, K.; Jancik, D.; Trapalis, C.; Otyepka, M. *Small* **2010**, *6*, 2885. (b) Karlicky, F.; Zboril, R.; Otyepka, M. *J. Chem. Phys.* **2012**, *137*, 034709. (c) Bourlinos, A. B.; Safarova, K.; Siskova, K.; Zboril, R. *Carbon* **2012**, *50*, 1425.
- (159) Savchenko, A. *Science* **2009**, *323*, 598.

- (160) (a) Tran, P.; Blaha, P. *Phys. Rev. Lett.* **2009**, *102*, No. 226401. (b) Kummel, S.; Kronik, L. *Rev. Mod. Phys.* **2008**, *80*, 3.
- (161) Lebegue, S.; Klintonbeg, M.; Eriksson, O.; Katsnelson, M. I. *Phys. Rev. B* **2009**, *79*, No. 245117.
- (162) Cudazzo, P.; Attaccalite, C.; Tokatly, I. V.; Rubio, A. *Phys. Rev. Lett.* **2010**, *104*, No. 226804.
- (163) Pulci, O.; Gori, P.; Marsili, M.; Garbuio, V.; Seitsonen, A. P.; Bechstedt, F.; Criscitiello, A.; del Sole, R. *Phys. Status Solidi A* **2010**, *207*, 291.
- (164) Onida, G.; Reining, L.; Rubio, A. *Rev. Mod. Phys.* **2002**, *74*, 601.
- (165) (a) Schwierz, F. *Nat. Nanotechnol.* **2010**, *5*, 487. (b) Du, A.; Smith, S. C. *J. Phys. Chem. Lett.* **2011**, *2*, 73.
- (166) (a) Balog, R.; Jorgensen, B.; Nilsson, L.; Andersen, M.; Rienks, E.; Bianchi, M.; Fanetti, M.; Lægsgaard, E.; Baraldi, A.; Lizzit, S.; Slijivancanin, Z.; Besenbacher, F.; Hammer, B.; Pedersen, T. G.; Hofmann, P.; Hornekær, L. *Nat. Mater.* **2010**, *9*, 315. (b) Gao, H.; Zhao, J.; Ding, F.; Lu, J. *J. Phys. Chem. C* **2011**, *115*, 3236.
- (167) Singh, A. K.; Yakobson, B. I. *Nano Lett.* **2009**, *9*, 1540.
- (168) Singh, A. K.; Penev, E. S.; Yakobson, B. I. *ACS Nano* **2010**, *4*, 3510.
- (169) Robinson, J. T.; Burgess, J. S.; Junkermeier, C. E.; Badescu, S. C.; Reinecke, T. L.; Perkins, F. K.; Zalalutdniov, M. K.; Baldwin, J. W.; Culbertson, J. C.; Sheehan, P. E.; Snow, E. S. *Nano Lett.* **2010**, *10*, 3001.
- (170) Withers, F.; Dubois, M.; Savchenko, A. K. *Phys. Rev. B* **2010**, *82*, No. 073403.
- (171) Nair, R. R.; Ren, W. C.; Jalil, R.; Riaz, I.; Kravets, V. G.; Britnell, L.; Blake, P.; Schedin, F.; Mayorov, A. S.; Yuan, S. J.; Katsnelson, M. L.; Cheng, H. M.; Strupinski, W.; Bulusheva, L. G.; Okotrub, A. V.; Grigorieva, I. V.; Grigorenko, A. N.; Novoselov, K. S.; Geim, A. K. *Small* **2010**, *6*, 2887.
- (172) Cheng, S. H.; Zou, K.; Okino, F.; Gutierrez, H. R.; Gupta, A.; Shen, N.; Eklund, P. C.; Sofo, J. O.; Zhu, J. *Phys. Rev. B* **2010**, *81*, No. 205435.
- (173) Hong, X.; Cheng, S. H.; Herding, C.; Zhu, J. *Phys. Rev. B* **2011**, *83*, No. 085410.
- (174) Bourlinos, A. B.; Bakandritsos, A.; Liaros, N.; Couris, S.; Safarova, K.; Otyepka, M.; Zboril, R. *Chem. Phys. Lett.* **2012**, *543*, 101.
- (175) Jeon, K. J.; Lee, Z.; Pollak, E.; Moreschini, L.; Bostwick, A.; Park, C. M.; Mendelsberg, R.; Radmilovic, V.; Kostecki, R.; Richardson, T. J.; Rotenberg, E. *ACS Nano* **2011**, *5*, 1042.
- (176) Leenaerts, O.; Peelaers, H.; Hernandez-Nieves, A. D.; Partoens, B.; Peeters, F. M. *Phys. Rev. B* **2010**, *82*, No. 195436.
- (177) Samarakoon, D. K.; Chen, Z. F.; Nicolas, C.; Wang, X. Q. *Small* **2011**, *7*, 965.
- (178) Takagi, Y.; Kusakabe, K. *Phys. Rev. B* **2002**, *65*, No. 121103(R).
- (179) Charlier, J. C.; Gonze, X.; Michenaud, J. P. *Phys. Rev. B* **1993**, *47*, 16162.
- (180) Sahin, H.; Topsakal, M.; Ciraci, S. *Phys. Rev. B* **2011**, *83*, No. 115432.
- (181) Heyd, J.; Scuseria, G. E.; Ernzerhof, M. *J. Chem. Phys.* **2003**, *118*, 8207.
- (182) Heyd, J.; Peralta, J. E.; Scuseria, G. E.; Martin, R. L. *J. Chem. Phys.* **2005**, *123*, No. 174101.
- (183) Ribas, M. A.; Singh, A. K.; Sorokin, P. B.; Yakobson, B. I. *Nano Res.* **2011**, *4*, 143.
- (184) Hamwi, A. J. *Phys. Chem. Solids* **1996**, *57*, 677.
- (185) (a) Li, B.; Zhou, L.; Wu, D.; Peng, H.; Yan, K.; Zhou, Y.; Liu, Z. *ACS Nano* **2011**, *5*, 5957. (b) Wu, J.; Xie, L.; Li, Y.; Wang, H.; Ouyang, Y.; Guo, J.; Dai, H. *J. Am. Chem. Soc.* **2011**, *133*, 19668.
- (186) Gopalakrishnan, K.; Subrahmanyam, K. S.; Kumar, P.; Govindaraj, A.; Rao, C. N. R. *RSC Adv.* **2012**, *2*, 1605.
- (187) Karousis, N.; Tagmatarchis, N. *Chem. Rev.* **2010**, *110*, 5365.
- (188) Tasis, D.; Tagmatarchis, N.; Bianco, A.; Prato, M. *Chem. Rev.* **2006**, *106*, 1105.
- (189) Meyer, E. A.; Castellano, R. K.; Diederich, F. *Angew. Chem., Int. Ed.* **2003**, *42*, 1210.
- (190) Burley, S. K.; Petsko, G. A. *Science* **1985**, *229*, 23.
- (191) Hong, B. H.; Lee, J. Y.; Lee, C. W.; Kim, J. C.; Bae, S. C.; Kim, K. S. *J. Am. Chem. Soc.* **2001**, *123*, 10748.
- (192) Singh, N. J.; Lee, H. M.; Hwang, I.-C.; Kim, K. S. *Supramol. Chem.* **2007**, *19*, 321.
- (193) Lee, J. Y.; Hong, B. H.; Kim, W. Y.; Min, S. K.; Kim, Y.; Jouravlev, M. V.; Bose, R.; Kim, K. S.; Hwang, I. C.; Kaufman, L. J.; Wong, C. W.; Kim, P.; Kim, K. S. *Nature* **2009**, *460*, 498.
- (194) Hong, B. H.; Bae, S. C.; Lee, C. W.; Jeong, S.; Kim, K. S. *Science* **2001**, *294*, 348.
- (195) Singh, N. J.; Lee, H. M.; Suh, S. B.; Kim, K. S. *Pure Appl. Chem.* **2007**, *79*, 1057.
- (196) Tarakeshwar, P.; Choi, H. S.; Kim, K. S. *Chem. Rev.* **2000**, *100*, 4145.
- (197) Riley, K. E.; Pitonak, M.; Jurecka, P.; Hobza, P. *Chem. Rev.* **2010**, *110*, 5023.
- (198) Hong, B. H.; Small, J. P.; Purewal, M. S.; Mullokandov, A.; Sfeir, M. Y.; Wang, F.; Lee, J. Y.; Heinz, T. F.; Brus, L. E.; Kim, P.; Kim, K. S. *Proc. Natl. Acad. Sci. U.S.A.* **2005**, *102*, 14155.
- (199) Hobza, P.; Bludský, O.; Selzle, H. L.; Schlag, E. W. *J. Chem. Phys.* **1992**, *97*, 335.
- (200) Tarakeshwar, P.; Kim, K. S.; Kraka, E.; Cremer, D. *J. Chem. Phys.* **2001**, *115*, 6018.
- (201) Tarakeshwar, P.; Choi, H. S.; Kim, K. S. *J. Am. Chem. Soc.* **2001**, *123*, 3323.
- (202) Lee, E. C.; Hong, B. H.; Lee, J. Y.; Kim, J. C.; Kim, D.; Kim, Y.; Tarakeshwar, P.; Kim, K. S. *J. Am. Chem. Soc.* **2005**, *127*, 4530.
- (203) Tarakeshwar, P.; Kim, K. S.; Brutschy, B. *J. Chem. Phys.* **2001**, *114*, 1295.
- (204) Grabowski, S. J. *J. Phys. Chem. A* **2007**, *111*, 13537.
- (205) Kwon, J. Y.; Singh, N. J.; Kim, H. A.; Kim, S. K.; Kim, K. S.; Yoon, J. *J. Am. Chem. Soc.* **2004**, *126*, 8892.
- (206) Vaupel, S.; Brutschy, B.; Tarakeshwar, P.; Kim, K. S. *J. Am. Chem. Soc.* **2006**, *128*, 5415.
- (207) Kim, E.; Paliwal, S.; Wilcox, C. S. *J. Am. Chem. Soc.* **1998**, *120*, 11192.
- (208) Hunter, C. A.; Sanders, J. K. M. *J. Am. Chem. Soc.* **1990**, *112*, 5525.
- (209) Hunter, C. A. *Chem. Soc. Rev.* **1994**, *23*, 101.
- (210) Hobza, P.; Selzle, H. L.; Schlag, E. W. *Chem. Rev.* **1994**, *94*, 1767.
- (211) Grimme, S. *Chem.—Eur. J.* **2004**, *10*, 3423.
- (212) Sinnokrot, M. O.; Sherrill, C. D. *J. Phys. Chem. A* **2006**, *110*, 10656.
- (213) Lee, E. C.; Kim, D.; Jurecka, P.; Tarakeshwar, P.; Hobza, P.; Kim, K. S. *J. Phys. Chem. A* **2007**, *111*, 3446.
- (214) Cabaco, M. I.; Danten, Y.; Besnard, M.; Guissani, Y.; Guillot, B. *J. Phys. Chem. B* **1998**, *102*, 10712.
- (215) West, A. P., Jr.; Mecozi, S.; Dougherty, D. A. *J. Phys. Org. Chem.* **1997**, *10*, 347.
- (216) Kim, H. G.; Lee, C. W.; Yun, S.; Hong, B. H.; Kim, Y. O.; Kim, D.; Ihm, H.; Lee, J. W.; Lee, E. C.; Tarakeshwar, P.; Park, S. M.; Kim, K. S. *Org. Lett.* **2002**, *4*, 3971.
- (217) Kim, K. S.; Suh, S. B.; Kim, J. C.; Hong, B. H.; Lee, E. C.; Yun, S.; Tarakeshwar, P.; Lee, J. Y.; Kim, Y.; Ihm, H.; Kim, H. G.; Lee, J. W.; Kim, J. K.; Lee, H. M.; Kim, D.; Cui, C.; Youn, S. J.; Chung, H. Y.; Choi, H. S.; Lee, C. W.; Cho, S. J.; Jeong, S.; Cho, J. H. *J. Am. Chem. Soc.* **2002**, *124*, 14268.
- (218) Geronimo, I.; Lee, E. C.; Singh, N. J.; Kim, K. S. *J. Chem. Theory Comput.* **2010**, *6*, 1931.
- (219) Wang, W.; Hobza, P. *ChemPhysChem* **2008**, *9*, 1003.
- (220) Dougherty, D. A.; Stauffer, D. *Science* **1990**, *250*, 1558.
- (221) Kim, D.; Hu, S.; Tarakeshwar, P.; Kim, K. S.; Lisy, J. M. *J. Phys. Chem. A* **2003**, *107*, 1228.
- (222) Kim, K. S.; Lee, J. Y.; Lee, S. J.; Ha, T. K.; Kim, D. H. *J. Am. Chem. Soc.* **1994**, *116*, 7399.
- (223) (a) Lee, J. Y.; Lee, S. J.; Choi, H. S.; Cho, S. J.; Kim, K. S.; Ha, T. K. *Chem. Phys. Lett.* **1995**, *232*, 67. (b) Choi, H. S.; Suh, S. B.; Cho, S. J.; Kim, K. S. *Proc. Natl. Acad. Sci. U.S.A.* **1998**, *95*, 12094.
- (224) Yi, H. B.; Lee, H. M.; Kim, K. S. *J. Chem. Theory Comput.* **2009**, *9*, 1709.
- (225) Yi, H. B.; Diefenbach, M.; Choi, Y. C.; Lee, E. C.; Lee, H. M.; Hong, B. H.; Kim, K. S. *Chem.—Eur. J.* **2006**, *12*, 4885.

- (226) Ihm, H.; Yun, S.; Kim, H. G.; Kim, J. K.; Kim, K. S. *Org. Lett.* **2002**, *4*, 2897.
- (227) Oh, K. S.; Lee, C. W.; Choi, H. S.; Lee, S. J.; Kim, K. S. *Org. Lett.* **2000**, *2*, 2679.
- (228) Chellappan, K.; Singh, N. J.; Hwang, I. C.; Lee, J. W.; Kim, K. S. *Angew. Chem., Int. Ed.* **2005**, *44*, 2899.
- (229) Singh, N. J.; Min, S. K.; Kim, D. Y.; Kim, K. S. *J. Chem. Theory Comput.* **2009**, *5*, 515.
- (230) Singh, N. J.; Shin, D.; Lee, H. M.; Kim, H. T.; Chang, H. J.; Cho, J. M.; Kim, K. S.; Ro, S. *J. Struct. Biol.* **2011**, *174*, 173.
- (231) Das, A.; Jana, A. D.; Seth, S. K.; Dey, B.; Choudhury, S. R.; Kar, T.; Mukhopadhyay, S.; Singh, N. J.; Hwang, I. C.; Kim, K. S. *J. Phys. Chem. B* **2010**, *114*, 4166.
- (232) Geronimo, I.; Singh, N. J.; Kim, K. S. *Phys. Chem. Chem. Phys.* **2011**, *13*, 11841.
- (233) Quinonero, D.; Garau, C.; Rotger, C.; Frontera, A.; Ballester, P.; Costa, A.; Deya, P. M. *Angew. Chem., Int. Ed.* **2002**, *41*, 3389.
- (234) Kim, D.; Tarakeshwar, P.; Kim, K. S. *J. Phys. Chem. A* **2004**, *108*, 1250.
- (235) (a) Geronimo, I.; Singh, N. J.; Kim, K. S. *J. Chem. Theory Comput.* **2011**, *7*, 825. (b) Kim, D. Y.; Geronimo, I.; Singh, N. J.; Lee, H. M.; Kim, K. S. *J. Chem. Theory Comput.* **2012**, *8*, 274. (c) Kim, K. S.; Karthikeyan, S.; Singh, N. J. *J. Chem. Theory Comput.* **2011**, *7*, 3471. (d) Min, S. K.; Lee, E. C.; Lee, H. M.; Kim, D. Y.; Kim, D.; Kim, K. S. *J. Comput. Chem.* **2008**, *29*, 1208.
- (236) Xu, Z.; Singh, N. J.; Kim, S. K.; Spring, D. R.; Kim, K. S.; Yoon, J. *Chem.—Eur. J.* **2011**, *17*, 1163.
- (237) Mascal, M.; Yakovlev, I.; Nikitin, E. B.; Fettingner, J. C. *Angew. Chem., Int. Ed.* **2006**, *45*, 2890.
- (238) Kim, D. Y.; Singh, N. J.; Lee, J. W.; Kim, K. S. *J. Chem. Theory Comput.* **2008**, *4*, 1162.
- (239) Henwood, D.; Carey, J. D. *Phys. Rev. B* **2007**, *75*, No. 245413.
- (240) Tkatchenko, A.; von Lilienfeld, O. A. *Phys. Rev. B* **2006**, *73*, No. 153405.
- (241) Umadevi, D.; Sastry, G. N. *J. Phys. Chem. C* **2011**, *115*, 9655.
- (242) Dion, M.; Rydberg, H.; Schröder, E.; Langreth, D. C.; Lundqvist, B. I. *Phys. Rev. Lett.* **2004**, *92*, No. 246401.
- (243) Chakarova-Käck, S. D.; Schröder, E.; Lundqvist, B. I.; Langreth, D. C. *Phys. Rev. Lett.* **2006**, *96*, No. 146107.
- (244) Granatier, J.; Lazar, P.; Otyepka, M.; Hobza, P. *J. Chem. Theory Comput.* **2011**, *7*, 3743.
- (245) Rochefort, A.; Wuest, J. D. *Langmuir* **2009**, *25*, 210.
- (246) Ortmann, F.; Schmidt, W. G.; Bechstedt, F. *Phys. Rev. Lett.* **2005**, *95*, No. 186101.
- (247) Gowtham, S.; Scheicher, R. H.; Ahuja, R.; Pandey, R.; Karna, S. P. *Phys. Rev. B* **2007**, *76*, No. 033401.
- (248) Umadevi, D.; Sastry, G. N. *J. Phys. Chem. Lett.* **2011**, *2*, 1572.
- (249) Antony, J.; Grimme, S. *Phys. Chem. Chem. Phys.* **2008**, *10*, 2722.
- (250) Berland, K.; Chakarova-Käck, S. D.; Cooper, V. R.; Langreth, D. C.; Schröder, E. *J. Phys.: Condens. Matter* **2011**, *23*, No. 135001.
- (251) Rajesh, C.; Majumder, C.; Mizuseki, H.; Kawazoe, Y. *J. Chem. Phys.* **2009**, *130*, No. 124911.
- (252) Giovannetti, G.; Khomyakov, P. A.; Brocks, G.; Karpan, V. M.; van den Brink, J.; Kelly, P. J. *Phys. Rev. Lett.* **2008**, *101*, No. 026803.
- (253) Uchoa, B.; Lin, C. Y.; Castro Neto, A. H. *Phys. Rev. B* **2008**, *77*, No. 035420.
- (254) Bertoni, G.; Calmels, L.; Altibelli, A.; Serin, V. *Phys. Rev. B* **2005**, *71*, No. 075402.
- (255) Youn, I. S.; Kim, D. Y.; Singh, N. J.; Park, S. W.; Youn, J.; Kim, K. S. *J. Chem. Theory Comput.* **2012**, *8*, 99.
- (256) Varchon, F.; Feng, R.; Hass, J.; Li, X.; Nguyen, B. N.; Naud, C.; Mallet, P.; Veuillen, J. Y.; Berger, C.; Conrad, E. H.; Magaud, L. *Phys. Rev. Lett.* **2007**, *99*, No. 126805.
- (257) Zhou, S. Y.; Gweon, G. H.; Fedorov, A. V.; First, P. N.; de Heer, W. A.; Lee, D. H.; Guinea, F.; Castro Neto, A. H.; Lanzara, A. *Nat. Mater.* **2007**, *6*, 770.
- (258) (a) Kim, W. Y.; Kim, K. S. *Nat. Nanotechnol.* **2008**, *3*, 408. (b) Lu, Y. H.; Chen, W.; Feng, Y. P.; He, P. M. *J. Phys. Chem. B* **2009**, *113*, 2. (c) Lee, G.; Kim, K. S.; Cho, K. *J. Phys. Chem. C* **2011**, *115*, 9719.
- (259) Cho, W. J.; Cho, Y.; Min, S. K.; Kim, W. Y.; Kim, K. S. *J. Am. Chem. Soc.* **2011**, *133*, 9364.
- (260) Cho, Y.; Choi, Y. C.; Kim, K. S. *J. Phys. Chem. C* **2011**, *115*, 6019.
- (261) (a) Kim, W. Y.; Choi, Y. C.; Min, S. K.; Cho, Y.; Kim, K. S. *Chem. Soc. Rev.* **2009**, *38*, 2319. (b) Kim, W. Y.; Choi, Y. C.; Kim, K. S. *J. Mater. Chem.* **2008**, *18*, 4510. (c) Kim, W. Y.; Kim, K. S. *J. Comput. Chem.* **2008**, *29*, 1073.
- (262) Cho, Y.; Kim, W. Y.; Kim, K. S. *J. Phys. Chem. A* **2009**, *113*, 4100.
- (263) Lee, E. C.; Choi, Y. C.; Kim, W. Y.; Singh, N. J.; Lee, S.; Shim, J. H.; Kim, K. S. *Chem.—Eur. J.* **2010**, *16*, 12141.
- (264) Cho, Y.; Min, S. K.; Kim, W. Y.; Kim, K. S. *Phys. Chem. Chem. Phys.* **2011**, *13*, 14293.
- (265) Min, S. K.; Cho, Y.; Mason, D. R.; Lee, J. Y.; Kim, K. S. *J. Phys. Chem. C* **2011**, *115*, 16247.
- (266) Jaegfeldt, H.; Kuwana, T.; Johansson, G. *J. Am. Chem. Soc.* **1983**, *105*, 1805.
- (267) Xu, Y.; Bai, H.; Lu, G.; Li, C.; Shi, G. Q. *J. Am. Chem. Soc.* **2008**, *130*, 5856.
- (268) Wang, Y.; Chen, X.; Zhong, Y.; Zhu, F.; Loh, K. P. *Appl. Phys. Lett.* **2009**, *95*, No. 063302.
- (269) An, X.; Butler, T. W.; Washington, M.; Nayak, S. K.; Kar, S. *ACS Nano* **2011**, *5*, 1003.
- (270) Yang, Q.; Pan, X.; Huang, F.; Li, K. *J. Phys. Chem. C* **2010**, *114*, 3811.
- (271) Kodali, V. K.; Scrimgeour, J.; Kim, S.; Hankinson, J. H.; Carroll, K. M.; de Heer, W. A.; Berger, C.; Curtis, J. E. *Langmuir* **2011**, *27*, 863.
- (272) Lopes, M.; Candini, A.; Urdampilleta, M.; Plantey, A. R.; Bellini, V.; Klyatskaya, S.; Marty, L.; Ruben, M.; Affronte, M.; Wernsdorfer, W.; Bendiab, N. *ACS Nano* **2010**, *4*, 7531.
- (273) Cheng, H. C.; Shiue, R. J.; Tsai, C. C.; Wang, W. H.; Chen, Y. T. *ACS Nano* **2011**, *5*, 2051.
- (274) Wang, X.; Tabakman, S. M.; Dai, H. *J. Am. Chem. Soc.* **2008**, *130*, 8152.
- (275) Liu, J.; Li, Y.; Li, Y.; Li, J.; Deng, Z. *J. Mater. Chem.* **2010**, *20*, 900.
- (276) Xu, Y.; Wu, Q.; Sun, Y.; Bai, H.; Shi, G. *ACS Nano* **2010**, *4*, 7358.
- (277) Tu, W.; Lei, J.; Zhang, S.; Ju, H. *Chem.—Eur. J.* **2010**, *16*, 10771.
- (278) Geng, J.; Jung, H. T. *J. Phys. Chem. C* **2010**, *114*, 8227.
- (279) Zhang, S.; Tang, S.; Lei, J.; Dong, H.; Ju, H. *J. Electroanal. Chem.* **2011**, *656*, 285.
- (280) Bai, H.; Xu, Y.; Zhao, L.; Li, C.; Shi, G. *Chem. Commun.* **2009**, 1667.
- (281) Wang, D. W.; Li, F.; Zhao, J.; Ren, W.; Chen, Z. G.; Tan, J.; Wu, Z. S.; Gentle, I.; Lu, G. Q.; Cheng, H. M. *ACS Nano* **2009**, *3*, 1745.
- (282) Wu, H.; Zhao, W.; Hu, H.; Chen, G. *J. Mater. Chem.* **2011**, *21*, 8626.
- (283) Choi, B. G.; Park, H.; Park, T. J.; Yang, M. H.; Kim, J. S.; Jang, S.-Y.; Heo, N. S.; Lee, S. Y.; Kong, J.; Hong, W. H. *ACS Nano* **2010**, *4*, 2910.
- (284) Ansari, S.; Kellarakis, A.; Estevez, L.; Giannelis, E. P. *Small* **2010**, *6*, 205.
- (285) Li, F.; Bao, Y.; Chai, J.; Zhang, Q.; Han, D.; Niu, L. *Langmuir* **2010**, *26*, 12314.
- (286) Liu, H.; Gao, J.; Xue, M.; Zhu, N.; Zhang, M.; Cao, T. *Langmuir* **2009**, *25*, 12006.
- (287) Saxena, A. P.; Deepa, M.; Joshi, A. G.; Bhandari, S.; Srivastava, A. K. *ACS Appl. Mater. Interfaces* **2011**, *3*, 1115.
- (288) Lim, H.; Lee, J. S.; Shin, H. J.; Shin, H. S.; Choi, H. C. *Langmuir* **2010**, *26*, 12278.
- (289) Fang, M.; Long, J.; Zhao, W.; Wang, L.; Chen, G. *Langmuir* **2010**, *26*, 16771.
- (290) Jo, K.; Lee, T.; Choi, H. J.; Park, J. H.; Lee, D. J.; Lee, D. W.; Kim, B. S. *Langmuir* **2011**, *27*, 2014.
- (291) Ghosh, A.; Rao, K. V.; George, S. J.; Rao, C. N. R. *Chem.—Eur. J.* **2010**, *16*, 2700.
- (292) Chen, C.; Zhai, W.; Lu, D.; Zhang, H.; Zheng, W. *Mater. Res. Bull.* **2011**, *46*, 583.
- (293) Liu, J.; Yang, W.; Tao, L.; Li, D.; Boyer, C.; Davis, T. P. *J. Polym. Sci., Part A: Polym. Chem.* **2010**, *48*, 425.
- (294) Yang, H. F.; Zhang, Q. X.; Shan, C. S.; Li, F. H.; Han, D. X.; Niu, L. *Langmuir* **2010**, *26*, 6708.

- (295) Guo, Y.; Deng, L.; Li, J.; Guo, S.; Wang, E.; Dong, S. *ACS Nano* **2011**, *5*, 1282.
- (296) Wang, Y.; Shi, Z.; Yin, J. *ACS Appl. Mater. Interfaces* **2011**, *3*, 1127.
- (297) Park, S.; Mohanty, N.; Suk, J. W.; Nagaraja, A.; An, J.; Piner, R. D.; Cai, W.; Dreyer, D. R.; Berry, V.; Ruoff, R. S. *Adv. Mater.* **2010**, *22*, 1736.
- (298) Green, A. A.; Hersam, M. C. *Nano Lett.* **2009**, *9*, 4031.
- (299) Zu, S. Z.; Han, B. H. *J. Phys. Chem. C* **2009**, *113*, 13651.
- (300) Chen, G.; Hoffman, A. S. *Nature* **1995**, *373*, 49.
- (301) Liu, S.; Tian, J.; Wang, L.; Li, H.; Zhang, Y.; Sun, X. *Macromolecules* **2010**, *43*, 10078.
- (302) Ghosh, A.; Rao, K. V.; Voggu, R.; George, S. J. *Chem. Phys. Lett.* **2010**, *488*, 198.
- (303) Choi, E. Y.; Han, T. H.; Hong, J. H.; Kim, J. E.; Lee, S. H.; Kim, H. W.; Kim, S. O. *J. Mater. Chem.* **2010**, *20*, 1907.
- (304) Paredes, J. I.; Villar-Rodil, S.; Alonso, A. M.; Tascon, J. M. D. *Langmuir* **2008**, *24*, 10560.
- (305) Qi, X.; Pu, K. Y.; Li, H.; Zhou, X.; Wu, S.; Fan, Q. L.; Liu, B.; Boey, F.; Huang, W.; Zhang, H. *Angew. Chem., Int. Ed.* **2010**, *49*, 9426.
- (306) Kim, T. Y.; Lee, H. W.; Kim, J. E.; Suh, K. S. *ACS Nano* **2010**, *4*, 1612.
- (307) Zhang, Y. H.; Zhou, K. G.; Xie, K. F.; Zeng, J.; Zhang, H. L.; Peng, Y. *Nanotechnology* **2010**, *21*, No. 065201.
- (308) Georgakilas, V.; Gournis, D.; Tzitzios, V.; Pasquato, L.; Guldi, D. M.; Prato, M. *J. Mater. Chem.* **2007**, *17*, 2679.
- (309) Wildgoose, G. G.; Banks, C. E.; Compton, R. G. *Small* **2006**, *2*, 182.
- (310) Shi, Y.; Kim, K. K.; Reina, A.; Hofmann, M.; Li, L. J.; Kong, J. *ACS Nano* **2010**, *4*, 2689.
- (311) Murphy, C. J.; Sau, T. K.; Gole, A. M.; Orendorff, C. J.; Gao, J.; Gou, L.; Hunyadi, S. E.; Li, T. *J. Phys. Chem. B* **2005**, *109*, 13857.
- (312) Kamat, P. V. *J. Phys. Chem. B* **2002**, *106*, 7729.
- (313) Daniel, M. C.; Astruc, D. *Chem. Rev.* **2004**, *104*, 293.
- (314) Tiwari, J. N.; Tiwari, R. N.; Kim, K. S. *Prog. Mater. Sci.* **2012**, *57*, 724.
- (315) Zhang, Q.; Xie, J.; Yang, J.; Lee, J. Y. *ACS Nano* **2009**, *3*, 139.
- (316) Luo, Z.; Somers, L.; Dan, Y.; Ly, T.; Kybert, N.; Mele, E.; Johnson, A. *Nano Lett.* **2010**, *10*, 777.
- (317) Granatier, J.; Lazar, P.; Prucek, R.; Safarova, K.; Zboril, R.; Otyepka, M.; Hobza, P. *J. Phys. Chem. C* **2012**, *116*, 14151.
- (318) Muszynski, R.; Seger, B.; Kamat, P. V. *J. Phys. Chem. C* **2008**, *112*, 5263.
- (319) Vinodgopal, K.; Neppolian, B.; Lightcap, I. V.; Grieser, F.; Ashokkumar, M.; Kamat, P. V. *J. Phys. Chem. Lett.* **2010**, *1*, 1987.
- (320) Myung, S.; Park, J.; Lee, H.; Kim, K. S.; Hong, S. *Adv. Mater.* **2010**, *22*, 2045.
- (321) Seger, B.; Kamat, P. V. *J. Phys. Chem. C* **2009**, *113*, 7990.
- (322) Si, Y.; Samulski, E. T. *Chem. Mater.* **2008**, *20*, 6792.
- (323) Yoo, E.; Okata, T.; Akita, T.; Kohyama, M.; Nakamura, J.; Honma, I. *Nano Lett.* **2009**, *9*, 2255.
- (324) Li, Y.; Gao, W.; Ci, L.; Wang, C.; Ajayan, P. M. *Carbon* **2010**, *48*, 1124.
- (325) Dong, L.; Reddy, R.; Gari, S.; Li, Z.; Craig, M. M.; Hou, S. *Carbon* **2010**, *48*, 781.
- (326) Xu, C.; Wang, X.; Zhu, J. *J. Phys. Chem. C* **2008**, *112*, 19841.
- (327) Nethravathi, C.; Anumol, E. A.; Rajamathi, M.; Ravishankar, N. *Nanoscale* **2011**, *3*, 569.
- (328) Zhou, Y. G.; Chen, J. J.; Wang, F.; Sheng, Z. H.; Xia, X. H. *Chem. Commun.* **2010**, *46*, 5951.
- (329) Hassan, H. M. A.; Abdelsayed, V.; El Rahman, A.; Khder, S.; Abou Zeid, K. M.; Terner, J.; El-Shall, M. S.; Al-Resayes, S. I.; El-Azhary, A. A. *J. Mater. Chem.* **2009**, *19*, 3832.
- (330) Bain, S. W.; Ma, Z.; Cui, Z. M.; Zhang, L. S.; Niu, F.; Song, W. G. *J. Phys. Chem. C* **2008**, *112*, 11340.
- (331) Ma, Z.; Liu, Q.; Cui, Z. M.; Bian, S. W.; Song, W. G. *J. Phys. Chem. C* **2008**, *112*, 8875.
- (332) Li, B. X.; Xie, Y.; Jing, M.; Rong, G. X.; Tang, Y. C.; Zhang, G. Z. *Langmuir* **2006**, *22*, 9380.
- (333) Liu, J. F.; Wang, X.; Peng, Q.; Li, Y. D. *Adv. Mater.* **2005**, *17*, 764.
- (334) Martinez, C. J.; Hockey, B.; Montgomery, C. B.; Semancik, S. *Langmuir* **2005**, *21*, 7937.
- (335) Cui, Z. M.; Hang, L. Y.; Song, W. G.; Guo, Y. G. *Chem. Mater.* **2009**, *21*, 1162.
- (336) Lou, X. W.; Wang, Y.; Yuan, C. L.; Lee, J. Y.; Archer, L. A. *Adv. Mater.* **2006**, *18*, 2325.
- (337) Lee, J. M.; Pyun, Y. B.; Yi, J.; Choung, J. W.; Park, W. *J. Phys. Chem. C* **2009**, *113*, 19134.
- (338) Chen, C.; Cai, W.; Long, M.; Zhou, B.; Wu, Y.; Wu, D.; Feng, Y. *ACS Nano* **2010**, *4*, 6425.
- (339) Zhang, L. S.; Jiang, L. Y.; Yan, H. J.; Wang, W. D.; Wang, W.; Song, W. G.; Guo, Y. G.; Wan, L. J. *J. Mater. Chem.* **2010**, *20*, 5462.
- (340) Wang, H.; Cui, L. F.; Yang, Y.; Casalongue, H. S.; Robinson, J. T.; Liang, Y.; Cui, Y.; Dai, H. *J. Am. Chem. Soc.* **2010**, *132*, 13978.
- (341) Yan, J.; Fan, Z.; Wei, T.; Qian, W.; Zhang, M.; Wei, F. *Carbon* **2010**, *48*, 3825.
- (342) Wang, B.; Wu, X. L.; Shu, C. Y.; Guo, Y. G.; Wang, C. R. *J. Mater. Chem.* **2010**, *20*, 10661.
- (343) Wu, Z. S.; Ren, W.; Wen, L.; Gao, L.; Zhao, J.; Chen, Z.; Zhou, G.; Li, F.; Cheng, H. M. *ACS Nano* **2010**, *4*, 3187.
- (344) Kim, H.; Seo, D. H.; Kim, S. W.; Kim, J.; Kang, K. *Carbon* **2011**, *49*, 326.
- (345) Chen, S. Q.; Wang, Y. J. *J. Mater. Chem.* **2010**, *20*, 9735.
- (346) Zhu, J.; Zhu, T.; Zhou, X.; Zhang, Y.; Lou, X. W.; Chen, X.; Zhang, H.; Hoon Hng, H.; Yan, Q. *Nanoscale* **2011**, *3*, 1084.
- (347) Zhang, M.; Lei, D.; Yin, X.; Chen, L.; Li, Q.; Wang, Y.; Wang, T. *J. Mater. Chem.* **2010**, *20*, 5538.
- (348) Wang, D.; Choi, D.; Li, J.; Yang, Z.; Nie, Z.; Kou, R.; Hu, D.; Wang, C.; Saraf, L. V.; Zhang, J.; Aksay, I. A.; Liu, J. *ACS Nano* **2009**, *3*, 907.
- (349) Shen, L.; Yuan, C.; Luo, H.; Zhang, X.; Yang, S.; Lu, X. *Nanoscale* **2011**, *3*, 572.
- (350) Lambert, T. N.; Chavez, C. A.; Hernandez-Sanchez, B.; Lu, P.; Bell, N. S.; Ambrosini, A.; Friedman, T.; Boyle, T. J.; Wheeler, D. R.; Huber, D. L. *J. Phys. Chem. C* **2009**, *113*, 19812.
- (351) Zhang, X. Y.; Li, H. P.; Cui, X. L.; Lin, Y. *J. Mater. Chem.* **2010**, *20*, 2801.
- (352) Zhang, H.; Lv, X.; Li, Y.; Wang, Y.; Li, J. *ACS Nano* **2010**, *4*, 380.
- (353) Zhou, K.; Zhu, Y.; Yang, X.; Jiang, X.; Li, C. *New J. Chem.* **2011**, *35*, 353.
- (354) Lightcap, I. V.; Kosel, T. H.; Kamat, P. V. *Nano Lett.* **2010**, *10*, 577.
- (355) Gao, E.; Wang, W.; Shang, M.; Xu, J. *J. Phys. Chem. Chem. Phys.* **2011**, *13*, 2887.
- (356) Williams, G.; Kamat, P. V. *Langmuir* **2009**, *25*, 13869.
- (357) Chang, H.; Sun, Z.; Ho, K. Y. F.; Tao, X.; Yan, F.; Kwok, W. M.; Zheng, Z. *Nanoscale* **2011**, *3*, 258.
- (358) Hwang, J. O.; Lee, D. H.; Kim, J. Y.; Han, T. H.; Kim, B. H.; Park, M.; No, K.; Kim, S. O. *J. Mater. Chem.* **2011**, *21*, 3432.
- (359) Jabeen, H.; Chandra, V.; Jung, S.; Lee, J. W.; Kim, K. S.; Kim, S. B. *Nanoscale* **2011**, *3*, 3583.
- (360) Yang, X.; Zhang, X.; Ma, Y.; Huang, Y.; Wang, Y.; Chen, Y. *J. Mater. Chem.* **2009**, *19*, 2710.
- (361) Cong, H. P.; He, J. J.; Lu, Y.; Yu, S. H. *Small* **2010**, *6*, 169.
- (362) Zhou, K.; Zhu, Y.; Yang, X.; Li, C. *New J. Chem.* **2010**, *34*, 2950.
- (363) He, F.; Fan, J.; Ma, D.; Zhang, L.; Leung, C.; Laiwa Chan, H. *Carbon* **2010**, *48*, 3139.
- (364) Bruchez, M., Jr.; Moronne, M.; Gin, P.; Weiss, S.; Alivisatos, A. P. *Science* **1998**, *281*, 2013.
- (365) Chan, W. C. W.; Nie, S. M. *Science* **1998**, *281*, 2016.
- (366) Huynh, W. U.; Dittmer, J. J.; Alivisatos, A. P. *Science* **2002**, *295*, 2425.
- (367) Schlamp, M. C.; Peng, X. G.; Alivisatos, A. P. *J. Appl. Phys.* **1997**, *82*, 5837.
- (368) Haremza, J. M.; Hahn, M. A.; Krauss, T. D.; Chen, S.; Calcines, J. *Nano Lett.* **2002**, *2*, 1253.
- (369) Chen, Z.; Bercaud, S.; Nuckolls, C.; Heinz, T. F.; Brus, L. E. *ACS Nano* **2010**, *4*, 2964.

- (370) Cao, A.; Liu, Z.; Chu, S.; Wu, M.; Ye, Z.; Cai, Z.; Chang, Y.; Wang, S.; Gong, Q.; Liu, Y. *Adv. Mater.* **2010**, *22*, 103.
- (371) Kim, Y. T.; Han, J. H.; Hong, B. H.; Kwon, Y. U. *Adv. Mater.* **2010**, *22*, 515.
- (372) Wang, Y.; Yao, H. B.; Wang, X. H.; Yu, S. H. *J. Mater. Chem.* **2011**, *21*, 562.
- (373) Lee, J. K.; Smith, K. B.; Hayner, C. M.; Kung, H. H. *Chem. Commun.* **2010**, 46, 2025.
- (374) Wang, G. W. B.; Wang, X.; Park, J.; Dou, S.; Ahn, H.; Kim, K. J. *Mater. Chem.* **2009**, *19*, 8378.
- (375) Chen, S.; Zhu, J.; Wang, X. *J. Phys. Chem. C* **2010**, *114*, 11829.
- (376) Li, X.; Wang, H.; Robinson, J. T.; Sanchez, H.; Diankov, G.; Dai, H. *J. Am. Chem. Soc.* **2009**, *131*, 15939.
- (377) Long, D.; Li, W.; Ling, L.; Miyawaki, J.; Mochida, I.; Yoon, S. H. *Langmuir* **2010**, *26*, 16096.
- (378) Lin, Y. C.; Lin, C. Y.; Chiu, P. W. *Appl. Phys. Lett.* **2010**, *96*, No. 133110.
- (379) Wei, D.; Liu, Y.; Wang, Y.; Zhang, H.; Huang, L.; Yu, G. *Nano Lett.* **2009**, *9*, 1752.
- (380) Panchokarla, L. S.; Subrahmanyam, K. S.; Saha, S. K.; Govindaraj, A.; Krishnamurthy, H. R.; Waghmare, U. V.; Rao, C. N. R. *Adv. Mater.* **2009**, *21*, 4726.
- (381) Deng, D.; Pan, X.; Yu, L.; Cui, Y.; Jiang, Y.; Qi, J.; Li, W. X.; Fu, Q.; Ma, X.; Xue, Q.; Sun, G.; Bao, X. *Chem. Mater.* **2011**, *23*, 1188.
- (382) Ci, L.; Song, L.; Jin, C.; Jariwala, D.; Wu, D.; Li, Y.; Srivastava, A.; Wang, Z. F.; Storr, K.; Balicas, L.; Liu, F.; Ajayan, P. M. *Nat. Mater.* **2010**, *9*, 430.
- (383) Zhao, L.; He, R.; Rim, K. T.; Schiros, T.; Kim, K. S.; Zhou, H.; Gutiérrez, C.; Chockalingam, S. P.; Arguello, C. J.; Pálková, L.; Nordlund, D.; Hybertsen, M. S.; Reichman, D. R.; Heinz, T. F.; Kim, P.; Pinczuk, A.; Flynn, G. W.; Pasupathy, A. N. *Science* **2011**, *333*, 999.
- (384) (a) Wehling, T. O.; Novoselov, K. S.; Morozov, S. V.; Vdovin, E. E.; Katsnelson, M. I.; Geim, A. K.; Lichtenstein, A. I. *Nano Lett.* **2008**, *8*, 173. (b) Park, S.; Hu, Y.; Hwang, J. O.; Lee, E. S.; Casabianca, L. B.; Cai, W.; Potts, J. R.; Ha, H. W.; Chen, S.; Oh, J.; Kim, S. O.; Kim, Y. H.; Ishii, Y.; Ruoff, R. S. *Nat. Commun.* **2012**, *3*, 638.
- (385) Dong, X.; Fu, D.; Fang, W.; Shi, Y.; Chen, P.; Li, L. *Small* **2009**, *5*, 1422.
- (386) Das, B.; Voggu, R.; Rout, C. S.; Rao, C. N. R. *Chem. Commun.* **2008**, 5155.
- (387) Liu, H.; Liu, Y.; Zhu, D. *J. Mater. Chem.* **2011**, *21*, 3335.
- (388) Das, A.; Pisana, S.; Chakraborty, B.; Piscanec, S.; Saha, S. K.; Waghmare, U. V.; Novoselov, K. S.; Krishnamurthy, H. R.; Geim, A. K.; Ferrari, A. C.; Sood, A. K. *Nat. Nanotechnol.* **2008**, *3*, 210.
- (389) Bostwick, A.; Ohta, T.; McChesney, J.; Emtsev, K.; Speck, F.; Seyller, T.; Horn, K.; Kevan, S.; Rotenberg, E. *New J. Phys.* **2010**, *12*, No. 125014.
- (390) Liu, Z.; Bol, A.; Haensch, W. *Nano Lett.* **2011**, *11*, 523.
- (391) (a) Lee, W. H.; Park, J.; Sim, S. H.; Lim, S.; Kim, K. S.; Hong, B. H.; Cho, K. *J. Am. Chem. Soc.* **2011**, *133*, 4447. (b) Lee, W. H.; Park, J.; Sim, S. H.; Jo, S. B.; Kim, K. S.; Hong, B. H.; Cho, K. *Adv. Mater.* **2011**, *23*, 1752.
- (392) (a) Lee, W. H.; Suk, J. W.; Lee, J.; Hao, Y.; Park, J.; Yang, J. W.; Ha, H. W.; Murali, S.; Chou, H.; Akinwande, D.; Kim, K. S.; Ruoff, R. S. *ACS Nano* **2012**, *6*, 1284. (b) Lee, W. H.; Suk, J. W.; Chou, H.; Lee, J.; Hao, Y.; Wu, Y.; Piner, R.; Akinwande, D.; Kim, K. S.; Ruoff, R. S. *Nano Lett.* **2012**, *12*, 2374.
- (393) Yu, Y. J.; Zhao, Y.; Ryu, S.; Brus, L. E.; Kim, K. S.; Kim, P. *Nano Lett.* **2009**, *9*, 3430.
- (394) Yang, J. W.; Lee, G.; Kim, J. S.; Kim, K. S. *J. Phys. Chem. Lett.* **2011**, *2*, 2577.
- (395) Dresselhaus, M. S.; Dresselhaus, G. *Adv. Phys.* **2002**, *51*, 1.
- (396) Kim, N.; Kim, K. S.; Jung, N.; Brus, L.; Kim, P. *Nano Lett.* **2011**, *11*, 860.
- (397) Yuk, J.; Kim, K.; Aleman, B.; Regan, W.; Ryu, J.; Park, J.; Ercius, P.; Lee, H.; Alivisatos, A.; Crommie, M.; Zettl, A. *Nano Lett.* **2011**, *11*, 3290.
- (398) (a) Pollak, E.; Geng, B.; Jeon, K.; Lucas, I.; Richardson, T.; Wang, F.; Kostecky, R. *Nano Lett.* **2010**, *10*, 3386. (b) Yoo, E.; Kim, J.; Hosono, E.; Zhou, H.; Kudo, T.; Honma, I. *Nano Lett.* **2008**, *8*, 2277.
- (399) Burrell, J.; Gadipelli, S.; Ford, J.; Simmons, J.; Zhou, W.; Yildirim, T. *Angew. Chem., Int. Ed.* **2010**, *49*, 8902.
- (400) Yu, D.; Dai, L. *J. Phys. Chem. Lett.* **2010**, *1*, 467.
- (401) Hong, T. K.; Lee, D. W.; Choi, H. J.; Shin, H. S.; Kim, B. S. *ACS Nano* **2010**, *4*, 3861.
- (402) Li, H.; Pang, S.; Wu, S.; Feng, X.; Müllen, K.; Bubeck, C. *J. Am. Chem. Soc.* **2011**, *133*, 9423.
- (403) Ji, Q.; Honma, I.; Paek, S. M.; Akada, M.; Hill, J. P.; Vinu, A.; Ariga, K. *Angew. Chem., Int. Ed.* **2010**, *49*, 9737.
- (404) Shen, J.; Hu, Y.; Li, C.; Qin, C.; Shi, M.; Ye, M. *Langmuir* **2009**, *25*, 6122.
- (405) Zhao, X.; Zhang, Q.; Hao, Y.; Li, Y.; Fang, Y.; Chen, D. *Macromolecules* **2010**, *43*, 9411.
- (406) Kulkarni, D. D.; Choi, I.; Singamaneni, S. S.; Tsukruk, V. V. *ACS Nano* **2010**, *4*, 4667.
- (407) Son, Y.; Cohen, M.; Louie, S. *Phys. Rev. Lett.* **2006**, *97*, No. 216803.
- (408) Son, Y.; Cohen, M.; Louie, S. *Nature* **2006**, *444*, 347.
- (409) Kim, W. Y.; Kim, K. S. *Acc. Chem. Res.* **2010**, *43*, 111.
- (410) Han, M.; Ozyilmaz, B.; Zhang, Y.; Kim, P. *Phys. Rev. Lett.* **2007**, *98*, No. 206805.
- (411) Jiao, L.; Zhang, L.; Wang, X.; Diankov, G.; Dai, H. *Nature* **2009**, *458*, 877.
- (412) Yu, Y. J.; Han, M. Y.; Berciaud, S.; Georgescu, A. B.; Heinz, T. F.; Brus, L. E.; Kim, K. S.; Kim, P. *Appl. Phys. Lett.* **2011**, *99*, No. 183105.
- (413) Cai, J.; Ruffieux, P.; Jaafar, R.; Bieri, M.; Braun, T.; Blankenburg, S.; Muoth, M.; Seitsonen, A.; Saleh, M.; Feng, X.; Müllen, K.; Fasel, R. *Nature* **2010**, *466*, 470.
- (414) Ding, Z.; Jiang, J.; Xing, H.; Shu, H.; Dong, R.; Chen, X.; Lu, W. J. *Comput. Chem.* **2011**, *32*, 737.
- (415) Lu, D.; Song, Y.; Yang, Z.; Li, G. *Appl. Surf. Sci.* **2011**, *257*, 6440.
- (416) Xu, J.; Wang, L.; Zhu, Y. *Langmuir* **2012**, *28*, 8418.
- (417) Huang, Z. H.; Zheng, X.; Lv, W.; Wang, M.; Yang, Q. H.; Kang, F. *Langmuir* **2011**, *27*, 7558.
- (418) Vasudevan, S.; Lakshmi, J. *RSC Adv.* **2012**, *2*, 5234.
- (419) Zhao, G.; Li, J.; Ren, X.; Chen, C.; Wang, X. *Environ. Sci. Technol.* **2011**, *45*, 10454.
- (420) Yang, S. T.; Chen, S.; Chang, Y.; Cao, A.; Liu, Y.; Wang, H. J. *Colloid Interface Sci.* **2011**, *359*, 24.
- (421) Zhao, G.; Jiang, L.; He, Y.; Li, J.; Dong, H.; Wang, X.; Hu, W. *Adv. Mater.* **2011**, *23*, 3959.
- (422) Chandra, V.; Kim, K. S. *Chem. Commun.* **2011**, 47, 3942.
- (423) Sui, Z.; Meng, Q.; Zhang, X.; Ma, R.; Cao, B. *J. Mater. Chem.* **2012**, *22*, 8767.
- (424) Geng, Z.; Lin, Y.; Yu, X.; Shen, Q.; Ma, L.; Li, Z.; Pan, N.; Wang, X. *J. Mater. Chem.* **2012**, *22*, 3527.
- (425) Zhang, J.; Xiong, Z.; Zhao, X. S. *J. Mater. Chem.* **2011**, *21*, 3634.
- (426) Zhang, K.; Kemp, K. C.; Chandra, V. *Mater. Lett.* **2012**, *81*, 127.
- (427) Chandra, V.; Yu, S. U.; Kim, S. H.; Yoon, Y. S.; Kim, D. Y.; Kwon, A. H.; Meyyappan, M.; Kim, K. S. *Chem. Commun.* **2012**, 48, 735.
- (428) Mishra, A. K.; Ramaprabhu, S. *J. Mater. Chem.* **2012**, *22*, 3708.
- (429) Liang, Y. T.; Vijayan, B. K.; Gray, K. A.; Hersam, M. C. *Nano Lett.* **2011**, *11*, 2865.
- (430) Ng, Y. H.; Iwase, A.; Kudo, A.; Amal, R. *J. Phys. Chem. Lett.* **2010**, *1*, 2607.
- (431) Xiang, Q.; Yu, J.; Jaroniec, M. *J. Am. Chem. Soc.* **2012**, *134*, 6575.
- (432) Liang, Y.; Li, Y.; Wang, H.; Zhou, J.; Wang, J.; Regier, T.; Dai, H. *Nat. Mater.* **2011**, *10*, 780.
- (433) Miao, X.; Tongay, S.; Petterson, M. K.; Berke, K.; Rinzler, A. G.; Appleton, B. R.; Hebard, A. F. *Nano Lett.* **2012**, *12*, 2745.
- (434) Bonaccorso, F.; Sun, Z.; Hasan, T.; Ferrari, A. C. *Nat. Photonics* **2010**, *4*, 611.
- (435) Gokus, T.; Nair, R. R.; Bonetti, A.; Bohmler, M.; Lombardo, A.; Novoselov, K. S.; Geim, A. K.; Ferrari, A. C.; Hartschuh, A. *ACS Nano* **2009**, *3*, 3963.

- (436) Eda, G.; Lin, Y. Y.; Mattevi, C.; Yamaguchi, H.; Chen, H. A.; Chen, I. S.; Chen, C. W.; Chhowalla, M. *Adv. Mater.* **2010**, *22*, 505.
- (437) Frangioni, J. V. *Curr. Opin. Chem. Biol.* **2003**, *7*, 626.
- (438) Baker, S. N.; Baker, G. A. *Angew. Chem., Int. Ed.* **2010**, *49*, 6726.
- (439) Chen, H.; Muller, M. B.; Gilmore, K. J.; Wallace, G. G.; Li, D. *Adv. Mater.* **2008**, *20*, 3557.
- (440) Luo, Z.; Vora, P. M.; Mele, E. J.; Johnson, A. T. C.; Kikkawa, J. M. *Appl. Phys. Lett.* **2009**, *94*, No. 111909.
- (441) Sun, X.; Liu, Z.; Welscher, K.; Robinson, J.; Goodwin, A.; Zaric, S.; Dai, H. *Nano Res.* **2008**, *1*, 203.
- (442) Peng, C.; Hu, W.; Zhou, Y.; Fan, C.; Huang, Q. *Small* **2010**, *6*, 1686.
- (443) Li, J. L.; Bao, H. C.; Hou, X. L.; Sun, L.; Wang, X. G.; Gu, M. *Angew. Chem., Int. Ed.* **2012**, *51*, 1830.
- (444) Zhu, S.; Zhang, J.; Qiao, C.; Tang, S.; Li, Y.; Yuan, W.; Li, B.; Tian, L.; Liu, F.; Hu, R.; Gao, H.; Wei, H.; Zhang, H.; Sun, H.; Yang, B. *Chem. Commun.* **2011**, *47*, 6858.
- (445) Peng, J.; Gao, W.; Gupta, B. K.; Liu, Z.; Romero-Aburto, R.; Ge, L.; Song, L.; Alemany, L. B.; Zhan, X.; Gao, G.; Vithayathil, S. A.; Kaiparettu, B. A.; Marti, A. A.; Hayashi, T.; Zhu, J. J.; Ajayan, P. M. *Nano Lett.* **2012**, *12*, 844.
- (446) Hu, S. H.; Chen, Y. W.; Hung, W. T.; Chen, I. W.; Chen, S. Y. *Adv. Mater.* **2012**, *24*, 1748.
- (447) Narayanan, T. N.; Gupta, B. K.; Vithayathil, S. A.; Aburto, R. R.; Mani, S. A.; Taha-Tijerina, J.; Xie, B.; Kaiparettu, B. A.; Torti, S. V.; Ajayan, P. M. *Adv. Mater.* **2012**, *24*, 2992.
- (448) Kim, H.; Namgung, R.; Singha, K.; Oh, I. K.; Kim, W. J. *Bioconjugate Chem.* **2011**, *22*, 2558.
- (449) Mao, X.; Tian, D.; Li, H. *Chem. Commun.* **2012**, *48*, 4851.
- (450) Kim, S.; Zhou, S.; Hu, Y.; Acik, M.; Chabal, Y. J.; Berger, C.; de Heer, W.; Bongiorno, A.; Riedo, E. *Nat. Mater.* **2012**, *11*, 544.
- (451) (a) Choi, B. G.; Yang, M. H.; Hong, W. H.; Choi, J. W.; Huh, Y. S. *ACS Nano* **2012**, *6*, 4020. (b) Chen, C. M.; Zhang, Q.; Huang, C. H.; Zhao, X. C.; Zhang, B.; Kong, Q. Q.; Wang, M.; Yang, Y.; Cai, R.; Su, D. *Chem. Commun.* **2012**, DOI: 10.1039/C2CC32189K. (c) Zhu, Y. W.; Murali, S.; Stoller, M. D.; Ganesh, K. J.; Cai, W. W.; Ferreira, P. J.; Pirkle, A.; Wallace, R. M.; Cychosz, K. A.; Thommes, M.; Su, D.; Stach, E. A.; Roff, R. S. *Science* **2011**, *332*, 1537.
- (452) Yong, Y. C.; Dong, X. C.; Chan-Park, M. B.; Song, H.; Chen, P. *ACS Nano* **2012**, *6*, 2394.
- (453) Li, X.; Huang, X.; Liu, D.; Wang, X.; Song, S.; Zhou, L.; Zhang, H. *J. Phys. Chem. C* **2011**, *115*, 21567.
- (454) Yang, H.; Heo, J.; Park, S.; Song, H. J.; Seo, D. H.; Byun, K. E.; Kim, P.; Yoo, I. K.; Chung, H. J.; Kim, K. *Science* **2012**, *336*, 1140.
- (455) Lee, W. C.; Lim, C. H. Y. X.; Shi, H.; Tang, L. A. L.; Wang, Y.; Lim, C. T.; Loh, K. P. *ACS Nano* **2011**, *5*, 7334.
- (456) Nair, R. R.; Wu, H. A.; Jayaram, P. N.; Grigorieva, I. V.; Geim, A. K. *Science* **2012**, *335*, 442.
- (457) Lee, H.; Heo, K.; Park, J.; Park, Y.; Noh, S.; Kim, K. S.; Lee, C.; Hong, B. H.; Jian, J.; Hong, S. *J. Mater. Chem.* **2012**, *22*, 8372.
- (458) Shin, S. Y.; Kim, N. D.; Kim, J. G.; Kim, K. S.; Noh, D. Y.; Kim, K. S.; Chung, J. W. *Appl. Phys. Lett.* **2011**, *99*, No. 082110.
- (459) Yuk, J. M.; Park, J.; Ercius, P.; Kim, K.; Hellebusch, D. J.; Crommie, M. F.; Lee, J. Y.; Zettl, A.; Alivisatos, A. P. *Science* **2012**, *336*, 61.